PNNL-11642
UC-2030

Pacific Northwest
National Laboratory
Operated by Battelle for the
U.S. Department of Energy

Mechanisms of Gas Retention and Release: Experimental Results for Hanford Waste Tanks 241-AW-101 and 241-AN-103

S. D. Rassat
P. A. Gauglitz
P. R. Bredt
L. A. Mahoney
S. V. Forbes
S. M. Tingey

September 1997

Prepared for the U.S. Department of Energy
under Contract DE-AC06-76RLO 1830

PNNL-11642

PACIFIC NORTHWEST NATIONAL LABORATORY
operated by
BATTELLE
for the
UNITED STATES DEPARTMENT OF ENERGY
under Contract DE-AC06-76RLO 1830

Printed in the United States of America

Available to DOE and DOE contractors from the Office of Scientific and Technical Information, P.O. Box 62, Oak Ridge, TN 37831; prices available from (615) 576-8401.

Available to the public from the National Technical Information Service, U.S. Department of Commerce, 5285 Port Royal Rd., Springfield, VA 22161


This document was printed on recycled paper.

PNNL-11642
UC-2030

Mechanisms of Gas Retention and Release: Experimental Results for Hanford Waste Tanks 241-AW-101 and 241-AN-103

S. D. Rassat
P. A. Gauglitz
P. R. Bredt
L. A. Mahoney
S. V. Forbes
S. M. Tingey

September 1997

Prepared for
the U.S. Department of Energy
under Contract DE-AC06-76RLO 1830

Pacific Northwest National Laboratory
Richland, WA 99352

Executive Summary

The 177 storage tanks at Hanford contain a vast array of radioactive waste forms resulting, primarily, from nuclear materials processing. Through radiolytic, thermal, and other decomposition reactions of waste components, gaseous species including hydrogen, ammonia, and the oxidizer nitrous oxide are generated within the waste tanks. Many of these tanks are known to retain and periodically release quantities of these flammable gas mixtures. The primary focus of the Flammable Gas Project is the safe storage of Hanford tank wastes. To this end, we strive to develop an understanding of the mechanisms of flammable gas retention and release in Hanford tanks through laboratory investigations on actual tank wastes. These results support the closure of the Flammable Gas Unreviewed Safety Question (USQ) on the safe storage of waste tanks known to retain flammable gases and support resolution of the broader Flammable Gas Safety Issue.

The overall purpose of this ongoing study is to develop a comprehensive and thorough understanding of the mechanisms of flammable gas retention and release. The first objective of the current study was to classify bubble retention and release mechanisms in two previously untested waste materials from Tanks 241-AN-103 (AN-103) and 241-AW-101 (AW-101). Results were obtained for retention mechanisms, release characteristics, and the maximum gas retention. In addition, unique behavior was also documented and compared with previously studied waste samples. The second objective was to lengthen the duration of the experiments to evaluate the role of slowing bubble growth on the retention and release behavior. Results were obtained for experiments lasting from a few hours to a few days.

Waste Materials and Method

The types of wastes in Hanford tanks are varied, and many must be studied to probe the full range of gas retention and release characteristics. Although each tank is unique, broad classification and categorization is attempted to reduce the number of waste types that must be studied individually. In previous laboratory studies of gas retention and release in Hanford tank wastes, the waste types included double-shell tank (DST) wastes from Tanks 241-SY-101 (SY-101), and 241-SY-103 (SY-103), both complex concentrate wastes, and single-shell tank (SST) waste from Tank 241-S-102, a saltcake waste. In the current study, the specific materials investigated include waste from AN-103, a double-shell slurry waste, and from Tank AW-101, a double-shell slurry feed waste. Both of these DST waste types are concentrated evaporator wastes, but the double-shell slurry in AN-103 is in a more concentrated form. These two tanks are of interest because they have a history of retaining large quantities of flammable gas. AN-103 continues to retain gas and has yet to exhibit large gas release events. The two tanks also represent waste types not previously investigated in laboratory gas retention studies.

The general experimental approach applied in the current and previous laboratory gas retention and release studies is similar. The waste sample of interest is loaded into a transparent vessel, allowed to settle, and irradiated with a cesium gamma source to generate a small amount of retained gas, on the order of 2–3% of the nonconvective layer volume. The sample is then evacuated in a controlled manner to nucleate additional gas bubbles and expand the existing gas bubbles. A new electronic vacuum pressure control system was developed, and pressure programs were applied that made it possible to attain very controlled growth rates in gas fraction. This system enables retention experiments to be run in a few hours or less or, preferably, for a day or longer. During an experiment, the volume of waste grows with gas retention and subsides with gas release, and both the level of the nonconvective solids layer and the convective supernatant liquid layer, when present, are monitored over time using a video camera and recording system. The relative contribution of the two primary mechanisms of gas retention, interstitial liquid-displacing

or particle-displacing bubbles, may be deduced from the relative growth of the liquid and nonconvective layers. Supporting evidence is obtained by directly observing the bubble shapes within the nonconvective layer using a zoom video camera.

A single composite was prepared using AN-103 nonconvective material and a sample of convective liquid. The AN-103 nonconvective material was obtained from an elevation of approximately 260–310 cm (segment 13, Core 167), which is near the top of the nonconvective layer in the tank core sample. AN-103 experiments were run at 42°C, near the measured tank temperature in the vicinity of where the sample was obtained. The AW-101 samples used in gas retention testing were recovered from two separate core sampling events (132 and 139) and from various depths in the waste tank. One composite, AW-101 Composite 2, was prepared from material located near the bottom of the tank, at 0–95 cm elevation (segments 21 and 22), and another, AW-101 Composite 1, was mixed from middle nonconvective layer segment (19; approximately 145–190 cm elevation) subsamples. These experiments were conducted at the ambient hot cell temperature (33–37°C), which is approximately equal to the measured tank temperature near the tank bottom. Four gas retention tests were conducted on samples from each of the waste tanks for a total of eight experiments.

Two types of gas retention experiments were conducted on both AN-103 and AW-101 composites. In the majority of experiments, an overlayer of supernatant liquid was present in the samples to mimic the actual conditions in a DST. For buoyant displacement to occur in these tests, the nonconvective layer must minimally retain enough gas that the bubble-laden material becomes neutrally buoyant in, or equal in density to, the liquid layer. However, gas retention greater than the neutral buoyancy gas fraction is possible and was observed in the retention-to-buoyancy experiments reported here due to waste strength and wall effects. In other experiments, the supernatant liquid layer was removed from waste samples, and buoyant displacement was thereby eliminated as a mechanism for gas release. An upper bound to the retained gas fraction was investigated in these experiments.

Bubble Retention Mechanisms

Through previous studies on actual and simulated tank wastes, it is recognized that two mechanisms of gas retention likely predominate in Hanford tanks: yield strength retention for particle-displacing bubbles and capillary retention for interstitial liquid-displacing bubbles. Photographic evidence obtained in this study showed that the AN-103 and AW-101 waste types retained gas exclusively in particle-displacing bubbles. These bubbles were typically round when small but tended to be slightly distorted from round at 1 mm in diameter or larger. The visual (shape) data indicate a moderate sample strength in each waste type, probably on the order of 50 to 75 Pa. Somewhat more deformed and elongated bubbles were observed in a portion of the AN-103 ultimate retention sample, indicative of a region containing higher-strength material.

New Observations: Stable Froths and Wall Effects

Stable foams, potentially resulting from an armored bubble retention mechanism and a viable pathway to crust formation, were observed on the supernatant liquid in the AN-103 composite retention-to-buoyancy experiments. Once the samples became buoyant, the bubbly mass formed a froth, which continued to retain more gas and expand with pressure reductions. In addition, anomalously high gas fractions (0.8–0.9) were observed near the vessel wall in the AN-103 retention-to-buoyancy experiments. This phenomenon, which was observed to a lesser extent in AW-101 samples and appeared unimportant in previous tests with SY-103, seems to be intimately linked to the attachment of bubbles to the plastic vessel walls. It is unclear what chemical or physical property resulted in this wall foaming characteristic or if it would occur in an actual steel tank. The high wall gas fractions and the wall interaction apparently contributed to maximum gas retention in the bulk nonconvective layer above the neutral buoyancy point.

Wall effects influenced the extent of gas retention in both AW-101 and AN-103 retention-to-buoyancy experiments, and the interaction strength between the waste samples and the vessel walls was quantified. In AW-101 Composite 1 and 2 tests, a maximum retained gas volume increase of 19% was observed, and only 9% growth was expected to reach neutral buoyancy. A wall-sample interaction strength of 9–10 Pa was calculated to account for the excess retained gas content. In the two-hour and one-day AN-103 experiments, a maximum 30–32% retained gas volume growth was measured and only 15-16% growth was predicted from density data (neutral buoyancy). The excess gas retention was attributed to a 16–19 Pa wall effect. In the four-day AN-103 experiment, the deviation of the neutral buoyancy predicted (20%) and measured (28%) maximum retained gas volume growths was considerably less. This corresponds to a lesser apparent wall interaction strength of 8 Pa. Additionally, in the long AN-103 test, the initiation of a slow buoyant rise of the nonconvective layer was detected at a retained gas volume growth of 22% or less, in very good agreement with the predicted neutral buoyancy gas content.

Role of Experiment Duration

A primary focus of the current experiments was to evaluate the effects of experiment duration and waste growth rate on gas retention behavior, because it is speculated that longer experiments would result in a more realistic bubble size distribution. In two-hour, half-day, and one-day AW-101 retention-to-buoyancy tests, the maximum retained gas fractions were essentially equal. However, gas release behavior was apparently affected by experiment duration: the nonconvective layer became buoyant in the supernatant liquid only in the most quickly evacuated sample, but the gas release rate (as a function of pressure) following maximum retention was greatest in the slowest (one-day) experiment. In these longer AW-101 tests, gas appeared to be released through a series of bubble disengagements. In the AN-103 retention-to-buoyancy tests, higher maximum void growth was observed in the two-hour and one-day experiments than in the four-day test. In addition, more gas release activity prior to maximum retention was evident in the longer AN-103 test. However, because of inhomogeneities in the AN-103 composite sample, differences in the AN-103 four-day test from the shorter tests cannot be attributed conclusively to variations in the experiment duration.

Maximum Gas Retention

To probe a bounding maximum gas retention, the supernatant liquid layer was removed from one AN-103 and one AW-101 sample to eliminate buoyant displacement as a mechanism for gas release. A maximum gas volume growth of 37% was measured in the AN-103 ultimate retention experiment, while only 27–32% growth was observed in the AN-103 retention-to-buoyancy tests. The AW-101 ultimate retention maximum retained gas volume increase (22–27%) was also greater than in the corresponding retention-to-buoyancy experiment (19%).

These reported maximum gas contents are determined from the growth in waste sample volume during an evacuation experiment. A 0% growth value was assigned at the start of evacuation. However, gas was present in the waste samples prior to evacuation due to sample irradiation and bubble entrainment in the vessel loading process. The initial sample growth rate during an evacuation was used to estimate the maximum initial (pre-evacuation) gas content and ranged from 3 to 5% of the nonconvective layer volume in all samples studied. Therefore, the absolute gas content of the waste samples is greater by a few percent than the reported maximum growth values.

Future Directions

The gas retention and release experimental results for AW-101 and AN-103 are indicative of novel waste behavior that may have been overlooked by broad classification or generalization of waste type. For example, AW-101, AN-103, and (previously) SY-103 waste samples all retained gas in slightly distorted round particle-displacing bubbles. But the consistency of this characteristic in these DST wastes does not represent the variability in the maximum gas retention of the various waste types, and it does not reflect the unique frothing behavior of the AN-103 material and the relatively weak foam stability in AW-101 and SY-103. The frothing in AN-103 also highlights a need to better understand the importance and role of bubble/particle interactions and to more clearly tie gas retention observations to tank chemistry, specifically, the presence or absence of surfactant-type chemical species.

To provide a comprehensive basis for understanding bubble retention mechanisms and maximum gas retention, experiments on additional significant waste tank samples and different experimental configurations are necessary. Although the focus of these tests should be waste tanks of highest priority to the Flammable Gas Project, some studies should be directed to address key needs. A particularly notable deficiency is the lack of evidence in actual waste data of retained interstitial liquid-displacing bubbles, which are indicative of a capillary retention mechanism. To date, experimental waste samples have been too small (short) to observe anything but the particle-displacing bubbles in yield strength retention. In order to observe gas retention by interstitial liquid-displacing bubbles, we propose to mimic a tall waste sample by placing a static load on top of a nonconvective layer during a gas retention experiment similar to those described in this report.

The overall objective of these studies is to quantify the pertinent mechanisms of gas bubble retention and release under conditions that, as accurately as reasonably possible, reflect the actual tank conditions. Even though the new pressure-controlled experimental apparatus described here permits tests longer than a day, the gas retention and release processes in this system occur on time scales that are rapid compared with the actual tank processes. An alternative is to accelerate the radiolytic gas generation mechanism naturally occurring in the tanks. In this approach, the experiment would take place over months, and it is anticipated that distinct gas retention and release characteristics would be observed. Gas diffusion and bubble migration should play a more significant role, and it is anticipated that a wider distribution of bubble sizes would result.

Acknowledgments

The authors would like to acknowledge other PNNL staff members who contributed significantly to this project. First, we thank Sheila Q. Bennett for her valuable editorial support. Loni M. Peurrung's assistance in developing the LabView software interface used to set, read, and record system pressures was critical to the success of the project. Finally, Charles W. Stewart's insight into gas retention and release phenomena led to helpful discussions and clarification of the interpretation of the results presented here.

Contents

Figures

Tables

1.0 Introduction

The Hanford Site has 177 underground storage tanks containing radioactive wastes that are complex mixtures of radioactive and chemical products. Some of these wastes are known to generate and retain bubbles of flammable gases that contain hydrogen, ammonia, and the oxidizer nitrous oxide. Because these gases are flammable and have the potential to be rapidly released, the mechanism of how gas is retained and released in these tank must be understood and quantified to establish the flammability hazard (Johnson et al. 1997a,b). While it would be helpful to have specific information about all tanks, a detailed understanding of bubble retention and release mechanisms on a representative selection of tanks should provide a sufficient understanding.

The established presence of large volumes of flammable gases in some Hanford tanks arguably poses the most significant current safety hazard. The flammable gas unreviewed safety question (USQ) was first declared in 1990[a] and has since been broadened to incorporate additional gases and facilities (Johnson et al. 1997b). The path for closing the USQ depends critically on establishing a technical basis for how gas is retained and potentially released from Hanford tanks because this establishes the potential hazard. Because of the potential ignition of these flammable gases, costly controls have been applied to all Hanford tanks (Grigsby and Leach 1996), and operations involving flammable gas tanks generally require extensive and restrictive safety assessments (WHC 1996a,b). Estimates of how retained bubbles are released play a pivotal role in determining the flammable gas hazard and the limits and controls imposed on operations. Developing a thorough understanding of gas retention and release is important because it will help establish the potential hazard and provide the analysis and documentation that form the basis for applying appropriate limits and controls. The current approach to closing the Flammable Gas USQ is using the SCOPE methodology (Slezak and Bratzel 1997), which involves inputting information on the uncertainty of important measurements and parameters. An improved understanding of bubble retention is valuable to the SCOPE process because it provides a basis for estimating the uncertainty and variability in retained gas among tanks and the range of likely releases and release mechanisms.

Resolving the Flammable Gas Safety Issue will follow the closure of the Flammable Gas USQ, and it is a broader topic (Johnson 1997). For gas retention and release, the challenge in closing the safety issue is developing a level of understanding thorough enough to prove that the flammable gas controls are always adequate (Johnson 1997). The retention and release of gas from waste tanks is complex because bubbles are retained and released by a variety of distinct mechanisms that depend on the often poorly understood waste properties and configuration. Because bubble retention and release is a central component in both closing the Flammable Gas USQ and resolving the safety issue, developing a broad and detailed understanding of the mechanisms pertinent to bubble retention and release is important.

A number of previous studies have focused on understanding the principal mechanisms of gas bubble retention in wastes because this is a critical step in quantifying the potential hazard. Recent laboratory studies on simulated and actual waste samples have provided a framework to classify bubble retention mechanisms (Gauglitz et al. 1994a, 1995, 1996), and additional recent experimental results can be classified by this framework (Walker et al. 1994; Bredt et al. 1995; Bredt and Tingey 1996; Rassat and Gauglitz 1995). In the previous studies, bubble retention measurements were made on waste samples from double-shell tanks (DSTs) SY-101 and SY-103 and single-shell tank (SST) S-102.[b] While these results have allowed improved understanding,

---

(a) Lawrence MJ. May 14, 1990. *Unreviewed Safety Question--Waste Storage Tanks.* Letter to LP Duffy, DOE-RL, Richland, Washington.

(b) Hanford tanks are formally designated with the prefix 241-. In this report, the prefix has been dropped, as it is in common usage.

results have been obtained for only three waste materials, and the experimental technique for creating gas bubbles was much faster than the actual process occurring in the tanks. Accordingly, further results are needed on additional waste types, and the previously used experimental technique requires improvement to allow for testing over longer time periods.

While the overall objective of this ongoing study is to quantify bubble retention and release behavior at the full tank scale, we are limited by both size and time in conducting laboratory studies. Typically, the laboratory experiments use waste depths on the order of 10 cm and experimental duration of hours to a few days. Actual bubble retention and release behavior in the tanks depends on the waste configuration (layering and depth) at the tank scale, and significant changes often occur over periods of years. Our approach has been to scale as many of the significant features as possible, but the actual tank waste configuration is not readily scaled. As a result, our results do not quantitatively predict all of the full tank behavior. In contrast, waste behaviors that are dominated by chemical interactions are largely independent of the tank-scale waste configuration and scale readily to laboratory studies. Gas generation experiments in actual wastes are an example of where laboratory scale studies have agreed quantitatively with full tank behavior (King et al. 1997). While our laboratory experiments miss certain aspects of tank-scale phenomena, these laboratory-scale observations of behavior at the scale of individual bubbles agree quite well with other documentation of individual bubbles in actual waste (Meyer et al. 1997) and gas retention theories (Gauglitz et al. 1994a, 1995, 1996).

1.1 Objectives

The focus of this laboratory study was to further quantify the pertinent mechanisms of gas bubble retention and release by measuring and observing the retention of gas bubbles and their release in actual waste samples. The first specific objective was to conduct bubble retention experiments with the previously developed but enhanced technique of creating retained bubbles by applying a vacuum to actual waste samples that have been exposed to a gamma source to accelerate gas generation. Actual waste samples from two tanks were studied. These experiments have provided quantitative information for two additional tanks on bubble retention (maximum retention), bubble shapes, and bubble release mechanisms. The second specific objective was to automate the apparatus used to apply vacuums to the waste samples. This automation provided two benefits: first, the changes in applied vacuum could be made very smoothly; and second, it allowed for multi-day, unattended testing that could be monitored with time-lapse video recording and data acquisition systems. To explore the role of experiment duration, bubble retention experiments were conducted over periods ranging from a few hours to a few days.

1.2 Significance

The significance of this work lies in further broadening the evidence of bubble retention and release mechanisms and waste behavior. This work supports the efforts to close the Flammable Gas USQ (Tri-Party Agreement Milestone M-40-09 [September 30, 1998], Johnson 1997), and is also directly focused on developing a sufficient understanding to support final resolution of the Flammable Gas Safety Issue (Tri-Party Agreement Milestone M-40-00 [September 30, 2001], Johnson 1997). In addition to directly supporting the issues associated with safe storage, a basic understanding of bubble retention and release mechanisms is crucial to future Hanford Site waste operations such as salt-well pumping, waste transfers, and sluicing/retrieval.

1.3 Gas Bubble Retention Mechanisms

The principal mechanisms of bubble retention that have been identified can be grouped into three categories: bubbles retained by the strength of the waste material, bubbles retained by capillary forces, and bubbles retained by direct attachment to particles (armored bubbles, bubble attachment, and aggregates) (Gauglitz et al. 1994a, 1995, 1996). In typical waste configurations, bubble retention is dominated by the waste strength and capillary forces (Johnson et al. 1997b, Gauglitz et al. 1996). Figure 1.1 shows the distinction between an interstitial-liquid-displacing bubble retained by capillary forces in a particulate material, and a particle-displacing bubble that is retained by the waste strength in a continuum material. For the particulate material, the bubble fingers between the waste particles. Here, the surface tension and pore throats between the particles give rise to forces that resist the upward force caused by gravity. For the bubble that displaces the waste particles, the waste is essentially a continuum material. When sufficiently strong, the strength of the continuum material overcomes the gravitational force and the bubble does not rise.

The distinction between the two dominant mechanisms of retention depends on two dimensionless groups that relate surface tension, gravitational, and waste strength forces (for details see Gauglitz et al. 1994a, 1995, 1996). These dimensionless groups are reproduced here because they will be used later when summarizing the current observations of bubble retention and comparing them with previous results. In general, fine particle materials such as sludges and some fine-particle slurries give rise to particle-displacing bubbles while coarser materials, such as many slurries and saltcakes, result in interstitial liquid-displacing bubbles. The forces affecting bubbles retained by these two mechanisms are substantially different, and the release mechanisms for these two retention mechanisms are expectedly different. Stewart et al. (1996) give a comprehensive discussion of bubble release mechanisms and their association to retention mechanisms. The two dimensionless groups, which quantify the transition between bubbles retained by the strength of the material (particle displacing) and by capillary forces (interstitial liquid displacing), are defined below:

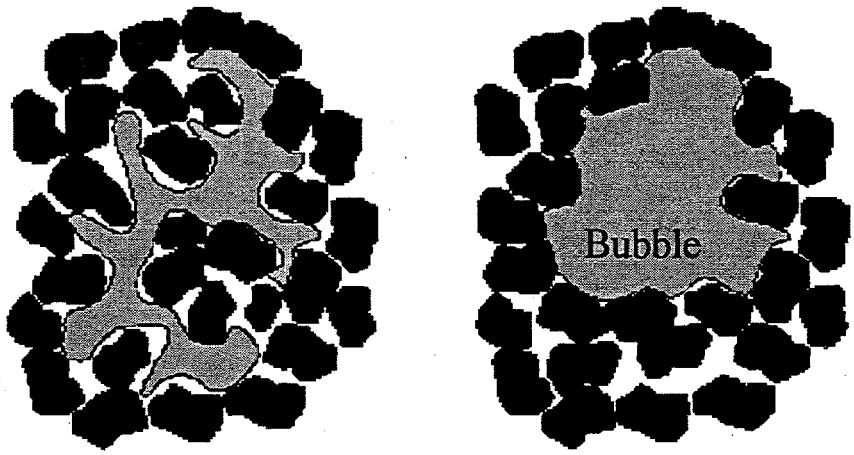

Figure 1.1. Schematic of a Bubble Fingering Between Particles in a Particulate Material and a Bubble Displacing Particles in a Continuum Material

$$\frac{\text{Gravitational Force}}{\text{Surface Tension Force}} = \frac{\Delta\rho g h D_{particle}}{4\gamma} \tag{1.1}$$

$$\frac{\text{Strength Force}}{\text{Surface Tension Force}} = \frac{\tau_s D_{particle}}{4\gamma}\left(\frac{A_2}{A_1}\right) \tag{1.2}$$

In the first dimensionless parameter, $\Delta\rho$ is the density difference between the settled solids, the liquid, g, is the gravitational acceleration, and h is the depth below the top of the settled solids. In the second dimensionless parameter, the constant A_2/A_1 is a ratio of areas that resulted from the original analysis, and τ_s represents the shear strength of the material. Although it is expected that the tensile and shear strengths are important in the growth of bubbles, these two measures of strength are commonly related (see Gauglitz et al. [1995] for a discussion of tensile and shear strength measurements). The shear strength is used here because it is the most easily measured and commonly reported measure of material strength. The surface tension (γ) force in these dimensionless parameters reflects the resistance the bubble experiences as it seeks to move between particles. Thus the appropriate length scale is the pore-throat diameter. For beds of packed particles, the median pore-throat diameter is roughly one-third the particle diameter (Dullien 1992). The actual pore-throat diameter (which is a distribution of sizes) can vary by an order of magnitude depending on the particle packing. For the purpose of this study, the pore-throat diameter is approximated as the particle diameter, $D_{particle}$. The two parameters shown above define the transition between two regimes of bubble retention: particle-displacing bubbles that are retained by yield strength forces and interstitial liquid-displacing bubbles that finger between the particles composing the particulate media, as seen in Figure 1.1.

A third dimensionless parameter further refines the range of bubble behavior for particle-displacing bubbles. When these bubbles grow in a deformable material, the dominant factors controlling their growth are surface tension forces, which seek to keep the bubbles round, and the strength of the material that the bubble must overcome to displace the particles. A detailed description of this process is given in Gauglitz et al. (1996). The relative importance of sludge strength to surface tension gives the third dimensionless group.

$$\frac{\text{Strength Force}}{\text{Surface Tension Force}} = \frac{\tau_s D_{bubble}}{\gamma} \tag{1.3}$$

where D_{bubble} is the bubble diameter. In this case, the surface tension (γ) force is related to the bubble size, so that the bubble diameter, D_{bubble} is the appropriate length scale. Again, for this dimensionless group, the strength of the material was chosen to be represented by the shear strength. This dimensionless group assumes that the particles composing the waste are sufficiently small that the bubbles never finger between the particles. Also, as reported in Gauglitz et al. (1995), the shear and tensile strengths of bubbly simulants decrease with increasing gas bubble content, a detail this simple analysis neglects.

The physical and chemical properties of Hanford tank waste vary greatly, but the waste has been classified both in broad characteristic groups and also in great detail. From the broad point of view, SST waste is typically classified as sludge, saltcake, or supernatant liquid (Hanlon 1997). Hanlon describes sludges as solids (insoluble) that were formed (precipitated) during sodium hydroxide additions to the waste. Sludges typically have very small particle sizes and are typically described as clay-like and plastic materials. Saltcake waste resulted from crystallization and precipitation after concentration of liquid waste and is composed of precipitated salt crystals. Generally, salt cake waste has a noticeable particulate character. Double-shell tank waste also has a range of physical properties, and the waste is also grouped into general waste types (Hanlon

1995). Often the physical behavior of some DST and SST wastes are described as clay- or sludge-like, although the chemical constituents do not conform to the standard definition.

In addition to the specific studies of bubble retention in Hanford wastes noted above, the general character of the bubble retention mechanisms has been described in the literature, although the associated applications are quite different from gas-bubble retention in waste tanks. Chhabra (1993) gives an extensive general review of bubbles in non-Newtonian fluids and discusses the specific situation of spheres (bubbles) retained by the strength of a fluid possessing a yield stress (Chhabra 1993; Chhabra and Uhlherr 1986). Dullien (1992) provides a general discussion of the capillary behavior of nonwetting fluids (bubbles) in particulate materials and provides a specific review of the mechanics and literature on capillary trapping.

1.4 Role of the Bubble Size Distribution on Retention Mechanisms

The size of retained bubbles and the distribution of bubble sizes is expected to vary over time. As the waste generates gas, existing bubbles grow, small new bubbles may nucleate, or the additional gas may escape via a release mechanism. Nucleation of new small bubbles slows, or perhaps stops, after a sufficient bubble population exists to deplete the surrounding liquid of dissolved gas by diffusion. In addition to these mechanisms, the process of Ostwald ripening causes smaller bubbles to shrink and larger bubbles to grow (Shaw 1980). The typical size of retained bubbles can be estimated from visual images of retained bubbles in actual waste in both laboratory experiments (Gauglitz et al. 1996; Bredt and Tingey 1996) and from visual images of dimples (presumably from bubbles) in extruded actual waste samples (Meyer et al. 1997). However, there have been no attempts to determine the distribution of bubble sizes.

All these phenomena will tend to cause the number and size of the larger bubbles to increase. Because larger bubbles have a greater buoyant force and are more likely to be released, the slow aging of bubbles may be an important step in providing a mechanism of slowly releasing gas. It is important to note that the classification of bubble retention mechanisms has not changed by considering a distribution of bubble sizes; instead, the distribution suggests that a few larger bubbles may exist and be released more readily. In the previous actual waste experiments (Gauglitz et al. 1996), the bubbles were created over a few hours, which is quite rapid compared with changes in the tanks that occur over months to years. If these laboratory experiments were conducted more slowly, the results should show a more realistic bubble size distribution, although the small size-scale of the experiment will exclude creation of bubbles larger than a few centimeters.

2.0 Actual Waste Samples

Gas retention tests described in this report were conducted using samples from waste Tanks AW-101 and AN-103. These actual waste samples were selected for testing based on a priority ranking that included both technical significance to the Flammable Gas Project and sample availability.[a] Previous studies have investigated bubble retention in DSTs SY-103 and SY-101, which contain complex concentrate (CC) wastes; retention has also been studied in waste samples from SST S-102, which contains double-shell slurry feed (DSSF) waste (Bredt et al. 1995; Bredt and Tingey 1996; Gauglitz et al. 1996; Hanlon 1997). AN-103 was selected because its double-shell slurry (DSS) waste type (Hanlon 1997) is different from the previously tested complex concentrate wastes. This tank also has 10.7% retained gas, based on retained gas sampler (RGS) and void fraction instrument (VFI) data (Meyer et al. 1997), the highest gas content for all of the DSTs on the Flammable Gas Watch List (FGWL). Even more interestingly, the GREs in AN-103 have the smallest release fraction of all the DSTs on the FGWL (Meyer et al. 1997). AW-101 was also selected for testing because its DSSF waste type (Hanlon 1997) is different from the complex concentrate and DSS wastes investigated in other samples. AW-101 was actually an alternate for SST S-106,[a] but waste samples from S-106 were not available when testing began.

Table 2.1 lists the samples used. Samples from Tank AW-101 were collected during the Core 132 and 139 sample events between February and May 1996 and delivered to PNNL's 325A hot cells between August and December 1996. Samples from Tank AN-103 were collected during the Core 166 and 167 sample events during September 1996. The liquid composite from AN-103 was delivered to PNNL's 325A hot cells in February 1997, and the solid samples were delivered in March 1997.

2.1 Tank AW-101

Tank AW-101 is a double-shell underground waste tank located in the Hanford 200 East Area. This tank contains about 4.26×10^6 L (1,125 kgal) of waste, 3.10×10^6 L (819 kgal) of liquid and 1.16×10^6 L (306 kgal) of solids, with a total waste height of 1,040 cm (409 in.) (Hanlon 1997). The waste is classified as DSSF, which is concentrated evaporator waste that is not saturated in sodium aluminate. This tank is currently on the FGWL because of observed level fluctuations (Sathyanarayana 1994).

Tank AW-101 was put into active service in July 1980. A detailed fill history for this tank has been compiled by Brager (1994). While the tank received several waste types including dilute noncomplexed waste, flush water, dilute phosphate waste, dilute sulfate waste, concentrated complexed waste, 300 and 400 Area laboratory wastes, salt-well liquid, as well as other smaller waste streams, the tank was almost completely drained in 1986. The waste currently stored in AW-101 resulted primarily from a transfer of 242-A evaporator waste in May 1986. The evaporator waste contained noncomplexed plutonium-uranium extraction waste from AW-102 as well as other wastes from Tanks AW-104 and AW-106. Before their transfer to AW-101, the 242-A evaporator concentrated these wastes until they were nearly saturated in sodium aluminate.

(a) In a September 2, 1996 memorandum from PA Gauglitz to JD Johnson entitled, "Prioritization of Tanks for Gas-Bubble Retention Studies," the results of two group discussions focusing on prioritizing waste samples for bubble retention testing and the basis for this prioritization are discussed.

Table 2.1. Samples Received for Gas Retention Testing

Tank	222-S ID	Jar #	Core	Segment	Location within Segment	Shear History
AW-101	S96T001936	9439	132	20	NA	Undisturbed
AW-101	S96T001939	9713	132	22	NA	Undisturbed
AW-101	S96T002477	10005	139	2	NA	Undisturbed
AW-101	S96T003553	10533	139	17R	Lower half	Mixed
AW-101	S96T003548	10531	139	17R	Upper half	Mixed
AW-101	S96T003559	10237	139	19	NA	Undisturbed
AW-101	S96T003562	10537	139	19	Lower half	Mixed
AW-101	S96T003569	10535	139	19	Upper half	Mixed
AW-101	S96T003574	10234	139	21	NA	Undisturbed
AW-101	S96T003576	10541	139	21	Lower half	Mixed
AW-101	S96T003583	10539	139	21	Upper half	Mixed
AN-103	S96T005989		166	3-4, 6-12	Drainable liquid	Mixed
AN-103	S97T000197	197	167	13	NA	NA
AN-103	S97T000198	198	167	13	NA	NA
AN-103	S97T000199	199	167	13	NA	NA
AN-103	S97T000200	200	167	13	NA	NA

Tank AW-101 was core-sampled in 1987, grab samples were collected in 1990, auger samples were collected in 1995, and two additional core samples were collected in 1996. The core samples collected in 1996 were used in the testing reported here. These last two core samples are referred to as Cores 132 and 139; each consists of 22 segments 19 inches long. Results from these core samples suggest the tank has three layers, a crust on top, a convective liquid layer beneath the crust, and a nonconvective layer with high solids content under the convective layer. The crust layer was contained in the top two segments; the convective layer was contained in segments 3 through 16. Segment 17 contained both convective and nonconvective material, and segments 17 through 22 contained nonconvective material.

Figure 2.1 presents the temperature and gas fraction profiles for Tank AW-101 (reproduced from Shekarriz et al. 1997, Figure 4.31). The waste in AW-101 has a total height of 1040 cm. The temperature profile shows a thermally nonconvective layer extending from the bottom of the tank to a height of 280 cm, with a thermally convective layer above. The convective layer has a temperature range of 38 to 42°C (101 to 107°F), as seen in both riser 4A and riser 15A. The temperature profile for the nonconvective layer shows a maximum temperature of approximately 43°C (110°F) with a minimum near 35°C (95°F). The samples used in these tests were taken from segments 19, 21 and 22. This material originated from an elevation between approximately 0 and 190 cm below riser 21A. Based on the temperature profile and the need to select one representative tank temperature, gas retention testing was conducted at the ambient cell temperature of 33–37°C (91–99°F).

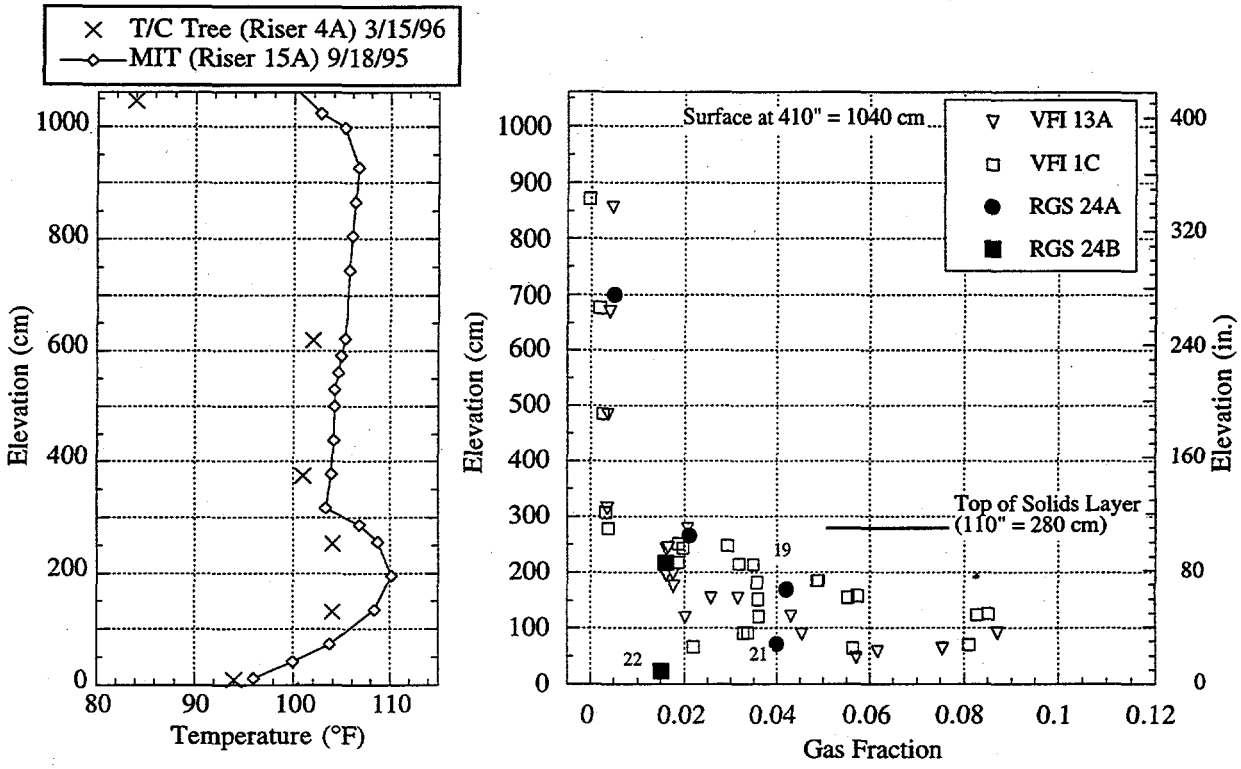

Figure 2.1. Temperature and Gas Fraction Profiles in Tank AW-101

The gas fraction profile in Figure 2.1 also shows the convective and nonconvective layering in Tank AW-101. Both the VFI and RGS show a significant gas retention in the waste below 280 cm. Above 280 cm, in the convective liquid, there is essentially no gas bubble retention. Below 280 cm, in the nonconvective solids, gas is retained with a maximum gas fraction of approximately 0.09 between 50 and 150 cm.

2.2 Tank AN-103

Tank AN-103 is a double-shell underground waste tank located in the Hanford 200 East Area. This tank contains about 3.62×10^6 L (955 kgal) of waste, 2.06×10^6 L (545 kgal) of liquid and 1.55×10^6 L (410 kgal) of solids, with a total waste height of 881 cm (347 in.) (Hanlon 1997). The waste is classified as DSS, which is concentrated evaporator waste that is saturated in sodium aluminate; this waste is more concentrated than DSSF.

A fill history for Tank AN-103 has been compiled by Brager (1994), and a more detailed history is being prepared[(a)] for inclusion in the AN-103 Tank Characterization Report. In general, Tank AN-103 received some of its waste from salt-well pumping of SSTs, but most of the tank contents were received from evaporator campaigns in 1984 and one in 1986.

(a) Document being prepared by NE Wilkins, Lockheed Martin Hanford Corporation, Richland, Washington, as noted in a personal communication.

Tank AN-103 was put into active service in December 1982. The tank was almost completely emptied in January 1983. From then until January 1984 the tank received 9.62×10^5 L (254 kgal) of dilute noncomplexed waste from laboratories in the 300 and 400 Areas, and 2.46×10^6 L (650 kgal) of dilute noncomplexed waste from salt-well pumping of several SSTs. In January 1984 the tank contents were removed, mixed with other waste, and concentrated. Approximately 3.41×10^6 L (900 kgal) of the concentrated slurry were returned to AN-103. An additional 7.57×10^5 L (200 kgal) of concentrated slurry was transferred to AN-103 in September 1984. In November 1984, 3.71×10^6 L (980 kgal) were transferred out of AN-103 to the evaporators, and in December, 2.99×10^6 L (790 kgal) of evaporated slurry were added back to the tank. In 1986, 2.65×10^6 L (700 kgal) were transferred out of AN-103 to the evaporators along with waste from AW-104, and 2.54×10^6 L (670 kgal) of the evaporated slurry were returned to Tank AN-103.

One core sample was collected from Tank AN-103 in December 1986, and two core samples were collected in September 1996. Materials from the 1996 core samples were used in the gas retention work reported here; these two core samples are referred to as Cores 166 and 167. Core 166 was taken from riser 12A, and Core 167 was taken from riser 21A. Results from these core samples suggest the tank has three layers, a crust on top, a convective liquid layer beneath the crust, and a nonconvective layer with high solids content under the convective layer. Cores 166 consisted of 19 segments, and Core 167 consisted of 18 segments. The first segment in both cores contained crust material. In Core 167, segments 2 through 11 contained convective material, and segments 12 through 18 contained nonconvective material. No information could be found on the contents of segment 2 of Core 166; however, segments 3 through 12 contained convective material, and segments 13 through 19 contained nonconvective material.

The nonconvective layer samples used in this testing originated from a failed RGS system test. The RGS system collects samples in a gas-tight stainless steel sampler. In the case of segment 13 from Core 167, the sampler failed to maintain a gas-tight seal, and therefore was of no use to the RGS project. However, since the sampler did not leak liquid, it was determined that the sample integrity was acceptable for the current task. This sample was not exposed to the mixing and evacuation that occur with the RGS measurements, although it is possible that the sample was hand-mixed prior to shipment to PNNL.

Figure 2.2 presents the temperature and gas fraction profiles for Tank AN-103 (reproduced from Shekarriz et al. 1997, Figure 4.35). The waste in AN-103 has a total height of 880 cm. The temperature profile shows a thermally nonconvective layer extending from the bottom of the tank to a height of 380 cm with a thermally convective layer above. The convective layer has an approximate temperature of 42°C (107°F) as seen in both riser 4A and riser 15A. The temperature profile for the nonconvective layer show a maximum of approximately 45°C (113°F) with a minimum near 36°C (97°F). The nonconvective layers used in the testing reported here were taken from Core 167, segment 13. This material originated from an elevation between approximately 260 and 310 cm. Based on the temperature profile, gas retention testing was conducted at 42°C (108°F).

The gas fraction profile in Figure 2.2 also shows the convective and nonconvective layering in Tank AN-103. Both the VFI and RGS show significant gas retention in the waste below 380 cm. Above 380 cm, in the convective liquid, there is essentially no gas bubble retention. Below 380 cm, in the nonconvective solids, gas is retained with a maximum gas fraction of approximately 0.16 between 250 and 350 cm.

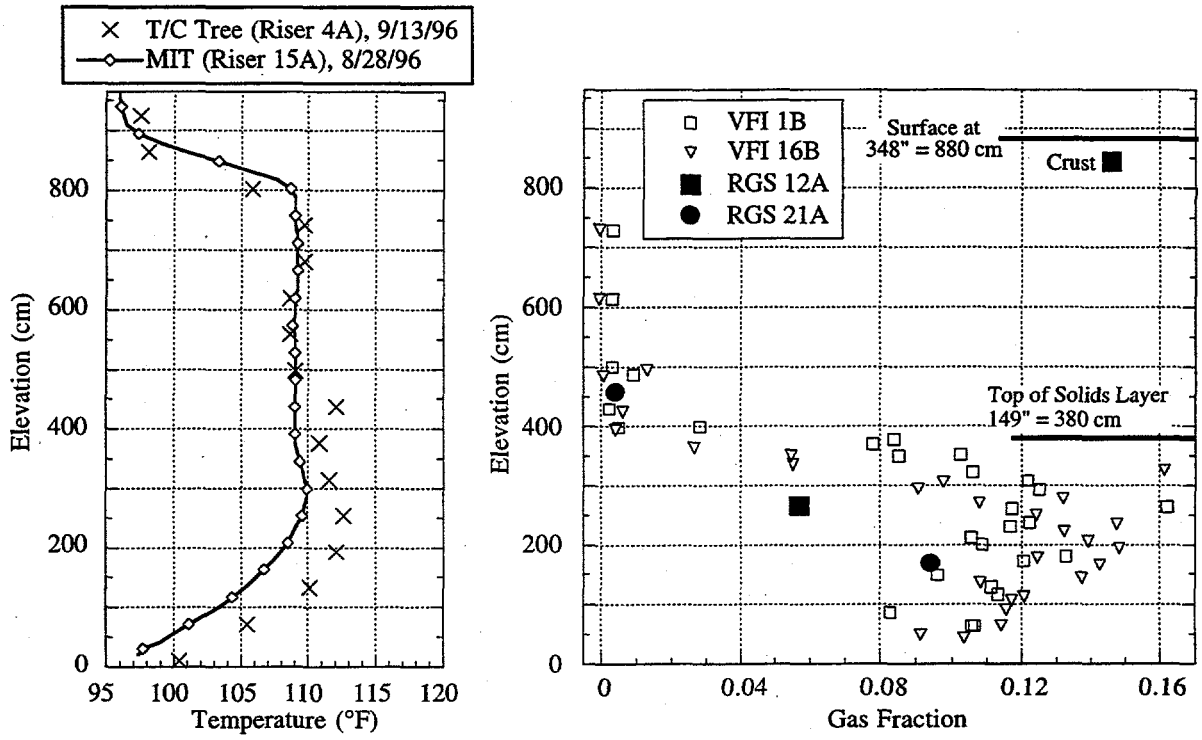

Figure 2.2. Temperature and Gas Fraction Profiles in Tank AN-103

3.0 Experimental

The experimental section describes the instrumentation used to measure the shear strengths of waste samples and the apparatus, approach, and methods applied in gas retention experiments.

3.1 Shear Strength Measurements

The shear strength (τ_s) of several samples from Tanks AN-103 and AW-101 was measured using a Haake M5 measuring head electronically remoted for in-cell operation and a shear vane manufactured at PNNL. Not all samples used in the composites contained enough material to perform the measurement, and several samples only contained enough for one. Technical Procedure PNL-ALO-501 was used to perform these measurements, which were made at the ambient cell temperature of 32°C. Shear strength (τ_s) is a measure of the force required to cause shear failure along a cylindrical surface created by the shear vane in a soft solid material (Nguyen and Boger 1992). Because this property is dependent upon sample history, the shear strength of the samples was measured in the original jars shipped to PNNL before mixing and after leaving them undisturbed for a minimum of two weeks. The shear vane, with dimensions H_v = 1.582 cm (height) and D_v = 0.800 cm (diameter), was placed in the sample and rotated at 0.6 rpm. The stress required to maintain the rotational speed was recorded as a function of time. The shear strength, τ_s, was then calculated according to Equation (3.1), where 4.9 x 10^5 is the maximum torque of the M5 head, $\%\tau/100$ is the fraction of the total torque that was set as full scale on the shear stress plot, and S_τ is the fraction of full scale recorded on the plot. For example, if the full scale on the plot was set to 25% and the shear strength was measured at 15% on the plot, then the total torque (the numerator of Equation 3.1) would be {(25/100) x 0.15 x 4.90 x 10^5} dyne•cm. Shear strength in the SI unit of Pascals (Pa; N/m^2) and as reported here are a factor of 10 less than the alternate units, $dyne/cm^2$.

$$\tau_s = \frac{4.90 \times 10^5 \frac{\%\tau}{100} S_\tau}{\frac{\pi H_v D_v^2}{2} + \frac{\pi D_v^3}{6}} \qquad (3.1)$$

3.2 Gas Retention Measurements

The apparatus for conducting the controlled pressure gas retention experiments, the composition of the waste samples used, and the experimental methods and approach are described in the following sections. Electronic pressure control is an important new feature developed for measuring gas retention in actual waste samples by evacuation. This advance allows for the application of controlled evacuations, and the duration of the experiment can be extended from a few hours to several days or more.

3.2.1 Apparatus

The gas retention experimental apparatus consists of three primary components: the leak-tight sample vessels, the vacuum pump and pressure control system, and the video system for recording visual observations. The components, integration, and application of these major systems are specified below.

3.2.1.1 Sample Vessels

Two sets of four vessels were constructed, one set with water jackets for temperature control and the other without. Each set consists of identical primary vessels constructed from nominally 2.54 cm (1 in.) inside diameter (ID) by 3.18 cm (1.25 in.) outside diameter (OD) acrylic tubes; they are ruled every 0.5 cm along their 25-cm length, and heights in millimeters are etched in the vessels each 1 cm. Photographs of the vessels, with and without water jackets, are shown in Figure 3.1, and the detail of the vessel graduations is depicted in Figure 3.2. Each vessel was calibrated for volume as a function of height using a water addition method, and the average height-specific volume is approximately 4.9 mL/cm. For waste sample analyses, the individual vessel calibration data were applied. The AW-101 gas retention experiments were conducted at cell temperature (~33–37°C) using unjacketed vessels such as the one on the right side of the figure. O-rings on the stainless steel top provide the seal on the inner surface of the vessel, and the fitting welded to the top connects to the vacuum system.

Figure 3.1 also shows a water jacketed vessel (without a stainless steel top). The temperature controlled sample vessels are identical to the unjacketed vessels except for a collar glued to the neck of the vessel. The double o-rings on the collar seal the outside of the vessel in the water jacket. The acrylic water jackets are square 5.1 cm (2.0 in.) inside diameter (ID) units,

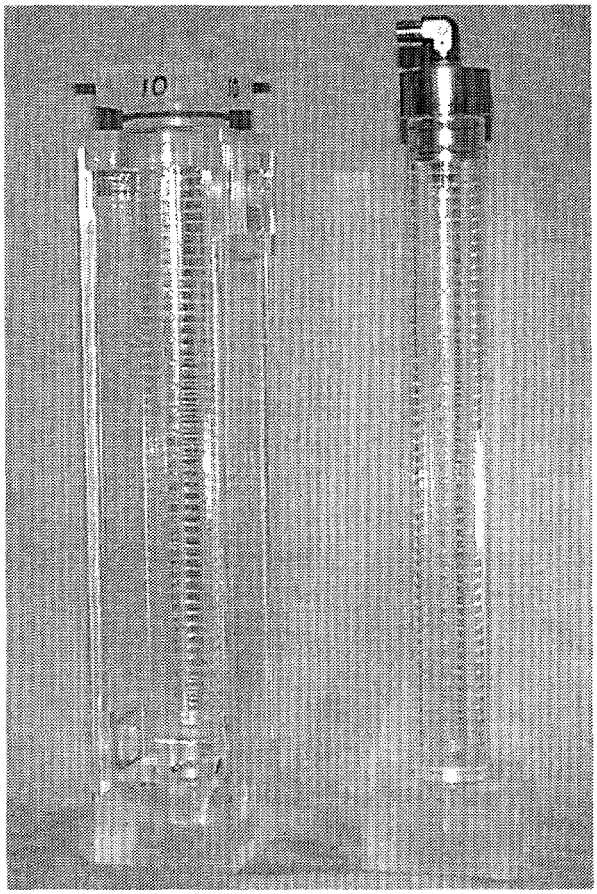

Figure 3.1. Gas Retention Vessels with Temperature Control Water Jacket (left) and Unjacketed (right). A stainless steel top shown only on the unjacketed vessel is used with both vessels.

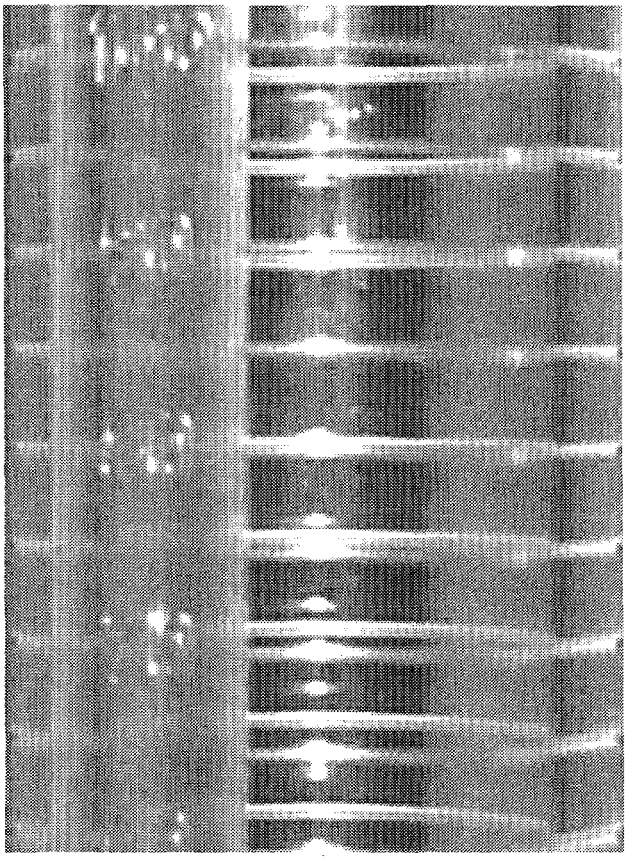

Figure 3.2. Photograph of Gas Retention Vessel Detail. Lines are etched every 0.5 cm.

which are threaded near the top and bottom of opposite faces to accept tube fittings for flow from the heated water bath. Four water jackets were connected in series and held securely in a specially designed stainless steel vessel holder. Type-K thermocouples calibrated to ± 0.5°C were located on the inlet and outlet water lines of the water jacket series, and typically the difference in feed and effluent water temperatures was less than 0.5°C. The four AN-103 samples were maintained at a representative tank temperature of 42 ± 1°C by flowing deionized water from the in-cell heat exchanger loop through the acrylic water jackets that surrounded the individual vessels. The water was pumped in the loop by a positive displacement pump flowing at approximately 3–4 L/min. The temperature in the recirculation loop in turn was controlled by a heated recirculating water bath (Neslab model RTE-EDD) located outside the hot cell.

3.2.1.2 Vacuum System and Pressure Control

A schematic of the vacuum control system for sample evacuations as set up in the 325 Building hot cell facility is shown in Figure 3.3. It consists of a Welch vacuum pump (gerotor type, model 8890-A), with a nominal pumping speed of 28 L/minute, and associated components. The gas flow rate through the 0.64 cm (1/4 in.) OD vacuum line is restricted by a needle valve (4.4 mm orifice) near the pump. The draw from the sample vessel is electronically controlled through an MKS Instruments model 248A control valve with a 500 sccm (0.5 L/min) N_2 flow rate range. A micrometering needle valve (0.81 mm orifice) is teed into the vacuum line between the control valve and the vessel to provide a slow constant bleed to the working control valve. Gas evacuated from the sample being tested is passed through a HEPA filter before contacting the control valve located outside the cell, and the pump exhaust is returned to the cell for added safety.

The electronic control valve is a key component of the pressure control system. The valve opening and the resulting evacuation of gas from the sample vessel are automatically regulated by a pressure control system. The signal applied to the control valve by the MKS model 250D proportional-integral-derivative (PID) pressure controller/readout is a function of the measured system and the set point pressures. The 0–1000-mm Hg absolute pressure transducer, an MKS model 621C operated at cell temperature, was located ~60 cm from a retention vessel during an evacuation and was connected to the O-ring sealed stainless steel top (see Figure 3.1) of the vessel by 0.25 in. OD tubing. The transducer outputs a 0-10-V signal, proportional to the pressure, to the pressure controller/readout. The signal is also sent to a personal computer data acquisition system for display and storage. This system consists of National Instruments data acquisition hardware and a LabView software interface. The system is also used to output pressure set point control voltages (0-5 V full scale) back to the 250D controller/readout.

3.2.1.3 Video System

Before and during an evacuation experiment, images of the waste sample were recorded for post-experimental analysis. In any given experiment, two video cameras were operated simultaneously. One camera was positioned to view both the liquid/solid and air/liquid interfaces, and these images were used to obtain the waste sample height information used to determine the magnitude of gas bubble retention. The second camera was typically located in the middle of the solids layer and focused on a 1–2 cm vertical segment of sample. These images provide detailed information on bubble shapes and the mechanisms of gas bubble retention. Three video cameras were used in the course of experimentation, though only two were employed in any given gas retention experiment. In some tests, a Rees Instruments R90 Series MK2 radiation-hardened color zoom camera, which is dedicated to A-cell of the 325 hot cell facility, was used to obtain waste level measurements. Alternatively, an Imaging & Sensing Technology 200 M, model ETV-1258 radiation-hardened black and white zoom camera was used to view sample levels. If the Rees color radiation-hardened camera was used for this purpose, the black and white camera was used for close-up sample images. When the black and white camera was used to view waste levels, a Sekai ISC-800A color zoom video camera was employed for close-up work.

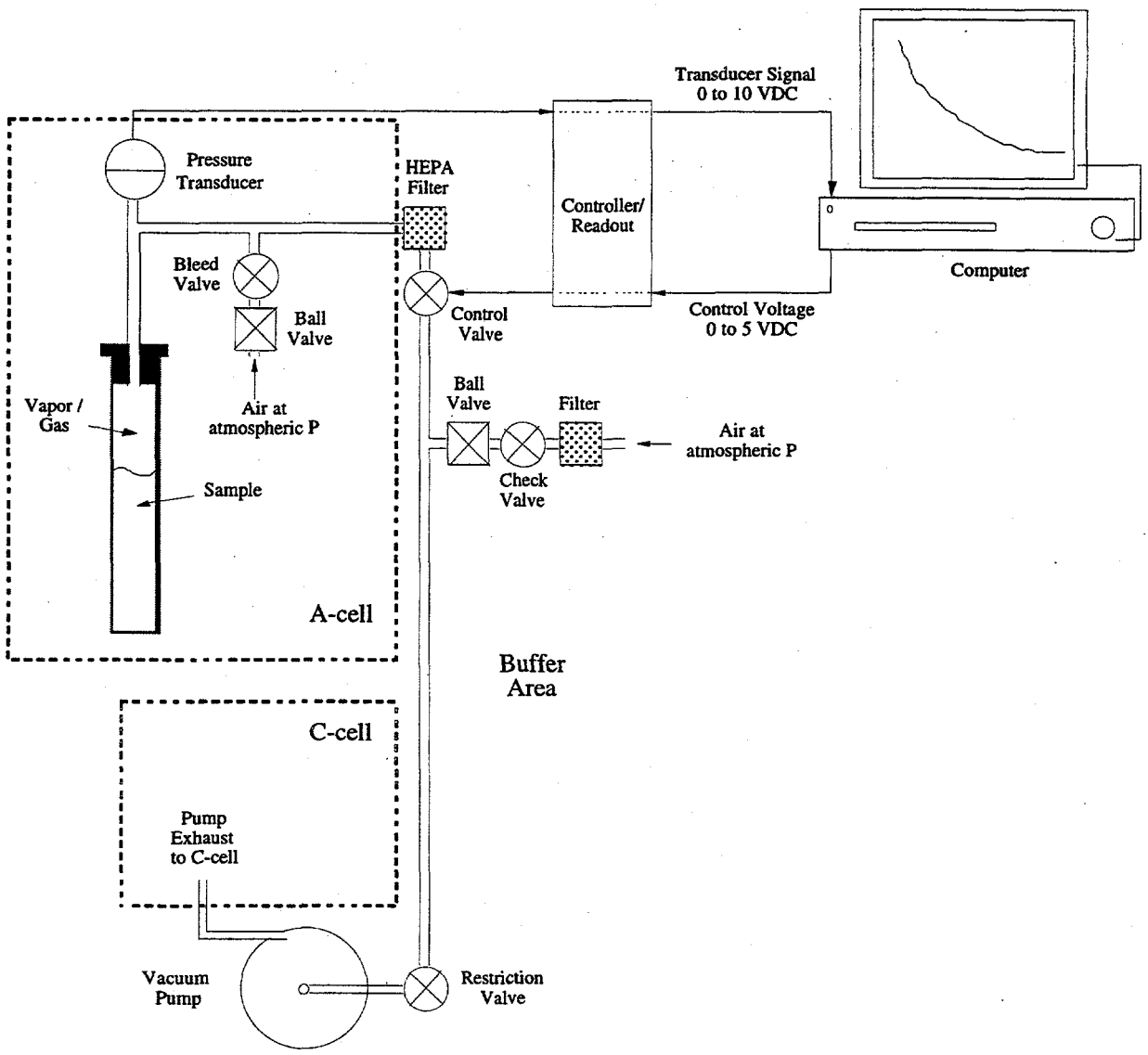

Figure 3.3. Pump and Vacuum Pressure Control System

Camera signals were recorded by two S-VHS format time-lapse video cassette recorders (Mitsubishi HS-S5600 and Panasonic AG-6760). Depending on the length of the experiment, the video recorders were operated in 2, 24, or 72 hour mode and the signals recorded on a standard 120-minute S-VHS tape. A date and time stamp was recorded simultaneously, and before each experiment the time was synchronized to within one second of the data acquisition system time. The camera signals were also sent to two Sony HR Trinitron monitors (model PVM-1353MD) for real-time viewing. Post-experimentally, still frame images from the video tape records were captured and printed with a Sony UP-5600 MD color video printer.

3.2.2 Waste Sample Composites

Tanks AW-101 and AN-103 actual wastes were used in the gas retention experiments. Eight retention experiments were completed, four samples from each of the two tanks. Because one of the primary goals was to probe the effect of evacuation rate on retention and release

behavior, it was important to have a relatively homogeneous sample for testing. To this end, a single AN-103 composite was prepared. For AW-101 samples, two composites were mixed. The individual waste samples used in composite preparation and the prepared composites were held at the ambient PNNL hot cell temperature (typically 32-37°C) prior to and during preparation. After transfer to the retention test vessels, the AN-103 samples were temperature controlled at 42 ± 1°C and the AW-101 samples were left at the ambient cell temperature.

3.2.2.1 AW-101 Composites

Two composite samples were prepared from six individual Tank AW-101 core samples. The jar identification, core string and segment numbers, location in the segment or sample history, and masses of individual waste samples added to the composites are shown in Table 3.1. The composite of the higher segment (19) samples have been identified as "AW-101 Composite 1," and the lower segment (21 and 22) composite is referred to as "AW-101 Composite 2." The composites were mixed by gently shaking, rocking, and inverting the sealed ~250 mL glass sample jars before their contents were transferred to individual retention vessels.

Table 3.1. Composition of AW-101 Composites

Composite ID	Jar Number	Core	Segment	Location / History	Mass Added, g
AW-101 Composite 1	10535	139	19	Upper Half	87.7
AW-101 Composite 1	10537	139	19	Lower Half	86.9
AW-101 Composite 1	10237	139	19	Undisturbed	97.5
AW-101 Composite 2	10234	139	21	Undisturbed	94.2
AW-101 Composite 2	10541	139	21	Lower Half	74.9
AW-101 Composite 2	9713	132	22	Lower Half	48.9

3.2.2.2 AN-103 Composite

A single composite sample was prepared from six individual Tank AN-103 sample jars, four containing solids and two containing convective layer liquid samples. The jar identification, core string and segment numbers, location in the segment or sample history, and masses of individual waste samples added to the composites are shown in Table 3.2. The composite is referred to as "AN-103 Composite" and was mixed by gently shaking, rocking, and inverting the sealed ~500 mL glass sample jar before and between transfers to individual retention vessels.

Table 3.2. Composition of AN-103 Composite

Jar Number	Core	Segment	History	Mass Added, g
197	167	13	RGS	96.9
198	167	13	RGS	96.4
199	167	13	RGS	100.7
200	167	13	RGS	25.6
12040	166		Drainable liquid composite	77.2
12040A	166		Drainable liquid Composite	57.8

3.2.3 Approach and Methods

Preparation of the waste samples for retention experiments, the approach used for pressure control in the experiments, and the methods used to evaluate the experimental results are described below.

3.2.3.1 Sample Loading, Settling, and Irradiation

Composited waste samples (see Section 3.2.2) were gently mixed by shaking, rocking, and inverting to homogenize, transferred to the retention vessels, weighed, and allowed to settle for approximately 14 days. To promote gas generation within the waste prior to evacuation, the settled samples were irradiated with a 2,200-Ci encapsulated and stainless steel jacketed cesium (^{137}Cs) source for four days. The samples were rotated 90° every 24 hours during the irradiation to provide a more uniform exposure. Little disturbance of and no gas release from the settled waste was observed during sample rotations. The horizontal center-to-center distance from the source to each of the four vessels was 3 in. (7.6 cm). At this distance, the estimated average dose rate is approximately 76 kR/hr, giving a total sample dose of about 7 MR in the four-day irradiation.[(a)]

3.2.3.2 Density Measurements and Buoyancy

All masses measured during vessel calibration and loading were obtained from calibrated balances accurate to the nearest 0.01 g or better. Supernatant liquid densities (ρ_l) were determined by measuring the volume and mass of liquid placed in a 10±0.1 mL graduated cylinder following a standard procedure.[(b)] The mass of supernatant liquid covering the solids layer of a waste sample in a retention vessel is estimated from its density and the observed volume of free liquid (V_l):

$$m_l = V_l \rho_l \tag{3.2}$$

The mass contained in the nonconvective solids layer is then computed as the difference from the total mass (m_{tot}) of added sample:

$$m_s = m_{tot} - m_l \tag{3.3}$$

Subsequently, the density of the solids layer is calculated from its estimated mass and the observed nonconvective solids layer volume (V_s) as follows.

$$\rho_s = \frac{m_s}{V_s} = \frac{m_{tot} - V_l \rho_l}{V_s} \tag{3.4}$$

A settled solids layer in a waste sample is expected to become buoyant in a surrounding liquid when sufficient gas is retained within the solids layer to reduce its density to that of the liquid. This is the predicted neutral buoyancy point, when a buoyant displacement (rollover) is

---

(a) For Tank 241-SY-103, Bryan et al. report a total (gamma and beta) dose rate of 469 R/hr in the nonconvective layer. Thus a 7 MR dose corresponds to 1.7 SY-103 tank years exposure (Bryan SA, CM King, LR Pederson, and SV Forbes, 1996, *Thermal and Radiolytic Gas Generation from Tank 241-SY-103 Waste: Progress Report*, letter report TWSFG96.17, Pacific Northwest National Laboratory, Richland, Washington).

(b) PNNL Technical Procedure PNL-ALO-501, "Laboratory Procedure for Measurement of Physical and Rheological Properties of Solutions, Slurries and Sludges," Section 5.0, "Procedure for Determination of Vol%, Wt% and Densities of Centrifuge Solids and Supernate," was used.

imminent. However, for buoyant displacement to occur, retained gas volumes greater than this neutral buoyancy gas fraction are required to overcome waste strength and wall effects. Meyer et al. (1997) discuss, from a theoretical basis, how waste strength and wall effects can hinder a buoyant rise at neutral buoyancy, and Stewart et al. (1996) have observed the phenomenon experimentally. In several experiments reported here, the volume of retained gas was greater than necessary to render the sample neutrally buoyant. In these cases, the solids layer density was less than the liquid density, and the magnitude of the difference in these values is representative of a density deficit in the solids layer or a density excess in the liquid layer. This density difference is used to calculate the effective force restraining buoyancy due to the combined waste strength and wall effects.

3.2.3.3 Gas Fraction Definitions and Gas Release Detection

The most accurately determined gas fraction data in these experiments result from the measured volume growth during an evacuation. The change in total sample volume from atmospheric pressure to some reduced pressure is the growth volume of retained gas. Because we observe negligible gas retention in the liquid layer, the volume change results from gas retained within the non-convective solids layer. The liquid growth volume accounts for both particle-displacing and interstitial liquid-displacing bubbles within the solids fraction. The solids layer growth gas fraction is simply the growth volume divided by the volume of the bubble-laden nonconvective layer at the same instant. This is equally represented in terms of a gas volume percentage. The maximum growth gas fraction reflects the peak sample growth, and the predicted neutral buoyancy growth gas fraction is calculated from the estimated growth volume necessary to render the solids layer buoyant.

The growth gas fraction results are not the absolute gas fractions within the sample, because the gas initially present within the solids layer is neglected. In previous work, Gauglitz et. al. (1996) applied a method based on the ideal gas law to estimate the volume of retained gas initially present in the sample. In this technique, the growth volumes early in an evacuation experiment are plotted against the inverse pressure and the slope of the line ($m = nRT$) is used to calculate the initial volume of gas retained ($V_i = m/P_i$). The volumes estimated in this manner may over-account for the initial volume, as initially dissolved gases may contribute to the volume expansion resulting from sample evacuation. Therefore, this estimated initial gas volume is an upper bound. The initial gas volume method was used here, and any reported absolute gas fractions have been computed as the sum of initial and growth volumes divided by the bubble-laden solids volume.

The ideal gas law has also been applied to detect gas release from experimental samples (Gauglitz et. al. 1996). The ideal gas law relationship

$$V_2 = V_1 \frac{P_1}{P_2} \tag{3.5}$$

is employed. Strictly speaking, the volumes V_1 and V_2 are absolute gas volumes. Here, however, V_1 is defined as the growth volume at system pressure P_1, where the growth volume is the change in the retained gas volume from the start of evacuation. V_2 is the estimated growth volume when the pressure is adjusted from P_1 to P_2. If V_2 exceeds the measured growth volume, gas release is indicated. In subsequent steps, V_1 is reset to the current measured growth volume, and a new V_2 is estimated. Since the absolute volume of retained gas is not used in this calculation, the method cannot be used to calculate gas release volumes. It is only applied as a gas release indicator.

3.2.3.4 Application of Pressure Control

To attain a consistent sample growth rate in the course of an evacuation experiment, the set point pressure (P_{set}) was adjusted continually using a pressure program given by the following function

$$P_{set} = P_{init}\left(\frac{1}{1+t/t_{set}}\right) \tag{3.6}$$

where P_{init} is the initial set point pressure in mm Hg, typically set to 760 mm Hg, t_{set} is the first pressure half-life in minutes, and t is the elapsed time in minutes from the start of the pressure program. The parameter $_{tset}$ was set to approximately 10 minutes during standard short-term (2–3 hr) evacuations, and a value of 100 minutes or more was applied for longer-term (≥1 day) experiments.

The following development shows the expected linear growth in sample volume resulting from the pressure program Equation (3.6). Rearranging Equation (3.6) gives

$$\frac{P_{init}}{P_{set}} - 1 = \frac{t}{t_{set}} \tag{3.7}$$

Assuming ideal gas law behavior for the volume of retained gas within a waste sample during a gas retention evacuation experiment, one finds that the change in volume resulting from a pressure change gives a functional form identical to Equation (3.7)

$$\frac{P_i}{P_f} - 1 = \frac{\Delta V}{V_i} \tag{3.8}$$

where V_i is the initial volume of retained gas, and P_i and P_f are the measured initial and final pressures associated with a pressure change. If it is assumed that the initial set point and initial measured pressures are equal ($P_{init} = P_i$) and that the final measured pressure is at the set point pressure ($P_f = P_{set}$), then the bracketed terms in Equations (3.7) and (3.8) are identical. Substituting from Equation (3.7) into Equation (3.8) gives

$$\Delta V = V_i\left(\frac{t}{t_{set}}\right) \tag{3.9}$$

It is apparent that the change in volume is proportional to the elapsed time, and thus, when the pressure program Equation (3.9) is applied, linear growth in retained gas volume is expected if no gas is released and the ideal gas law holds.

Figure 3.4 shows the measured pressure and the inverse of the pressure as a function of elapsed time for an actual waste experiment. The pressure program parameters were P_{init} = 760 mm Hg and t_{set} = 12 minutes. Note the nearly linear response of the inverse pressure, particularly early in the experiment. At longer times and lower absolute pressures (<100 mm Hg), the linear inverse pressure is approximated by a series of small steps. The steps result from slight overshoots in the targeted pressure and the subsequent delay until the set point pressure falls below the system pressure. In this experiment, the effect was exacerbated by improper functioning of an in-cell bleed valve used to dampen the steps. Although not shown in the figure, the set point

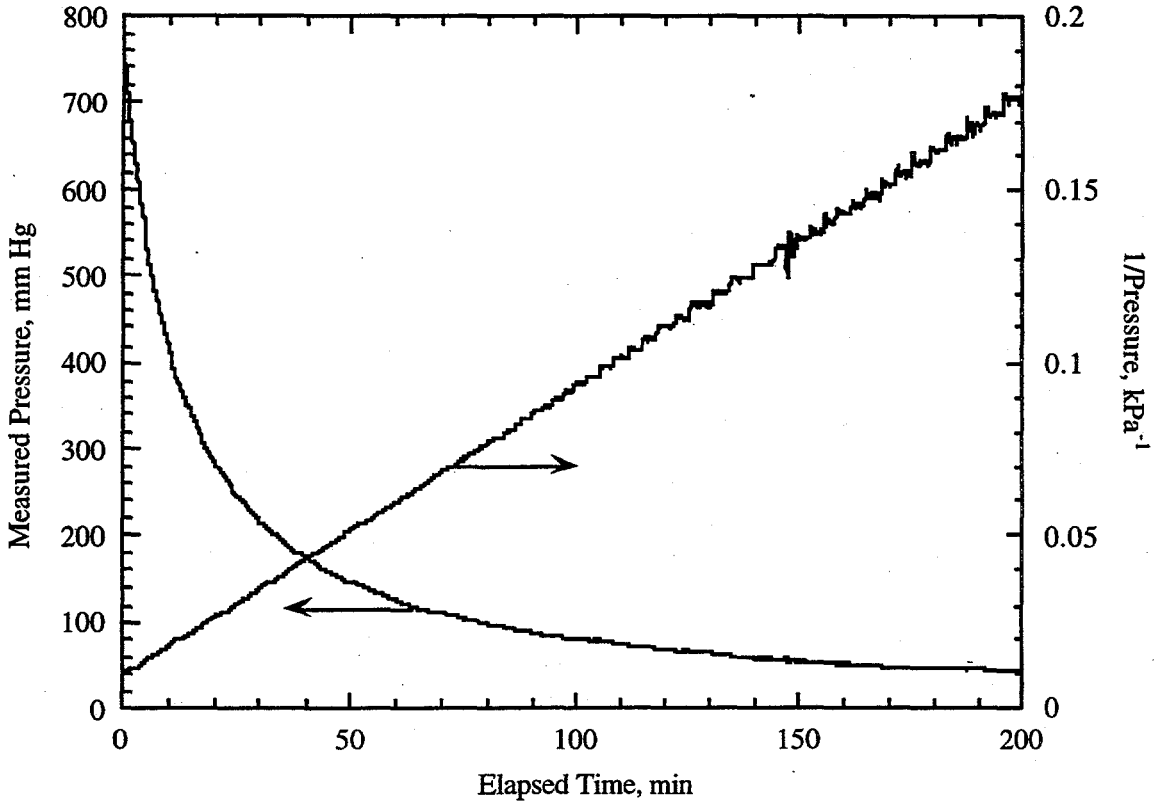

Figure 3.4. Application of a Typical Pressure Program and the Approximately Linear Time Dependence of the Measured Inverse Pressure

pressure program is linear and step free when plotted in this fashion. In Figure 3.4, the sudden decrease in the inverse pressure just before 150 minutes elapsed time corresponds to a moderate gas release from the waste sample.

4.0 Quantitative Results and Discussion

In this section quantitative results pertinent to the gas retention experiments on AW-101 and AN-103 waste types are discussed, and in Section 5 qualitative visual evidence of the retention and release mechanisms are presented. Throughout this analysis of the gas retention and release experiments, three primary parameters are investigated: 1) the effect of evacuation rate and experiment duration; 2) variations resulting from waste sample differences; and 3) the effects related to the presence or absence of a supernatant liquid layer. Quantitative results are presented from the studies for AW-101 in Section 4.2, and the details of AN-103 tests are described in Section 4.3. Maximum retained gas fractions above the neutral buoyancy point were measured in both AW-101 and AN-103 experiments when a supernatant liquid layer was present, and Section 4.4 relates these observations to the effects of waste/vessel wall interactions and waste strength. Quantitative results include shear strength measurements used to support our understanding of both the magnitude and mechanism of gas retention, and these are presented in Section 4.1.

4.1 Sample Shear Strengths

Selected samples from Tanks AW-101 and AN-103 and two AW-101 composites were analyzed for shear strength. Results from these analyses are listed in Table 4.1. Since the shear strength of a material can depend on its shear history, several of the samples from AW-101 were analyzed prior to any shearing; these samples are identified in Table 4.1 as undisturbed. With the exception of the shear induced during the tank core sampling and sampler extrusion process, the undisturbed samples have no significant shear history. The undisturbed samples have not been stirred, mixed, shaken, or homogenized. A group of homogenized samples from AW-101 were also analyzed for shear strength. The samples from Tank AN-103 may have been hand-mixed prior to shipment to PNNL but were left undisturbed for at least one month before analysis.

Table 4.1. Measured Shear Strengths for Samples from Tanks AW-101 and AN-103

Jar	Tank	Shear History	Shear Strength (Pa)
10237	AW-101	Undisturbed	4.8×10^2
10537	AW-101	Mixed	3.9×10^2
10535	AW-101	Mixed	2.1×10^3
10234	AW-101	Undisturbed	2.9×10^2
10541	AW-101	Mixed	1.3×10^3
10539	AW-101	Mixed	$<3 \times 10^2$
9713	AW-101	Undisturbed	1.6×10^3
10005	AW-101	Undisturbed	5.1×10^3
AW-101 Comp 1	AW-101	Mixed	$<3 \times 10^2$
AW-101 Comp 2	AW-101	Mixed	$<3 \times 10^2$
197	AN-103	NA	7.5×10^3
198	AN-103	NA	4.8×10^3
199	AN-103	NA	4.4×10^3

For most tank materials, the measured shear strength decreases after a sample has been mixed.[a] However, this is not indicated by the results in Table 4.1 for material from AW-101 prior to compositing. Three samples were measured from each of segments 19 and 21. These samples were either mixed material from the lower half of the segment, mixed material from the upper half of the segment, or undisturbed material from an unknown location within the segment. The shear strength of the undisturbed sample was not the highest in either segment; the upper half of segment 1 and the lower half of segment 21 had the highest shear strengths. It is likely that shear strength did not decrease with mixing because of the extended period these samples were allowed to rest before shear strength measurements were taken, approximately one year. During this one-year period it is possible that a significant regrowth in shear strength occurred. A second possibility is a lack of homogeneity within the segments. This is supported by the variation in results between the upper and lower half samples within the same segments.

The shear strengths of the two AW-101 composite samples prepared for gas retention tests were below the instrument detection limits. The shear strength technique is only semi-quantitative; the analyst must make a subjective identification of the point in the rheogram at which flow is observed. Based on the dimensions of the vane used in this analysis, a value of 300 Pa was determined to be the detection limit for these samples. These measurements were made only a few days after the composites were prepared, and the results indicate a lower bound on the strength for recently mixed material. The strength was apparently degraded as a result of the mixing in preparing the composites and is expected to increase with settling time.

From retained bubble shapes and gas release data, as presented in the following sections, the strengths of the settled bubble-laden AW-101 and AN-103 composites in the retention vessels were estimated to be on the order of 50 Pa. These values are much lower than the shear strengths presented in Table 4.1, which range from <300 Pa to 2100 Pa on the as-received AW-101 samples and from 4400 to 7500 Pa on the as-received AN-103 samples. In-tank ball rheometer data for these tanks indicate waste strengths that are generally lower than the results presented in Table 4.1. Meyer et al. (1997) report typical ball rheometer yield stresses of 142 ± 15 Pa for AN-103 and 159 ± 37 Pa for AW-101. These data are representative values selected from the full set of ball rheometer data, which varied from zero to greater than 900 Pa (Meyer et al. 1997).

The differences in strength results determined by the various methods, particularly shear vane and ball rheometer tests, is not unexpected (Heath 1987). These two tests measure distinct properties in the same material. Shear strength is determined from the peak torque required to rotate a shear vane at low shear rate in the undisturbed solid-like material. On the other hand, the ball rheometer method is a viscosity measuring technique in which the yield stress in a fluid is evaluated from measurements at a series of shear rates (ball velocities). A reported ball rheometer datum for the yield stress results from extrapolating calculated shear stresses to zero shear rate. In general, the shear strength is expected to be different, and greater, than the yield stress (Heath 1987). The discrepancy will be enhanced in materials where a considerable solid-like structure has developed prior to disturbance by a shearing force in a shear strength test. In the current studies, the relatively high shear strength results may relate to a higher degree of solids settling in the laboratory samples than in the actual tanks. Also, the shear strength data were obtained at the hot cell temperature, which is generally cooler than the actual tank temperatures, and, as a result, more crystallization of the shear strength samples may have occurred.

(a) Bredt, PR, JD Hudson, and JM Tingey. 1995. *Effects of Dilution on the Physical and chemical Properties of Tank 241-SY-103 Waste*. Letter Report PNL MIT 092995, Pacific Northwest Laboratory, Richland, Washington.

4.2 Maximum Gas Retention in AW-101 Samples

In this section the quantitative gas retention results for AW-101 samples are discussed. Four separate experiments were conducted, two on each of the two AW-101 composite samples. An experimental suite was selected to probe the maximum gas retention under a variety of conditions that are summarized in Table 4.2. In three of the experiments, a layer of supernatant liquid was present on the samples, and in this way the actual conditions in a DST were mimicked. In these gas retention-to-buoyancy (RB) experiments, it was observed that AW-101 waste composites retained gas up to and beyond the neutral buoyancy point, and the data are presented. In a fourth AW-101 experiment, the supernatant liquid was removed from the settled sample before gas retention was measured. This type of experiment is referred to as ultimate retention (UR) because it is expected that eliminating the possibility of buoyant gas release may ultimately allow more gas to be retained in the waste (Gauglitz et al. 1996). This was confirmed in the AW-101 experiments described below. An initial investigation into the effect of evacuation rate and experiment duration on gas retention in AW-101 samples showed little effect on maximum gas retention, but gas release was affected. These results are discussed here, and additional quantitative details for each AW-101 gas retention experiment are provided in Appendix A.

4.2.1 Effects of Experiment Duration

The experimental time frame of gas retention studies using sample evacuation as a means of accelerated gas volume growth is much more rapid than actual tank growth cycles (e.g., on the order of 100 days for Tank SY-101 [Meyer et al. 1997]). In previous studies using this technique (Rassat and Gauglitz 1995; Bredt et al. 1995; Bredt and Tingey 1996; Gauglitz et al. 1996), the samples were expanded from minimal to maximum gas fraction in a few hours or less. Through the use of a pressure control system, the range of practical growth rates is expanded from a few hours to several days or longer. Although there is no feasible limitation to the duration of an electronically controlled evacuation, practical factors (i.e., risk of power failure, sample dryout) limit the length of such an experiment. The effects of experiment duration (evacuation rate) on gas bubble retention in AW-101 and AN-103 waste types were studied. The AW-101 results are presented here, and the AN-103 results follow in Section 4.3.

The approximate length of the experiment and the pressure program parameters used to control the length of the AW-101 experiments are tabulated in Table 4.2. In several cases, two sets of pressure program parameters were applied because it was necessary to correct the initial evacuation rate during the course of the experiment. For example, in the first AW-101 Composite 1 test (vessel 1), approximately seven minutes into the evacuation, at a pressure of 391 mm Hg, the sample appeared to be growing too rapidly. Accordingly, the evacuation was stopped

Table 4.2. Experimental Conditions Applied in AW-101 Experiments

Sample	Type	Vessel	Duration (approx.)	Initial P_{init}, mm Hg	Initial t_{set}, min.	Final P_{init}, mm Hg	Final t_{set}, min.
AW-101 Composite 1	RB	1	2 hours	760	8	394	32
AW-101 Composite 1	RB	2	1 day	760	190	93	420
AW-101 Composite 2	RB	3	1/2 day	760	120	NA	NA
AW-101 Composite 2	UR	4	1 day	760	120	55	600

briefly (~five minutes) and the system pressure held nearly constant while the pressure program was revised. Using the combination of initial and final parameter values (initial: P_{init} = 760 mm Hg, t_{set} = 8 min; revised: P_{init} = 394 mm Hg, t_{set} = 32 min), approximately 90 minutes total evacuation time was required to reach the maximum retention at a pressure of 109 mm Hg. If the parameters had not been reset, we estimated that the maximum retention point would have been attained in less than 50 minutes. In the other AW-101 experiments, in which two sets of pressure program parameters are shown in Table 4.2, the final parameters were selected to expedite the experiments. In the other AW-101 Composite 1 sample (vessel 2), the parameters were reset approximately seven hours after the maximum retention had been achieved (117 mm Hg, ~17 hr elapsed time) to allow the retention/release behavior to be followed to lower pressures in a reasonable time frame. This latter experiment is assigned an approximate duration of one day, and the faster experiment is designated as a two-hour test.

The AW-101 Composite 1 samples were used to probe the effect of evacuation rate on gas bubble retention in retention-to-buoyancy experiments. The conditions in the two experiments, except for pressure program parameters, were essentially identical: the same waste sample was used; each vessel was filled, settled, and irradiated under the same conditions; and each settled sample contained a 2.1–2.25 cm supernatant liquid layer over a 10.75–10.95 cm nonconvective solids layer. Figure 4.1 shows the measured growth fraction in the solids layer as a function of the system pressure for both samples. In each case, the growth gas fraction increases essentially linearly with the inverse pressure to near the maximum gas retention, and the samples grow at essentially the same rate (with respect to pressure). However, in both samples, gas releases large enough (minimally 0.05 cm level change or approximately 0.25 mL) to be detected in waste level measurements were observed at gas volume growth greater than ~17%, and these corresponded to visual observations of individual bubble releases (bubble disengagement). Some of the release points are indicated on the figure. It should be noted that smaller individual gas releases were observed occasionally from each sample at lower gas fractions.

As shown in Figure 4.1, the maximum gas retention in the two AW-101 Composite 1 experiments was also comparable. Maximum growth gas fractions of 0.19 were measured in both the two-hour (vessel 1) and one-day (vessel 2) experiments, and the maximum absolute gas fractions are estimated to be up to 3% higher (gas fraction of 0.22) due to gas bubbles initially present in the samples. Additional discussion of absolute gas fractions is included in the AW-101 results summary in Section 4.2.4. At the maximum retention, the volume of retained gas in the two AW-101 Composite 1 samples was about twice that needed for the bulk nonconvective layer to reach neutral buoyancy in the supernatant liquid. A maximum growth gas fraction of only 0.09 is predicted based on measured and estimated layer densities.

As noted previously, gas retention above neutral buoyancy is not unexpected because of waste strength and tank or vessel wall interactions (Section 3.2.3.2) (Meyer et al. 1997). These wall effects are discussed in detail in Section 4.4. Another consideration for retention beyond neutral buoyancy is that insufficient supernatant liquid was present for the nonconvective layer to readily become buoyant. This scenario seems less likely, because a buoyant rise was observed in the two-hour experiment. Also, in the longer experiment the supernatant liquid layer was present beyond the maximum retention point, suggesting that the liquid layer was not lost because of infiltration into the nonconvective layer, and a buoyant rise should have been feasible.

The lack of buoyant displacement in the day-long experiment is the primary distinguishing factor from the comparable two-hour test. This difference was deemed significant enough that longer experiments became the new standard. The two experiments are also distinguished by the gas release behavior after the maximum gas retention and at lower pressures, as depicted in Figure 4.1. In the shorter experiment, the buoyant displacement occurred shortly after a partial release of gas from the solids layer. Following the rollover, the sample continued to retain (and release) gas and actually attained a secondary maximum growth gas fraction nearly as great as the original (0.19) at a considerably lower pressure (76 mm Hg versus 109 mm Hg). Beyond this

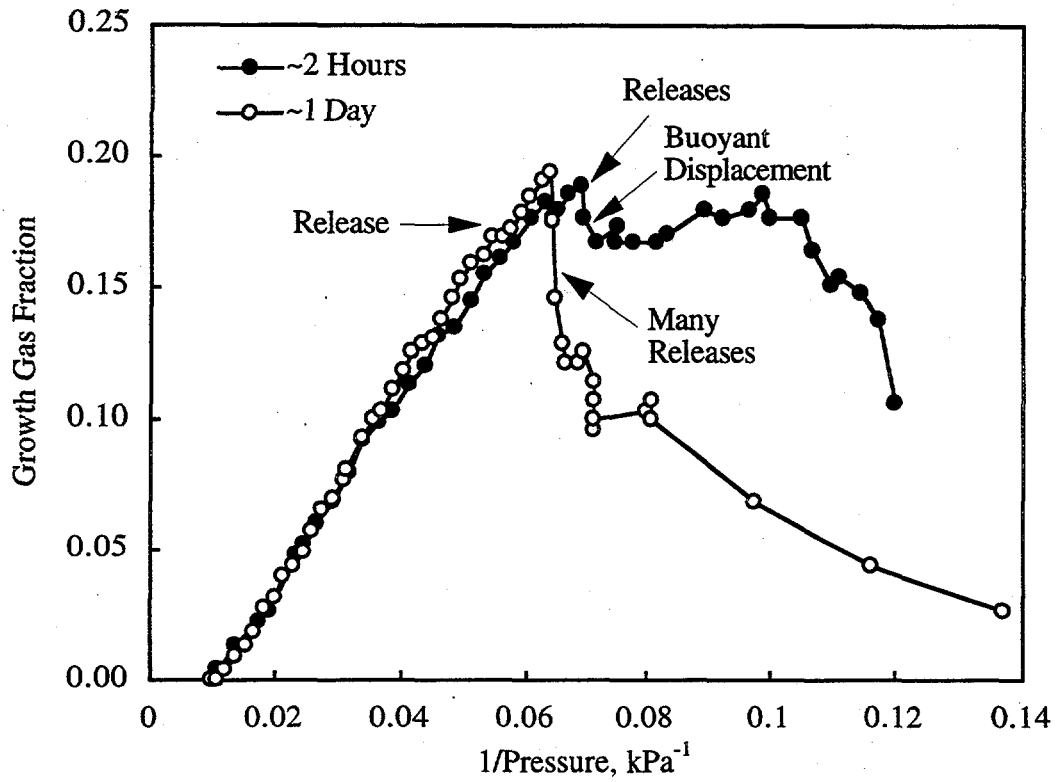

Figure 4.1. Effect of Evacuation Rate on Gas Bubble Retention in Two Samples of AW-101 Composite 1

second peak, the waste released considerable gas. In the one-day experiment, gas was released relatively quickly, on a pressure basis, immediately after maximum retention was reached. A series of about a dozen individual bubble gas releases resulted in a retained gas volume decrease of 5.4 mL, corresponding to a growth gas fraction decrease from 0.19 to 0.12 during a pressure reduction from 117 mm Hg to 113 mm Hg. At still lower pressures, the sample continued to release gas without attaining a discernible secondary retention maximum.

The average gas volume per individual bubble release for the series noted above is estimated at approximately 0.4 mL, which equates to an average bubble diameter of ~0.9 cm. This size was used to estimate the sludge yield strength necessary to retain the gas bubbles. A value on the order of 25 Pa was calculated assuming the strength of the yielding material simply balanced the buoyant upward force acting on the trapped bubble (Stewart et al. 1996). A bubble-laden solids density equal to the convective liquid density (1.43 g/mL) was used in the calculation. The calculated strength does not conflict with the measured composite strength, which was below the 300-Pa detection limit.

4.2.2 Comparison of Two Composites

The retention-to-buoyancy experimental results for an AW-101 Composite 2 sample are very similar to those for the AW-101 Composite 1 samples. Figure 4.2 compares the gas fraction profiles as a function of system pressure for the one-day Composite 1 experiment (vessel 2) to an approximately half-day test for Composite 2 in vessel 3. Again, a 19% maximum gas growth was observed, and only 9% gas growth to attain neutral buoyancy was expected. As shown in Figure 4.2, the gas growth rate with respect to pressure is similar for the two waste types, with the Composite 2 sample attaining maximum retention at a slightly higher pressure (122 mm Hg) or faster rate than the Composite 1 test (117 mm Hg). The only really notable distinction in the

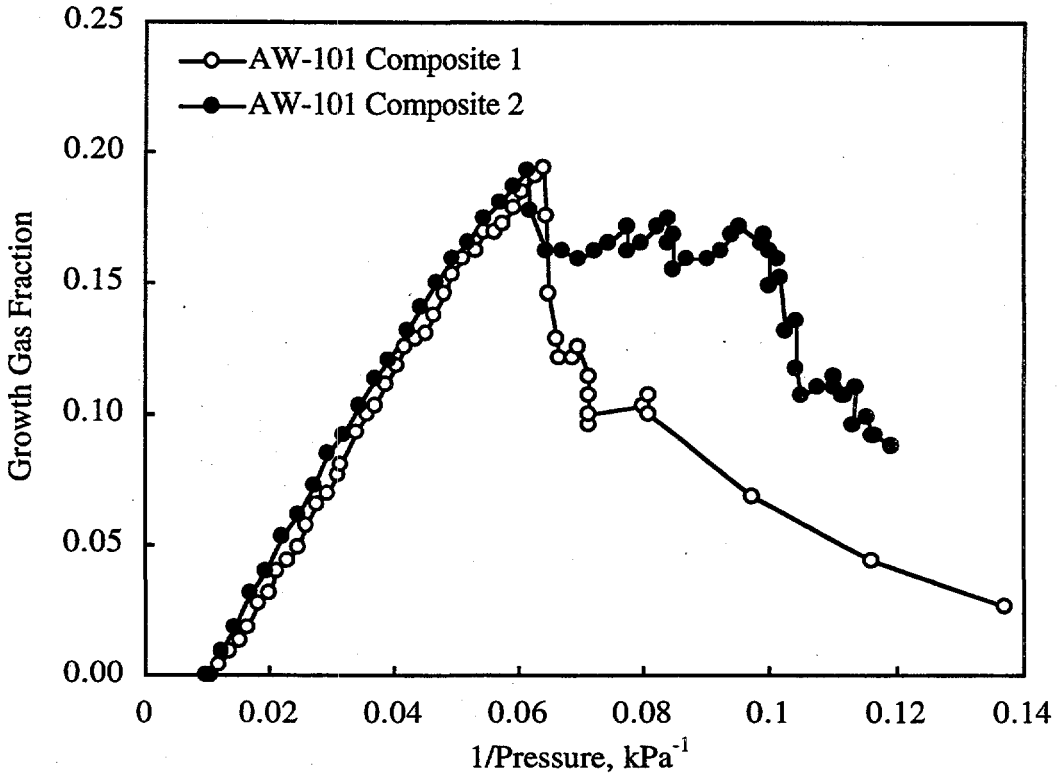

Figure 4.2. Comparison of Retention-to-Buoyancy in Samples of AW-101 Composites 1 and 2

Composite 2 experiment is in the buoyant displacement and gas release behavior, which was observed to fall between the two Composite 1 tests described previously. In the Composite 2 experiment, the nonconvective layer never rolled over, which compares well with the longer Composite 1 experiment depicted in both Figures 4.1 and 4.2; on the other hand, the gas release following maximum retention in the Composite 2 sample was somewhat more lethargic or delayed, much like the shorter Composite 1 experiment (see Figure 4.1 for comparison). After maximum retention was reached in the Composite 2 test, a relatively rapid release period followed in which growth gas fraction decreased from 0.19 to 0.16 and then retained additional gas to reach a secondary maximum of nearly 0.18 growth gas fraction.

Although the specific purpose of comparing results in multiple composites was to evaluate differences associated with unique waste properties, the effect of the length of experiment must also be considered. In the Composite 2 test, the pressure parameters were set to P_{init} = 760 mm Hg and t_{set} = 120 min, so the pressure at maximum retention (122 mm Hg) was reached in just over 10 hours compared with nearly 17 hours for the longer Composite 1 test and ~90 minutes for the fastest run. (In some respects, the Composite 2 test could also be considered a one-day experiment because approximately 22 hours were required to carry the test beyond the maximum gas retention through the release phase shown in Figure 4.2.) The somewhat distinct gas release behaviors in the three AW-101 retention-to-buoyancy experiments may be a result of the different evacuation rates.

The similarity in maximum gas retention results for the two AW-101 composites is not surprising, because the composite physical properties, by chance, and the experimental operating conditions, by design, were very comparable. For example, the estimated nonconvective layer densities following irradiation and prior to evacuation were both 1.57 g/mL, and the initial settled solids and overall sample heights (10.75-10.9 cm and 12.8-13.0 cm, respectively) were also very

closely matched. In addition, the shear strengths of the individual samples (Table 4.1) that constitute the composites (Table 3.1) were of similar magnitude, as were the measured strengths (<300 Pa) of the composited samples after minimal settling.

4.2.3 Ultimate Retention

The supernatant liquid layer was removed from a second AW-101 Composite 2 sample (vessel 4) prior to evacuation so that the ultimate retention in the waste could be investigated. The initial evacuation rate parameters in the two Composite 2 experiments (ultimate retention and retention to buoyancy) were identical, but while the retention-to-buoyancy experiment was considered a ~half-day experiment, the ultimate retention experiment is clearly a full-day test. This is a consequence of the much lower pressure (<60 mm Hg) required to attain maximum retention in the ultimate retention experiment than the buoyant retention case (122 mm Hg). Figure 4.3 shows the gas fraction progression for the first 25 hours of the ultimate retention experiment using the initial pressure program parameters (P_{init} = 760 mm Hg, t_{set} = 120 min). The figure also includes projected gas fraction data assuming ideal gas law behavior in the retained gas. The estimated retained volume at some pressure P_1 is used to predict the gas volume at the next measured pressure P_2 (see the discussion in Subsection 3.2.3.3). When the measured growth volume is less than predicted, gas release is implied. The initial gas release at a growth gas fraction of 0.18 and several subsequent releases are indicated on Figure 4.3. This ultimate retention gas fraction profile is distinct from the retention-to-buoyancy profiles shown in Figures 4.1 and 4.2. Whereas the buoyancy experiments attain maximum retention followed by a general decay in gas fraction after the onset of the first major release phase, the ultimate retention sample recovers from the initial release series to grow to greater gas fractions. In this way, the Figure 4.3 depicts three distinct growth phases. The maximum growth gas fractions in these stages were 0.18 (108 mm Hg, 0.070 kPa^{-1}), 0.20 (77 mm Hg, 0.098 kPa^{-1}), and 0.22 (59 mm Hg, 0.127 kPa^{-1}).

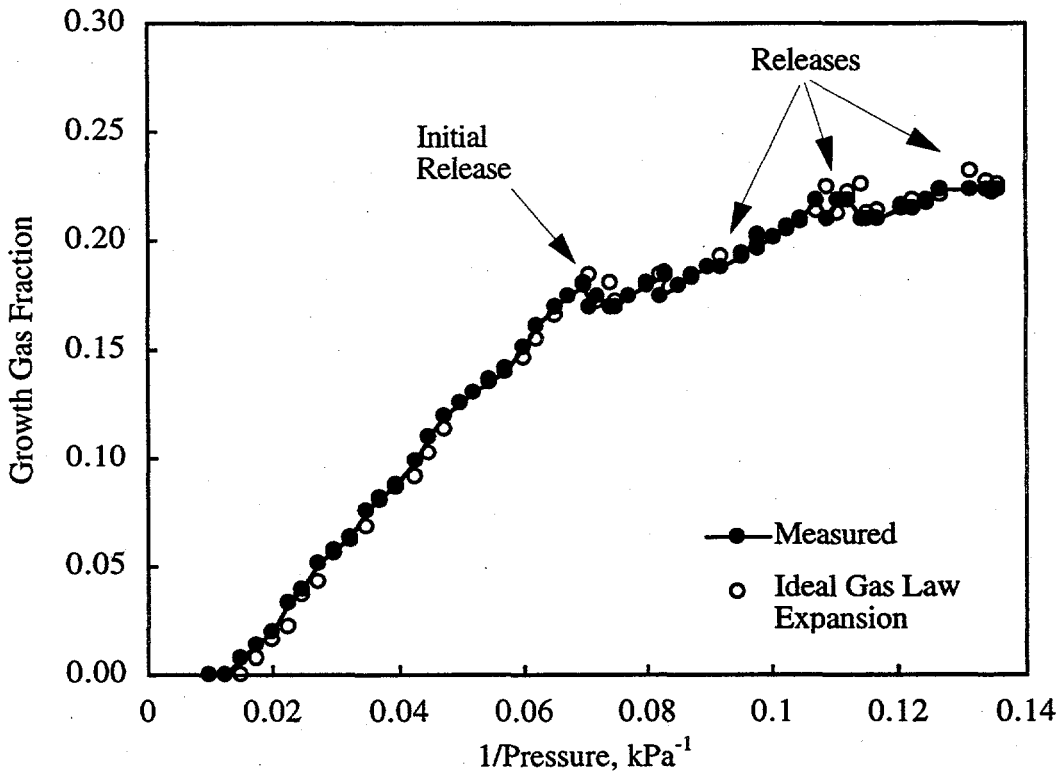

Figure 4.3. Ultimate Gas Retention in AW-101 Composite 2

The growth pattern in Figure 4.3 is similar to those observed in previous simulated waste gas retention studies (Gauglitz et al. 1996) using moderately weak (~67 Pa) bentonite clay sludges in an equivalent diameter apparatus. The clay simulant study showed that both the maximum retention and the retention and release characteristics were dictated by the material strength. Although no direct correlation of the actual waste and clay simulant results may be made due to differences in physical, chemical, and rheological properties of the materials, the simulant studies should provide an order of magnitude guide to the strength of the actual waste. A strength on the order of 50 Pa is in good agreement with that estimated previously for AW-101 Composite 1 on the basis of release volume (see Section 4.2.1).

The data shown in Figure 4.3 indicate a stable maximum gas fraction plateau at 0.22. At this point in the experiment, a decision was made to increase the evacuation rate (P_{init} = 55 mm Hg, t_{set} = 600 min) such that release behavior could be observed in a timely manner (~one additional day). Unfortunately, the transition from the initial to final pressure programs was not as smooth as anticipated; controller overshoot at the start of the second control program resulted in a very rapid increase in gas volume to approximately 0.27 growth gas fraction, as shown in Figure 4.4. Although it is unclear whether this additional 4–5% volume growth would have been attained with more consistent pressure control, the higher gas fraction (0.27) should be considered an upper bound. In either case, the maximum gas content measured in the ultimate retention experiment is greater than the 0.19 growth gas fraction obtained in the retention-to-buoyancy experiment. This is expected, because removing the supernatant liquid eliminates buoyancy as a pathway to gas release in the ultimate retention experiment.

The unique growth and release characteristics resulting from the pressure upset noted above are depicted in Figure 4.4. The figure shows both the set point and measured system pressures as a function of the elapsed time from the start of the final evacuation program. In spite of the smooth set-point pressure profile, the measured pressures attained a damped sawtooth pattern with a rapid initial pressure swing from 56 to 38 mm Hg. Corresponding to this pressure decrease, the sample growth gas fraction increased sharply from 0.22 to 0.27 (this is shown in the figure as well). During the first vacuum subsidence (pressure rise), the gas fraction smoothly decreased to 0.17, below those previously measured at the same pressure (0.22 to 0.27). Perhaps most interesting is the sudden sample collapse just after the second downward pressure swing. The retained gas volume did not increase when the pressure decreased, and as the pressure began to rise toward the set point, the sample rapidly released a large fraction of its retained gas, falling to about 0.05 growth gas faction. Apparently, the pressure upset significantly destabilized the waste structure, and it collapsed in the absence of a constant vacuum pressure. Although not shown, at still lower pressures the waste gas fraction cycled three times from a minimum of 0.03 to about 0.11 maximum growth gas fraction as the pressure was reduced from 52 to 20 mm Hg.

4.2.4 Summary of Gas Fraction Data

Table 4.3 summarizes the maximum growth gas fraction data for the AW-101 samples discussed in detail in the preceding sections. Also shown in the table are additional maximum retained gas volume data including the expected growth to sample buoyancy and the estimated absolute sample gas content obtained in consideration of initial gas content. Two values of the initial gas content, determined as a percentage of the nonconvective layer volume, were calculated and are presented in the table. The sample growth resulting from the four-day irradiation provides an estimate of the minimum absolute initial gas content. The value obtained from initial growth data upon sample evacuation, using the ideal gas law approach, provides an upper bound on the initial gas fraction, because the volume expansion during depressurization should be affected by retained gas volume created through gas entrainment, by gas generation, and during gas/vapor desupersaturation. The minimum initial gas content in the four samples ranged from 1.8 to 2.3%, and the maximum was about twice that (3.7–4.6%). The maximum initial gas content values were used in calculating the maximum absolute gas fractions, which were typically 3–4 % higher gas content than those obtained directly from measured growth data.

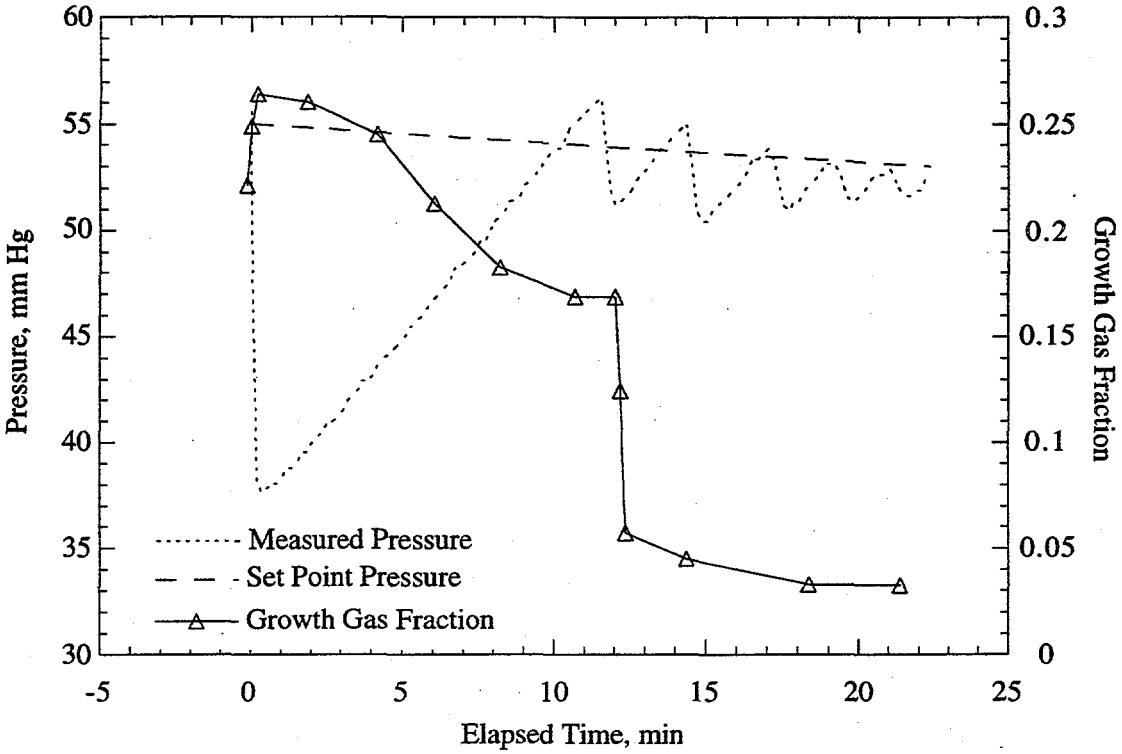

Figure 4.4. Detail of a Pressure Upset and Gas Release in the AW-101 Ultimate Retention Experiment

In summary, the maximum growth values obtained in retention-to-buoyancy experiments (19%) were about 10% higher in gas content than expected for the nonconvective layer to become neutrally buoyant in the supernatant liquid. The ultimate retention maximum gas growth of 22–27% was somewhat greater than that for the corresponding buoyancy experiment with the same composite sample. The range of maximum gas volume growth values in the latter experiment reflects maximum gas contents before and during a pressure upset.

4.3 Maximum Gas Retention in AN-103 Samples

A single Tank AN-103 composite sample was prepared and used in the four gas retention analyses discussed in this section. The experimental conditions are summarized in Table 4.4. As with the AW-101 tests, the primary focus of these experiments was to develop an understanding of and to quantify gas retention under conditions that most closely reflect the actual tank. These are

Table 4.3. Summary of Gas Retention Data for AW-101 Samples

Sample	Vessel	Initial Gas Volume, %		Maximum Gas Volume, %		
		Irradiation Growth	Ideal Gas Law	Expected Growth to Buoyancy	Measured Growth	Estimated Including Initial
Composite 1	1	2.3	3.7	8.7	18.9	21.9
Composite 1	2	1.8	3.7	9.3	19.4	22.4
Composite 2	3	1.8	4.6	9.2	19.3	23.0
Composite 2	4	2.0	4.2	NA	22.1 (26.6)	25.5 (29.6)

Table 4.4. Experimental Conditions Applied in AN-103 Experiments

Sample	Type	Vessel	Duration (approx.)	P_{init}, mm Hg	t_{set}, min
AN-103 Composite	RB	6	2 hours	760	12
AN-103 Composite	RB	7	1 day	760	100
AN-103 Composite	RB	8	4 days	760	400
AN-103 Composite	UR	9	1 day	760	100

retention-to-buoyancy (RB) experiments on samples containing a thick layer of supernatant liquid. In the three AN-103 experiments of this type, where the primary variable was the experimental duration or evacuation rate, gas fractions well above the neutral buoyancy point were measured in all cases. However, the maximum amount of gas retained was less in the longest test. To complete the AN-103 experimental suite, a single ultimate retention (UR) experiment was run, and again the maximum gas retention was greater than in the corresponding RB test. The quantitative gas retention results are discussed below; additional details are summarized in Appendix B.

4.3.1 Effects of Experiment Duration

To further investigate the effects of experiment duration on gas retention and release characteristics, three AN-103 composite samples were evacuated with separate pressure programs (see Table 4.4) giving experiment durations ranging from about two hours to more than 30 times as long (four days). Figure 4.5 shows the gas growth as a function of pressure for each of the three retention-to-buoyancy experiments. In the two-hour test (P_{init} = 760 mm Hg, t_{set} = 12 min), a maximum growth gas fraction of 0.30 was measured just prior to a small gas release and the subsequent buoyant displacement. The maximum retention occurred at an elapsed time of almost exactly two hours and a pressure of 67 mm Hg. A slightly higher maximum growth gas fraction of 0.32 was observed in the new standard one-day experiment (P_{init} = 760 mm Hg, t_{set} = 100 min) at essentially the same pressure and 17 hours elapsed time. The lowest maximum retention (0.28 growth gas fraction) in the series was obtained in the longest experiment (P_{init} = 760 mm Hg, t_{set} = 400 min). This experiment took about 71 hours to reach maximum retention at 64 mm Hg and was continued an additional day to monitor the retention and release characteristics. In this four-day experiment, gas releases observed at intermediate growth gas fractions of 0.10 (~167 mm Hg, 0.045 kPa^{-1}) and 0.18 (99 mm Hg, 0.076 kPa^{-1}) effectively reduced the growth rate in the sample compared with the two-hour and one-day experiments shown in Figure 4.5. Some small intermediate gas releases were also observed in these faster experiments, but none was as substantial as the release activity at 18% growth in the four-day test. Apparently, in this latter experiment, enough gas collected near the surface of the nonconvective layer to overcome the waste strength resistance, and gas was released.

Although the difference in the magnitude at maximum retention in the AN-103 tests is quite small, and all growth volumes are in the range of 28 to 32%, the effect of a slower evacuation rate may be greater than this suggests. The expected gas volume growth to neutral buoyancy for the long-term experiment (vessel 8) was 20%, or about 8% retained gas volume less than the observed maximum. On the other hand, the expected growth to buoyancy for each of the shorter experiments (vessels 6 and 7) was 15 to 16%, which is nearly half of the measured peak values of 30 to 32%. The higher expected retained gas volume growth to neutral buoyancy in the long-term experiment is a result of inhomogeneities within the AN-103 composite sample. Some of the inhomogeneities were visually obvious in loading the vessels, particularly in the last two filled

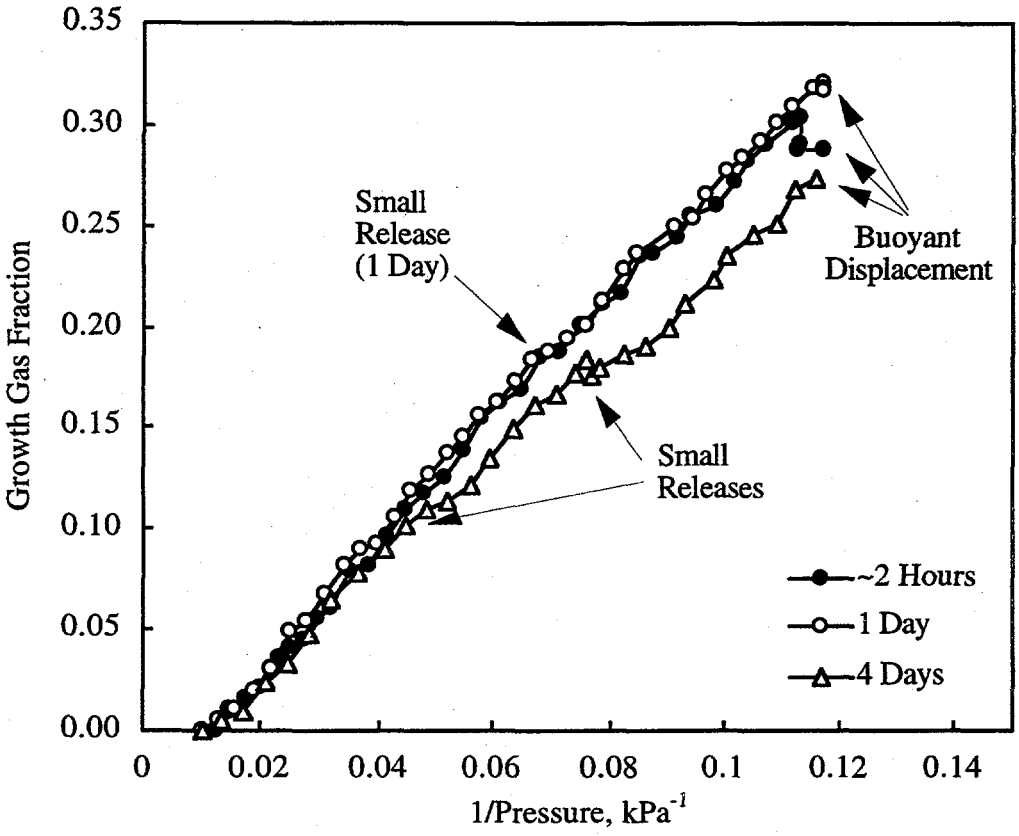

Figure 4.5. Effect of Evacuation Rate on Gas Bubble Retention in Three Samples of AN-103 Composite

(vessels 8 and 9). In each of these samples the composite was thicker, and in loading the final vessel (9), a pliable waste slug of notably greater strength was observed. The inhomogeneities resulted in more dense settled nonconvective layers in vessels 8 and 9 (1.86 g/mL) than in vessels 6 and 7 (1.77 and 1.76 g/mL, respectively), and compared with the measured supernatant liquid density (1.49 g/mL), a greater retained gas volume growth to neutral buoyancy is estimated in the four-day experiment sample (vessel 8) over the faster samples (vessels 6 and 7). Another consequence of the composite inconsistency is that vessel 8 had a thinner initial supernatant liquid layer (2.85 cm) than vessels 6 and 7 (5.3 and 4.9 cm, respectively). As a result of the sample nonuniformity, it cannot be stated conclusively that the reduced maximum retention in the four-day experiment is a direct result of the relatively slow growth process. However, the early release behavior in the long-term experiment (see Figure 4.5 and the discussion above) and other evidence presented in Section 4.4 suggest that the evacuation rate does play a role.

In contrast to the AW-101 experiments, in which only the most quickly evacuated sample became buoyant in the supernatant liquid, each of the AN-103 bubble-laden nonconvective samples rose in the liquid near the point of maximum retention in a buoyant displacement. However, quite distinct from the AW-101 results and gas retention experiments with Tank SY-103 waste (Gauglitz et al. 1996; Bredt and Tingey 1996), the AN-103 samples were not observed to release gas during or following rollover. Rather, the risen bubbly waste became a froth beneath a layer of stable pre-existing foam that continued to expand with further pressure decreases. (The stability of the AN-103 foams is addressed separately in Section 5.3.) For this reason, gas retention plots in Figure 4.5 are abruptly terminated at the point of buoyant displacement, and this event has been selected to define the maximum retention in these experiments.

4.3.2 Ultimate Retention

The AN-103 composite ultimate retention growth gas fraction data are plotted as a function of pressure in Figure 4.6. In this day-long experiment (P_{init} = 760 mm Hg, t_{set} = 100 min), a maximum gas growth of 37% was measured at a pressure of 43 mm Hg (0.174 kPa^{-1}) after approximately 27 hours elapsed time. To detect gas release from the sample, the ideal gas law volume growth prediction technique was applied. The equivalent ideal gas law estimated growth gas fractions are shown with the experimental data in Figure 4.6, and when these exceed the measured growth datum at a given pressure, gas release is implied. Prior to an initial gas release at a growth gas fraction of 0.25, the sample volume (and gas fraction) increased essentially linearly with the inverse pressure, characteristic of ideal gas law behavior. Beyond the initial release, the slope of the growth curve decreased slightly, and after subsequent releases, the growth rate continually declined. The shape of the gas retention and release curve in Figure 4.6 is, as noted with the respect to the AW-101 ultimate retention experiment and Figure 4.3, similar to that for a bentonite clay with a moderate shear strength of about 100 Pa (Gauglitz et al. 1996).

As with the AW-101 results, the difference between the maximum gas fractions in ultimate retention (0.37) and retention-to-buoyancy (0.28–0.32) experiments is not as great as might be expected, primarily due to the substantial excess retained gas volume in the buoyancy experiments and the apparent ineffectiveness of the buoyant release mechanism in those tests. This issue is addressed in the discussion of wall effects in Section 4.4.

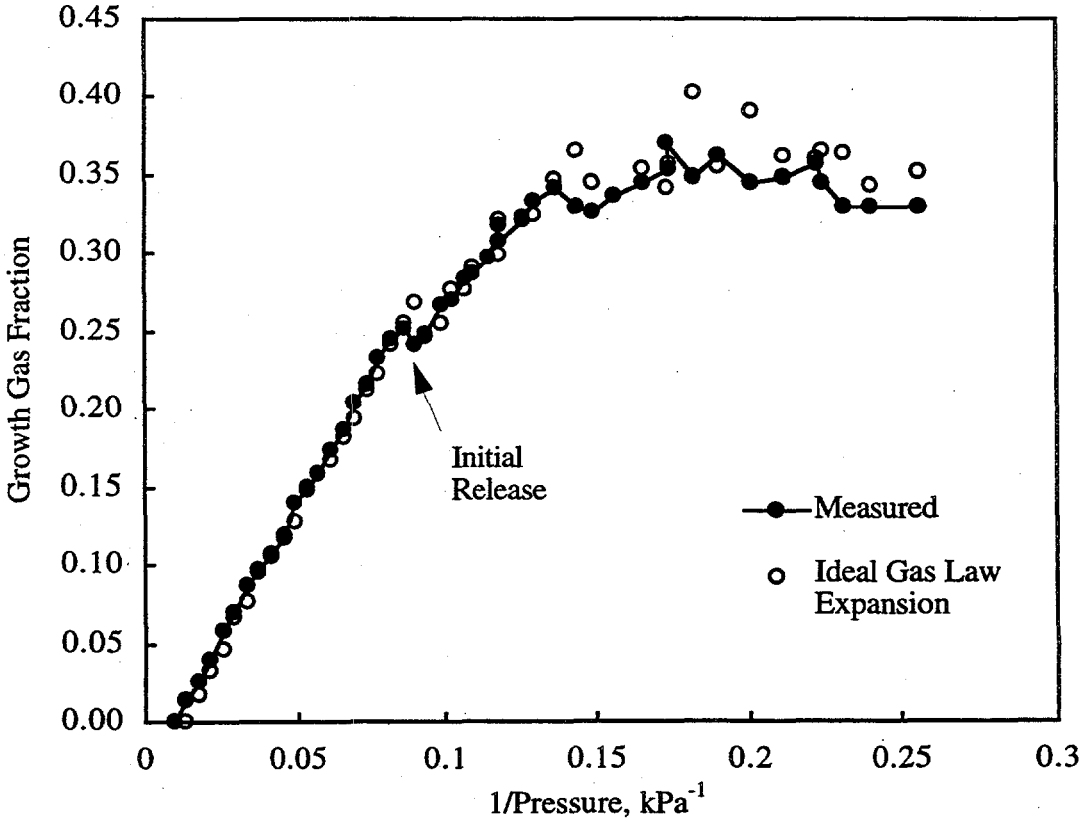

Figure 4.6. Ultimate Gas Retention in AN-103 Composite

4.3.3 Summary of Gas Fraction Data

Measured and estimated initial and maximum gas fractions for each of the four AN-103 gas retention experiments are summarized in Table 4.5. The initial nonconvective layer gas contents determined from sample growth during irradiation ranged from 2.1 to 2.7%. Measured sample growth during the initial stages of the evacuation experiments and application of the ideal gas law resulted in initial gas content estimates of 2.9 to 4.1%. Between 28 and 32% maximum growth in retained gas volume was measured in retention-to-buoyancy tests, with the smallest value coinciding with a long (four-day) experiment. A somewhat greater gas volume growth (37%) was observed in the ultimate retention experiment. The estimated absolute gas content, taking into consideration the maximum initial gas volume, is 2 to 3% greater in gas content than the measured growth percentage for each sample. The measured maximum growth for each of the retention-to-buoyancy experiments exceeds the expected growth by 8 to 17% gas content, and the difference was least in the slowest growth rate experiment.

4.4 Wall Effects

It has been suggested that gas retention beyond neutral buoyancy is an expected outcome resulting from waste strength (Meyer et al. 1997) and wall interaction effects. In our experiments in narrow vessels, compared with tanks of large diameter, it is reasonable to assume that wall effects contribute proportionately more to retention beyond neutral buoyancy. This is a result of simple geometry, which shows that the ratio of the waste/wall interaction area to the waste volume scales inversely with the vessel diameter. Since we are not able to uniquely distinguish between the wall and waste strength effects, and because strong interactions between the retention vessel walls and retained gas in AN-103 samples were deduced from visual observations (Sections 5.2 and 5.3), gas retention above neutral buoyancy is here attributed to wall effects. It must be emphasized, however, that waste strength also plays a role.

Gas retention above the neutral buoyancy gas fraction was observed in both the AW-101 and AN-103 retention-to-buoyancy experiments. The retained gas excess becomes apparent when the estimated nonconvective layer density falls below the supernatant liquid density. At maximum

Table 4.5. Summary of Gas Retention Data for AN-103 Samples

Vessel #	Initial Gas Volume, %		Maximum Gas Volume, %		
	Irradiation Growth	Ideal Gas Law	Expected Growth to Buoyancy[(a)]	Measured Growth	Estimated Including Initial
6	2.1	4.1	15.8	30.4	33.2
7	2.7	3.4	15.4	32.1	34.4
8	2.7	2.9	20.2	27.8	29.8
9	2.1	3.0	NA	36.9	39.4

(a) These values are based on AN-103 Composite densities (Table 4.6) determined in the current experiments. A lower estimated neutral buoyancy gas content, 11.6 for AN-103 based on bulk tank densities (liquid density of 1530±50 kg/m^3 and nonconvective layer density of 1730±110 kg/m^3, is reported in CW Stewart's *A Discussion of the Potential for Large Flammable Gas Releases from Tank 241-AN-103* (TWSFG97.38, PNNL, 1997).

retention, the difference between the minimum density of the bubbly solid layer ($\rho_{s,min}$) and that of the liquid layer density (ρ_l) gives the maximum buoyancy of the solids layer. To maintain this unstable configuration, a force other than gravity must act downward to hold the bubbly solids layer in place. This is likely an interaction force between the vessel walls and the nonconvective layer (or a waste strength effect).

Knowing the volume (V_{max}) of nonconvective material at the maximum retention and the estimated density deficit in the layer, one can calculate the apparent excess mass supported by the walls and an associated wall force:

$$F_w = (\rho_{s,min} - \rho_l) V_{max} g = (\rho_{s,min} - \rho_l) \frac{\pi}{4} d^2 h_{max} g \quad (4.1)$$

Here, d is the vessel diameter, h_{max} is the nonconvective layer height at maximum retention, and g is the gravitational acceleration. Considering the vessel wall area (A_w) over which the wall force acts, the average strength of the wall interaction can be estimated:

$$\tau_w = \frac{F_w}{A_w} = \frac{F_w}{\pi d h_{max}} = (\rho_{s,min} - \rho_l) \frac{d}{4} g \quad (4.2)$$

Equation (4.2) has been applied to each AW-101 and AN-103 retention-to-buoyancy experiment, and the estimated wall interaction strengths are tabulated in Table 4.6 along with the various supporting density values.

In the three AW-101 experiments, the interaction strength is consistently estimated as 9–10 Pa. This rather minimal strength is enough to attain growth gas fractions (0.19) approximately twice those expected to reach neutral buoyancy (0.09). Whereas the AW-101 interaction strengths are uniform, the AN-103 results are more scattered (8–19 Pa), and this may be a result of the wider variation in experiment durations. The interaction strengths in the two-hour and one-day experiments were nearly equal, 16 and 19 Pa, respectively, and in the four-day test, the interaction was estimated to be about half as strong (8 Pa). However, as noted in Section 4.3.1, the differences between the four-day experiment and the shorter tests cannot be attributed conclusively to variations in the experiment duration due to inhomogeneities in the AN-103 composite sample.

It is important to note that this wall strength is different, and typically less, than the shear strength measured with a vane. In particular, it is known that slurries will slip on a fluid layer along walls (Gauglitz et al. 1994b), although some slurries will also tend to stick. In contrast, shear vanes cause shear failure within the sample rather than along a wall. While previous testing with SY-103 waste samples did not suggest wall interactions (Gauglitz et al. 1996), the AW-101 and AN-103 waste samples behaved differently.

The AN-103 wall interaction strength data shown in Table 4.6 suggest lesser wall effects in the four-day experiment. Supporting photographic evidence (Section 5.2), shows a lower gas fraction at the vessel walls than in the shorter AN-103 tests. In addition, evidence of reduced wall effects in the long AN-103 experiment are found in the convective and nonconvective level measurement data leading up to the maximum retention and buoyant displacement.

Figure 4.7 shows the liquid layer volume, normalized by the maximum measured liquid volume, as a function of the evacuated system pressure for each of the three AN-103 experiments. At buoyancy, which essentially corresponds to the point of maximum gas growth in each AN-103 test, the free liquid volume is zero, since it has been displaced by the bubble-laden nonconvective waste. Any shrinkage of the liquid layer thickness in the course of a retention experiment suggests either liquid infiltration into the nonconvective layer or relative upward movement of the solids

Table 4.6. Estimated Strengths of Waste/Wall Interactions in AW-101 and AN-103 Samples

Sample	Duration, Approx.	Densities, g/mL				Interaction Strength, Pa
		Liquid	Solids Layer, Initial	Solids Layer, Minimum	Solids Layer, Deficit	
AW-101 Composite 1	2 Hours	1.43	1.56	1.27	0.16	9
AW-101 Composite 1	1 Day	1.43	1.57	1.27	0.16	10
AW-101 Composite 2	1/2 Day	1.43	1.57	1.27	0.16	10
AN-103 Composite	2 Hours	1.49	1.77	1.23	0.26	16
AN-103 Composite	1 Day	1.49	1.76	1.17	0.32	19
AN-103 Composite	4 Days	1.49	1.86	1.36	0.12	8

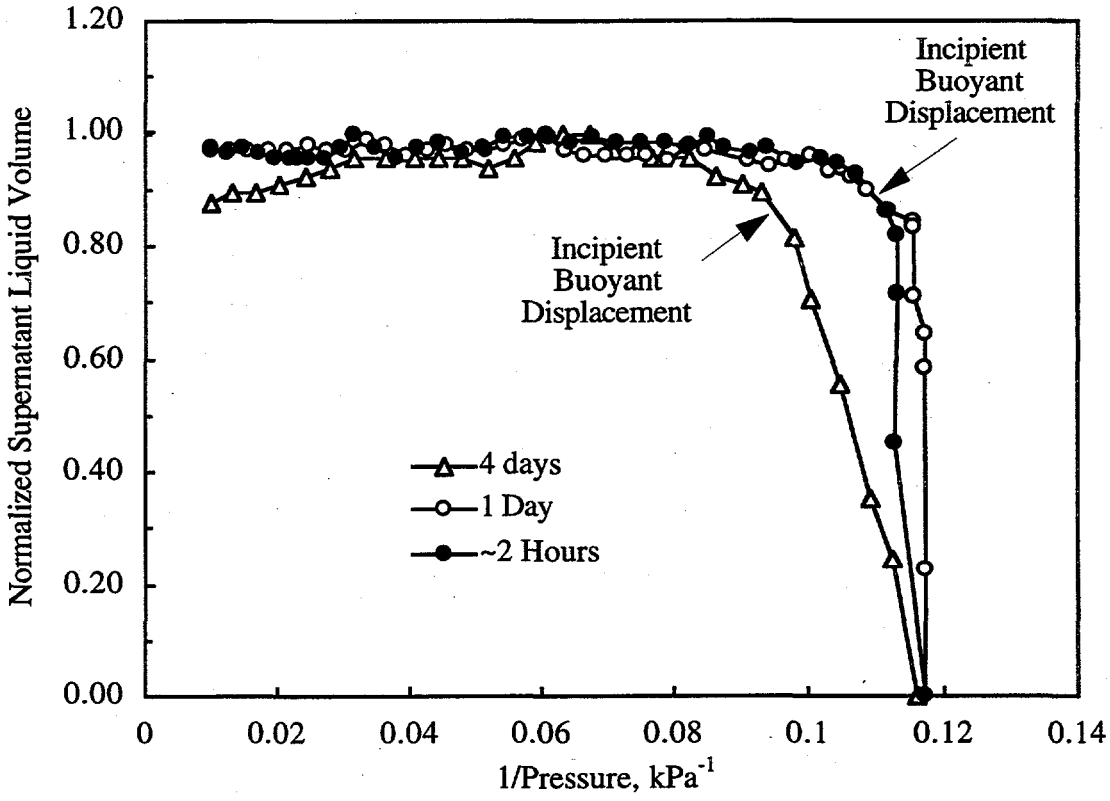

Figure 4.7. Effect of Evacuation Rate on the Rise of Buoyant AN-103 Sludge Determined from Changes in the Supernatant Liquid Volume

layer into the liquid. The liquid level profile in Figure 4.7 for the longer experiment is somewhat distinct from the shorter ones. In the four-day test the liquid layer thickness has clearly begun to subside at an inverse pressure of less than 0.10 kPa^{-1} (~77 mm Hg). At this point of initial non-convective layer rise, identified on the figure as the point of incipient buoyant displacement, the measured gas growth fraction was about 0.22, in very good agreement with the expected neutral buoyancy growth gas fraction for this sample (0.20).

On the other hand, Figure 4.7 shows that in the shorter AN-103 experiments the waste samples do not begin to rise much before the pressure at which buoyancy was attained; thus the gas fractions at the point of incipient buoyant displacement are nearly equal to their maximum retention values. The data indicate enhanced wall slip or reduced wall interaction with decreased sample growth rate (or longer experiment duration).

The buoyant rise at relatively low gas fraction in the four-day AN-103 experiment does not appear to be related to the absolute thickness of the supernatant liquid layer. In a previous study of buoyant retention in Tank SY-103 waste, Gauglitz et al. (1996) observed that, in experiments with relatively thick supernatant liquid layers (3–4 cm; 25–35 volume percent liquid), buoyancy occurred at measured gas fractions very near the expected value (suggesting minimal wall effects); and in cases of thin supernatant liquid layers (0.2–0.7 cm; 4–10% liquid), the measured maximum gas fractions exceeded the expected neutral buoyancy gas content. It was surmised that the maximum measured gas fraction tended to increase as the thickness of the supernatant liquid layer volume decreased below some critical minimum value. This conclusion is supported by the ultimate retention experiments in the present study. In these extreme experiments where no supernatant liquid is present, the observed maximum gas fractions in AN-103 and AW-101 waste types exceeded the maximum buoyant retention gas fractions. All these data suggest that the four-day AN-103 experiment, with a thinner (2.85 cm) supernatant liquid layer than in the two-hour and one-day tests (4.9-5.3 cm), should have retained relatively more gas if the liquid layer thickness were a critical factor. Apparently, experiment duration or waste physical properties were the overriding factors in the AN-103 retention-to-buoyancy results.

5.0 Results and Discussion: Mechanisms of Gas Bubble Retention and Release

Qualitative visual evidence of gas bubble retention and release mechanisms supporting the quantitative retention data (Section 4) are presented in this section. Images obtained from the AW-101 and AN-103 experiments are shown and discussed, with a primary emphasis on waste structure details within the nonconvective layer. An additional section (5.3) is dedicated to a discussion of observed frothing behavior in the AN-103 retention-to-buoyancy tests.

Throughout this section, both black-and-white and color photographs are shown. It should be noted that the colors in these pictures generally do not reflect the colors of actual waste. The reproduced colors are affected by the lighting conditions in the hot cell and the digital enhancement process used to generate photographic prints from videotape.

5.1 AW-101 Composites

A discussion of gas bubble retention mechanisms in AW-101 composites is presented first, with a comparison of the retention-to-buoyancy and ultimate retention experimental results. A demonstration of gas release behavior, including buoyant displacement (rollover), in a retention-to-buoyancy experiment follows.

5.1.1 Retention Mechanisms

Figure 5.1 shows the retained bubbles within an AW-101 Composite 1 sample (vessel 1, ~2-hour duration) at various stages of the retention-to-buoyancy experiment. The center of the field of view in the photographs is about 5.3 cm above the bottom of the retention vessel, corresponding to roughly half the initial height of the nonconvective layer. For reference, the retention vessels are grooved every 0.5 cm along their height. The upper photographs in Figure 5.1 demonstrate the nucleation and growth of bubbles resulting from the four-day exposure to the cesium gamma radiation source. Approximately 2% gas growth resulted from this irradiation process. The irradiated sample (upper right in figure), at least at the observable waste/vessel interface, was found to be quite uniformly distributed throughout the nonconvective layer with round gas bubbles about 200 μm diameter and smaller. Before irradiation, the sample was observed to contain considerably fewer and generally smaller gas bubbles (upper left).

The lower images in Figure 5.1 show gas bubbles at the same location in the vessel at two points during evacuation. The lower left image represents 9% gas volume growth in the solids layer, which is near the gas content at which the nonconvective layer was expected to reach neutral buoyancy. At this stage the bubbles, as large as 2.5 mm across and more typically 0.8 mm, are essentially round with only minor distortion and elongation. The shape of these particle-displacing bubbles is consistent with the behavior of fine-particle simulants of moderate strength. In bentonite clay simulants, Gauglitz et al. (1996) observed slightly distorted round bubbles in material with an initial (gas-free) shear strength of ~67 Pa. The lower right photograph of Figure 5.1 was taken at 18% gas growth, just shy of the maximum 19% growth. Through a combination of gas expansion and bubble coalescence, the typical size of bubbles increased to about 2 mm with bubbles as large as 5 mm observed. Larger bubbles are significantly distorted and show some fingering characteristics; however, this distortion appears to be more a function of the close packing of bubbles and shape changes resulting from coalescence than an increase in waste strength. Bright spots, which are particularly noticeable in the larger bubbles, are light-reflected from irregular particle surfaces located either in the liquid film at the vessel wall or, more likely, at the inner bubble/waste interface.

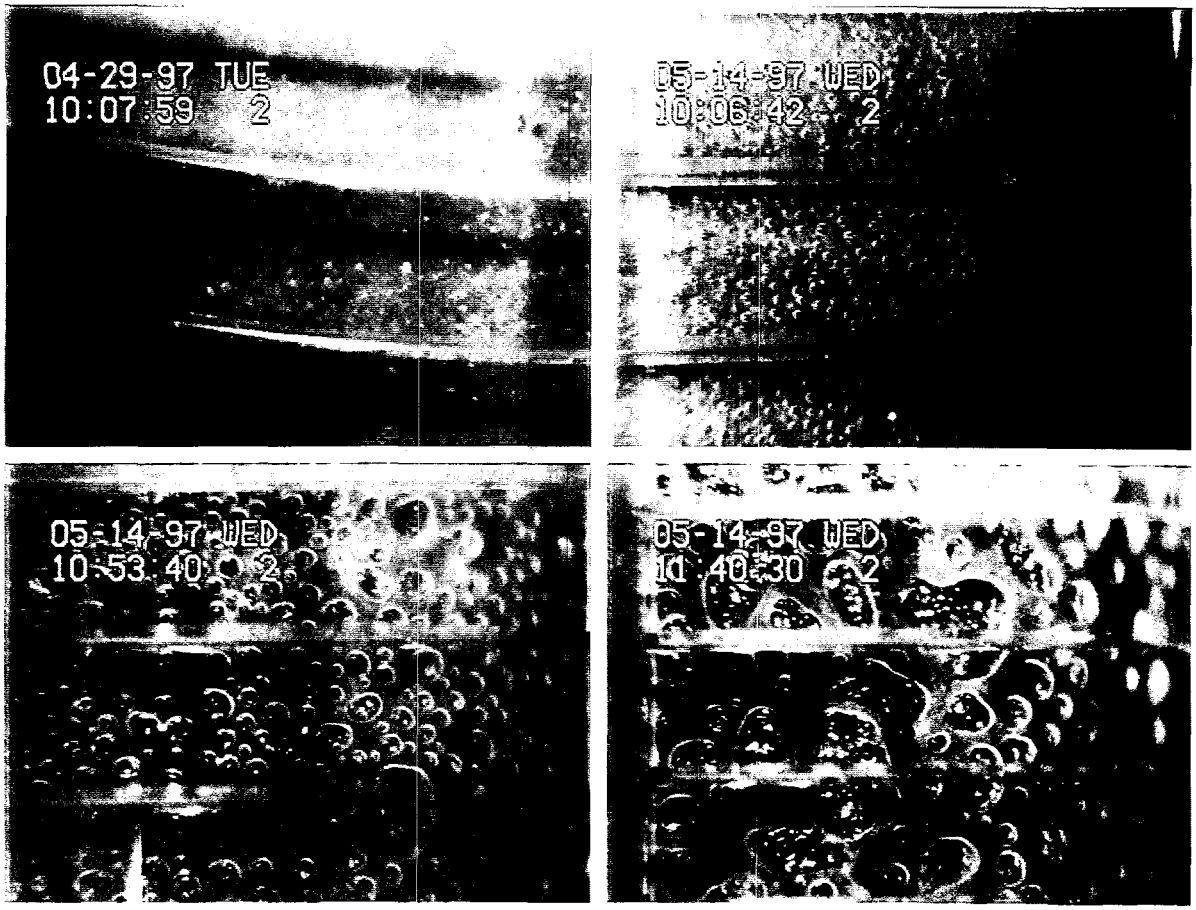

Figure 5.1. Gas Bubbles in AW-101 Composite 1 as a Function of Gas Fraction: (UL) Pre-Irradiation; (UR) Pre-Evacuation, 0% Growth; (LL) 9% Gas Growth; and (LR) 18% Gas Growth

The observed bubble shapes at the comparable stages of growth in the longer AW-101 Composite 1 (one-day) and AW-101 Composite 2 (half-day) retention-to-buoyancy tests were very similar to those depicted in Figure 5.1 and are not shown. (A more thorough analysis of the effect of experiment duration on gas bubble retention mechanisms is presented for the AN-103 experiments in Section 5.2). As noted in Section 4.2, the primary distinction among the AW-101 retention-to-buoyancy experiments is not in the growth phase of the samples, as is characterized by the bubbles shown in the figure and the gas growth profiles (Figures 4.1 and 4.2), but rather in the attainment of buoyancy and the rate of subsequent gas release.

Figure 5.2 is a series of photographs taken during the AW-101 Composite 2 ultimate retention experiment showing gas bubbles at different gas fractions. These detail images were taken at about half-height (initial) in the solids layer. The first image in the set (Figure 5.2 upper left) was taken after a four-day gamma irradiation and prior to the start of evacuation. The round bubbles have typical diameters of about 200 μm, much like those observed in the AW-101 Composite 1 sample, with the largest bubble in the image about twice as large. After gas growth to

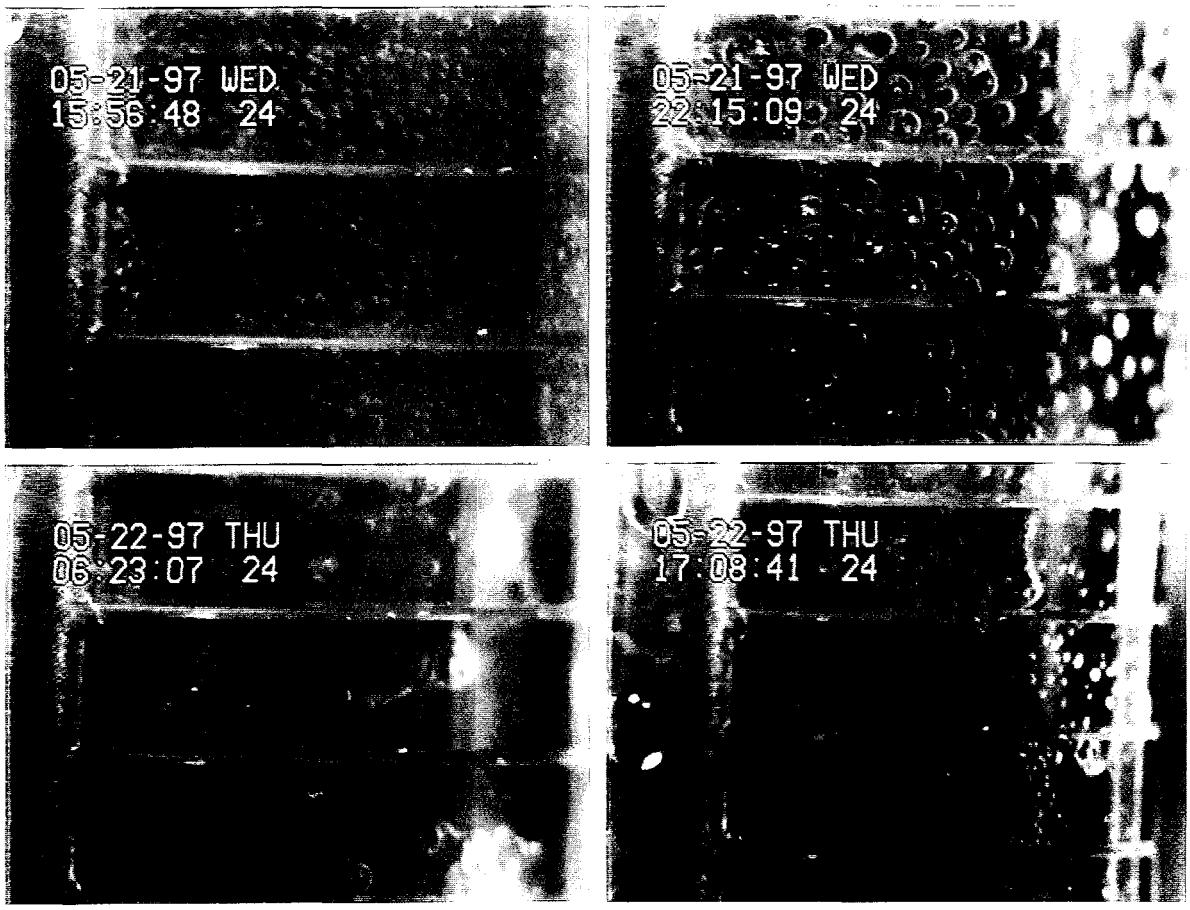

Figure 5.2. Gas Bubbles in AW-101 Composite 2 During an Ultimate Retention Experiment: (UL) Pre-Evacuation, 0% Growth; (UR) 9% Gas Growth; (LL) 18% Gas Growth; (LR) ~24% Gas Growth

9% (upper right), the typical bubble diameter increased to about 0.8 mm, and the bubbles are uniformly distributed in the field of view. Again, this is almost identical to the results of the buoyant retention experiment (Figure 5.1) at approximately the same gas content.

However, the ultimate retention experiment images at greater gas content are distinctly different. At 18% gas growth, both the visible bubble size and the bubble distribution are heterogeneous. Bubbles ranging from 250 μm or smaller to more than 3 mm are observed, and the larger bubbles are generally distorted from round. At the time the photograph was captured, the sample was in an initial gas release phase (as depicted in Figure 4.3). This suggests that a connected path to the waste surface, from some unknown depth, had been established, and the waste column likely attained this channeled structure via coalescence and bubble movement. Some evidence of channels is noted in Figure 5.2 (18% gas growth), where an apparently liquid-filled void nearly 5 mm long is observed in the lower left side of the photograph. At high gas content

(18–24% growth, lower photographs), the magnitude of the gas fraction is less obvious at the observable waste-vessel interface than at lower gas growth (9%); this again is indicative of an internal gas network. Interestingly, a second generation of small round bubbles, similar in size to those nucleated and grown during irradiation, is observed in the highest gas fraction image (~24% growth) shown in Figure 5.2. These bubbles apparently are the result of dissolution of dissolved species, diffusion to nucleation sites, and growth with pressure reductions.

5.1.2 Release Characteristics

Figure 5.3 shows a gas release from the same AW-101 Composite 1 sample photographed in detail in Figure 5.1. The pictures in Figure 5.3 were obtained at a growth gas fraction of 0.18 and 10 minutes before buoyant displacement at 0.19 growth gas fraction. In a span of 3 seconds, an approximately 4-mm-diameter gas bubble located 2.5–3 cm below the nonconvective layer surface and in contact with the vessel wall grew to more than 2 cm long and 1 cm wide (Figure 5.3 upper) and suddenly erupted out of the waste. Apparently, the smaller, initial bubble was connected to a channel that supplied gas for the rapid expansion. The waste was not strong enough to prevent the buoyant rise of this single bubble. The lower photograph in Figure 5.3 captures the released gas in a single bubble of nearly 1 cm diameter just prior to rupture at the liquid-air interface. The picture also shows the substantial deformation of the solid-liquid interface resulting from the bubble motion. Considering a simple force balance, the minimum yield strength of a material needed to retain a 1-cm-diameter bubble against a buoyant rise in a 1.4 g/mL density slurry is estimated to be about 27 Pa (Stewart et al. 1996; see also Section 4.2.1). Thus it appears that the upper portion of the waste sample shown in Figure 5.3 has a strength of this order and is consistent with visual comparisons to bentonite clay samples, as discussed with reference to Figure 5.1.

Figures 5.4 and 5.5 show the buoyant rise of bubble-laden nonconvective material in the same AW-101 sample from two perspectives. The first figure is a set of photographs taken at the upper surface level, which displays the rise of the nonconvective layer into the supernatant liquid over the period of about one minute. The first photograph in the series (upper left) was captured before any appreciable movement of the waste; the surface deformation on the left side of the solids layer resulted from the gas release indicated in Figure 5.4. Only a relatively small amount, less than 10% of the total retained gas volume, was released in the buoyant displacement depicted in Figure 5.4. Stewart et al. (1996) estimate that, in actual tank conditions, a supernatant liquid height about equal to the nonconvective layer thickness is necessary for buoyant displacement to have sufficient kinetic energy to release all the retained gas. Therefore, it is not surprising that only a small amount of gas is released during buoyant displacement in a laboratory experiment of small total height (~15.5 cm) and with a thin liquid layer (~2.2 cm).

In spite of the relatively lethargic appearance of the buoyant displacement from a gas release perspective, close-up images obtained from the middle of the nonconvective column clearly show activity throughout the waste volume. Detailed photographs taken synchronously with those of Figure 5.4 are shown in Figure 5.5. The full vertical scale of each quadrant in Figure 5.5 is approximately 1.8 cm, with demarcations every 0.5 cm. The second line from the bottom of each photograph is the 5.0-cm reference from the bottom of the sample. The upper left of the figure shows the bubble shapes and a relatively stagnant condition prior to the buoyant displacement. As in the 18% gas growth photograph reviewed earlier (Figure 5.1, lower right), bubbles ranging in diameter from about 0.5 to 4 mm are present with a typical size of ~2 mm. As shown in the upper right image of Figure 5.5, gas bubbles within the middle height of the solids layer, above the 5.0 cm reference line, were disappearing (coalescing, rising) in conjunction with the rise of the

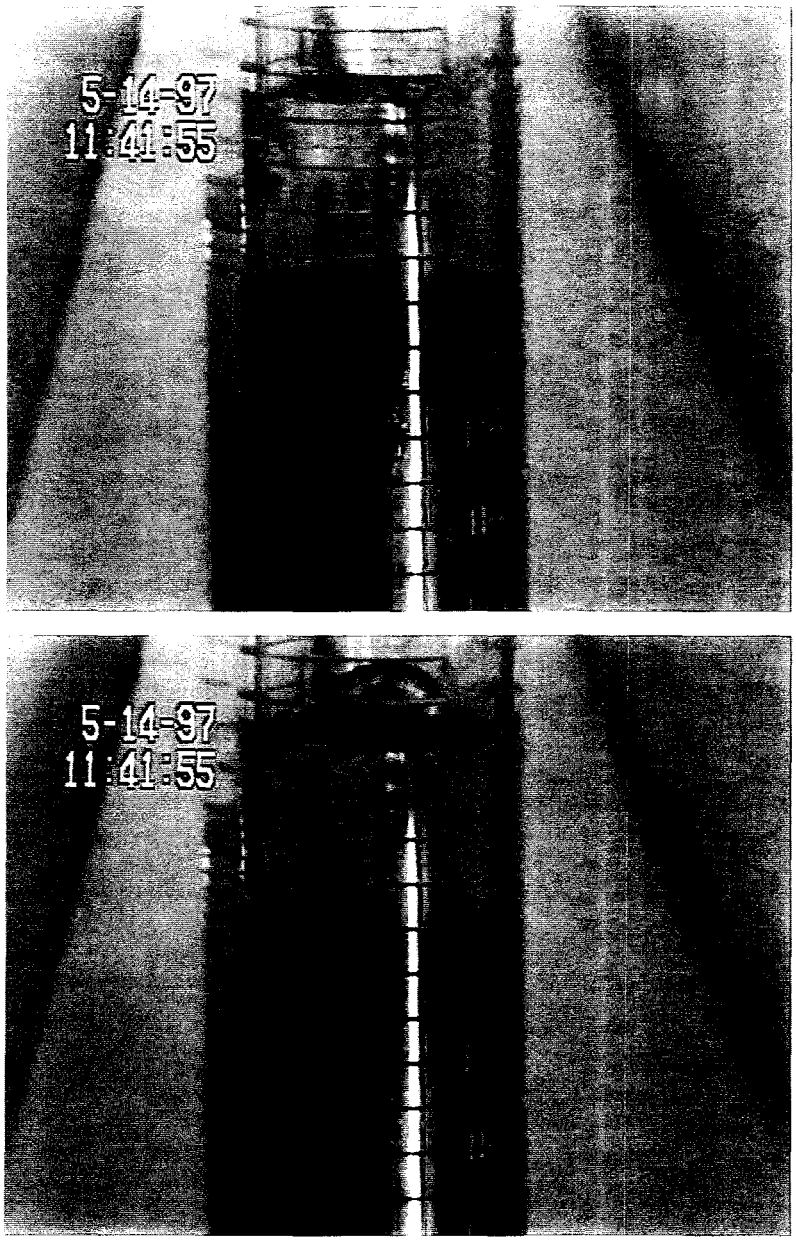

Figure 5.3. A Large Bubble Gas Release from AW-101 Composite 1 (upper) Just Before and (lower) Just After the Event

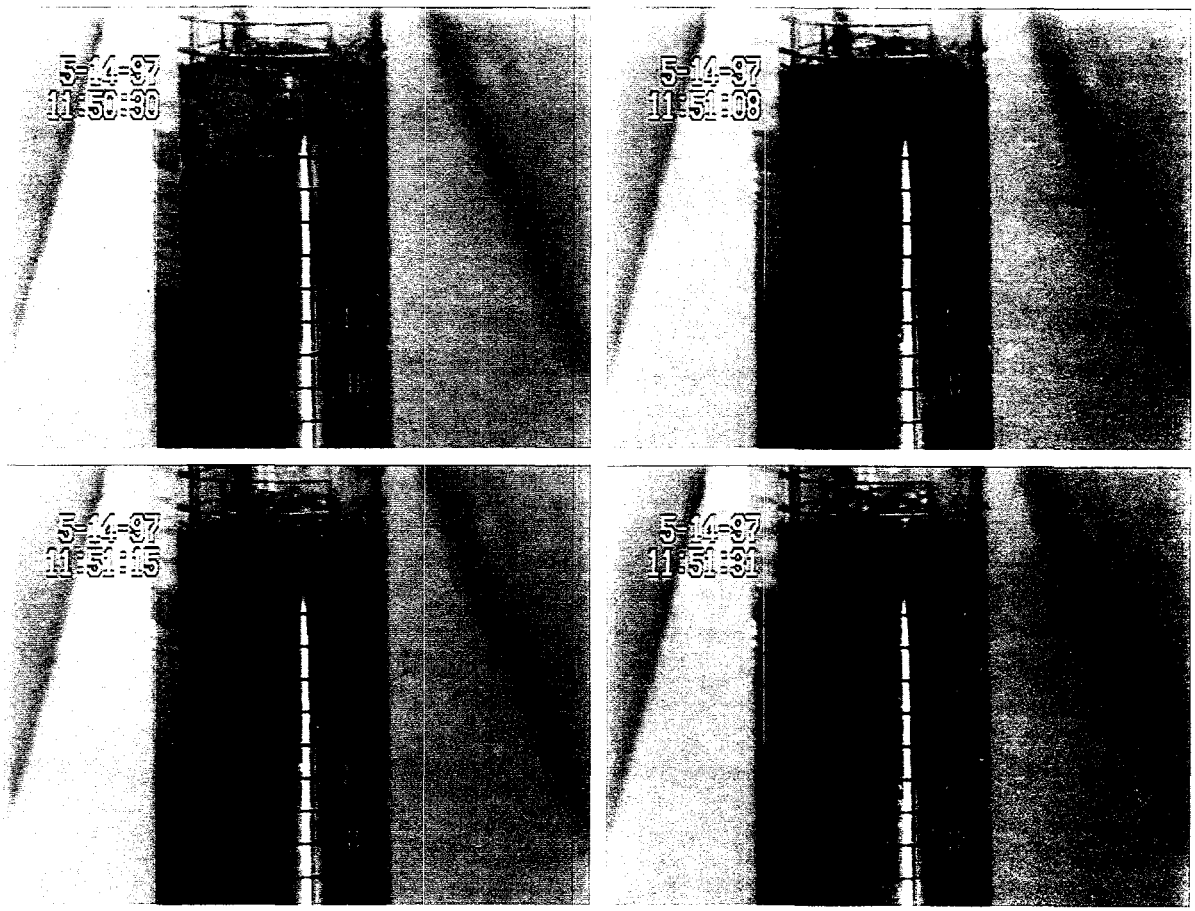

Figure 5.4. Surface View of AW-101 Composite 1 During the Rollover: (UL) Just Before the Event; (UR) After Some Rise in the Solids Layer; (LL) Solids Layer Approaching the Liquid Surface; and (LR) Solids Layer at the Liquid Surface

bubbly mass into the supernatant liquid. Below the reference line, the movement of gas bubbles was less pronounced. Note, for example, a group of bubbles in the lower left corner of each of the first two photographs in the series. Furthermore, in the video recording from which these photographs were captured, downward liquid convection (liquid infiltration) was obvious to just below the 5.0-cm reference at the time the photograph on the upper right was snapped. During the continued buoyant rise of the solids layer, waste deeper in the vessel became involved. In the lower left image of Figure 5.5, the group of bubbles (lower left corner) noted above is expanding and pushing upward. As the nonconvective layer reached the supernatant liquid surface, the bubble-laden solids layer was weakened enough that even relatively small bubbles (~0.5 mm) readily moved upward from below and through the camera's view (Figure 5.5 lower right).

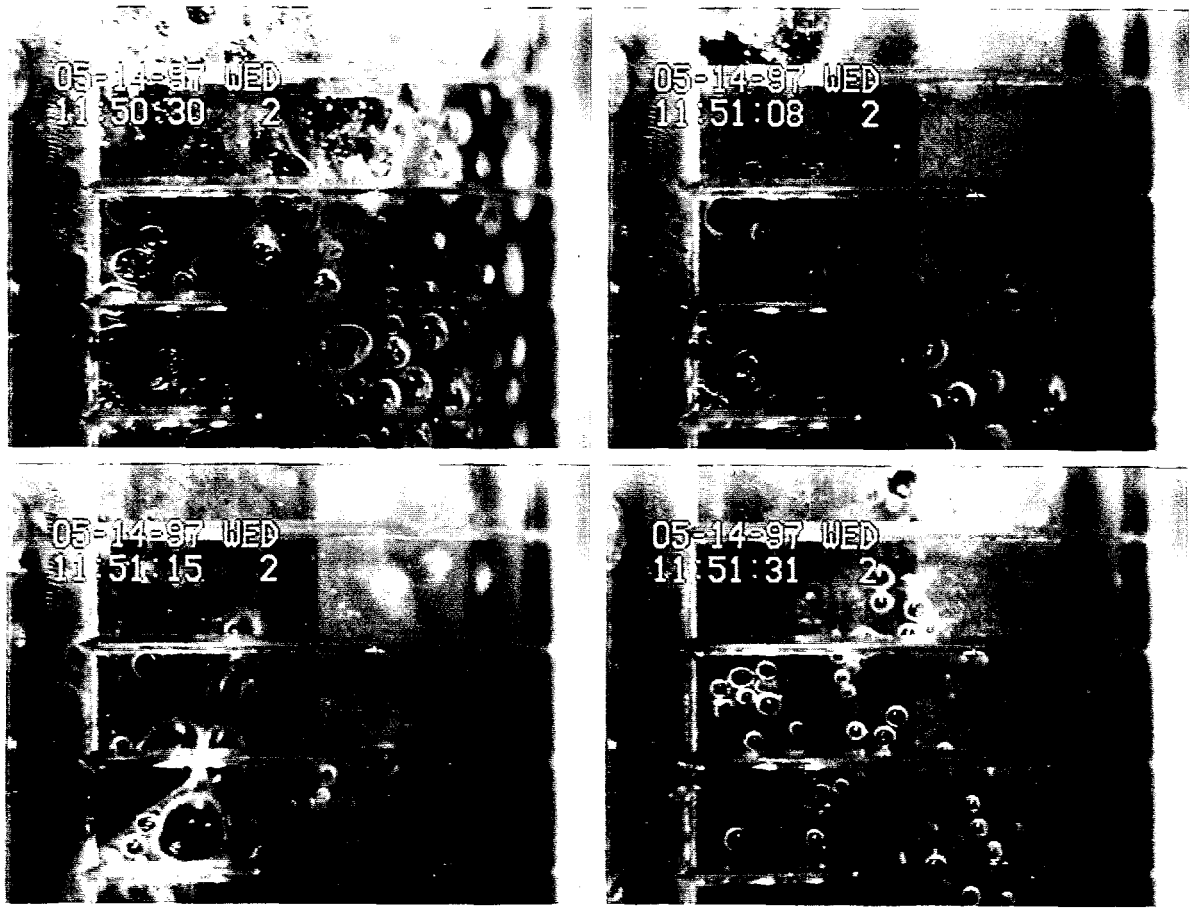

Figure 5.5. Close-Up of Gas Bubbles in AW-101 Composite 1 During the Rollover: (UL) Just Before the Event; (UR) Movement Above 5 cm Line; (LL) Movement Below 5 cm Line; and (LR) Migration of Small Bubbles Through Weakened Waste

5.2 AN-103 Composite

Photographic evidence of retained bubble shapes in the nonconvective layer of AN-103 Composite in both retention-to-buoyancy and ultimate retention experiments are provided in this section. The effect of experiment duration on the mechanism of gas bubble retention in neutral buoyancy tests is presented first. Section 5.3 contains a discussion of gas retention by foam and froth, as observed in the AN-103 experiments, and the armored bubble retention mechanism.

5.2.1 Effect of Experiment Duration on Retention Mechanism

Figures 5.6, 5.7, and 5.8 demonstrate the apparent effects of experiment duration on the mechanisms of gas retention in the AN-103 composite. Each of the figures includes four photographs: the upper left frame shows the irradiated waste prior to sample evacuation; the upper right image was taken at a growth gas fraction of ~0.08; the lower left photograph reveals bubble shapes at 0.14–0.15 growth gas fraction; and the lower right frame shows the bubble-laden nonconvective layer at still higher gas fraction (0.25–0.27), approaching maximum retention. Again, the camera in each test was set such that bubble detail images are obtained from near the (initial) middle of the nonconvective layer column, ~5 cm above the vessel bottom. Of course, as the sample retains gas, the relative distance of the fixed camera to the top surface of the nonconvective layer increases. When comparing the photographic evidence, it should be noted that the images in Figure 5.6 (1.3 cm vertical) are somewhat more magnified than those of Figures 5.7 and 5.8 (1.7 cm vertical). Where reported, the average bubble diameter was determined by measuring the visible dimensions of 10 randomly selected bubbles in each photograph, averaging the values, and normalizing by the measured width of the 0.5-cm line spacing.

The gas fraction at the vessel wall in the early to middle stages of the long-duration experiment (Figure 5.8) and throughout the two-hour and day-long experiments (Figures 5.6 and 5.7, respectively) appears to be very large. A quantitative analysis of the magnitude of the gas content adjacent to the walls was made as follows. If one assumes that the gas bubbles visible at the wall form a sheath of gas one average bubble diameter thick throughout the waste height, then a wall-bound gas content can be estimated. This method of analysis was applied to the sample depicted in Figure 5.6 for the three highest gas fractions shown. Bubble diameters of 0.6, 1.1, and 1.9 mm were estimated for gas growths of 8, 15, and 25%, respectively. Using the known nonconvective layer height corresponding to each of the gas fractions and the vessel diameter, the volume of material (gas and waste) contained in the bubbly sheath can be calculated. These volumes were estimated at 4.7, 9.0, and 17 mL (with increasing gas fraction). The corresponding measured sample growth volumes (retained gas growth) at the same times were slightly less, at 4, 7.9, and 15.7 mL, respectively. If all the sample growth volume is retained in the gas sheath, local gas fractions in the sheath of 85, 88, and 91% are estimated. These are in reasonable agreement with values (70–90%) estimated on the basis of visual observations alone. The analysis confirms that a significant gas volume in these AN-103 experiments was retained near the vessel wall and indicates nonuniformity in the radial distribution of gas through the waste column.

The images from the two-hour experiment (Figure 5.6) are very similar to those in the one-day test (Figure 5.7) at each gas fraction. The semblance of the behavior in these two tests is supported by quantitative gas retention results as well (Section 4.3.1). In both the two-hour and one-day experiments, a high density of small (~0.2 mm and smaller) round bubbles present following irradiation (0% growth due to evacuation) increase to ~0.6 mm at 8% gas growth and remain round (particle displacing). At still higher gas growth, the average visible diameter increases to ~1.1 mm at 14–15% gas growth and to ~1.9 mm at 25–27% gas growth. However, at these larger diameters, distortion of the bubbles from round is more apparent. The distortion in this case appears to be more a result of the close packing of bubbles (and froth strength) than a deformation resulting from the inherent strength of the AN-103 waste. The bubbly waste images, particularly at high gas fractions, indicate a highly lamellar structure where the bubble walls are composed of relatively thin layers of waste particulate and liquid.

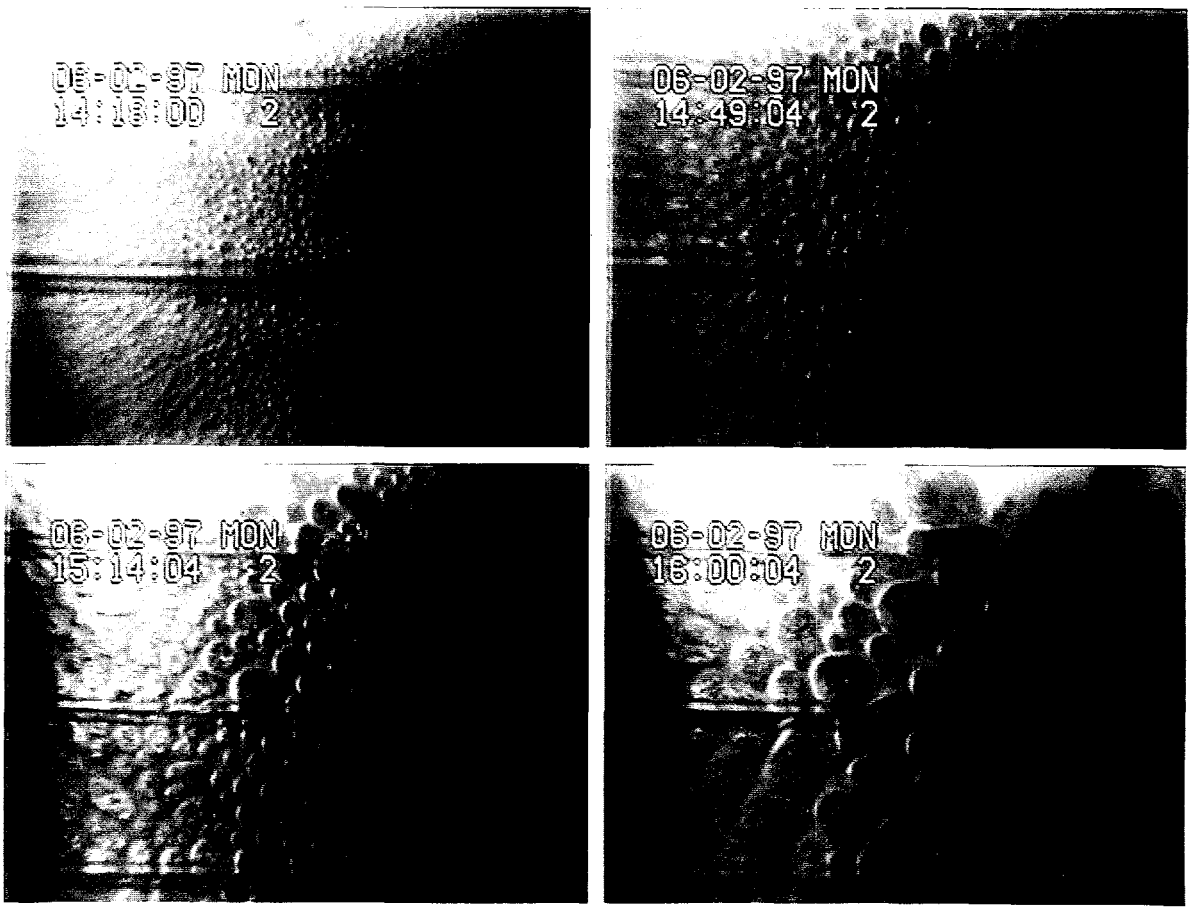

Figure 5.6. Gas Bubbles in the Two-Hour AN-103 Composite Experiment: (UL) Pre-Evacuation, 0% Growth; (UR) 8% Gas Growth; (LL) 15% Gas Growth; (LR) 25% Gas Growth

This phenomenon is believed to be related to the specific AN-103 chemistry (e.g., the type and amount of organic constituents) rather than an inherent feature resulting from the gas retention method. For example, Figure 5.9 is an image of Tank SY-103 nonconvective layer composite at approximately 21% gas growth and appears to have distinctly lower gas fraction at the vessel walls. This photograph is reproduced from the work of Gauglitz et al. (1996), in which a nearly identical gas retention system, including vessel fabrication material, was used. A similar irradiation procedure was also applied in the earlier experiment, although the total gamma dose in the current tests (~7 MR) is estimated to be about twice as large due to differences in the size and location of the cesium sources.

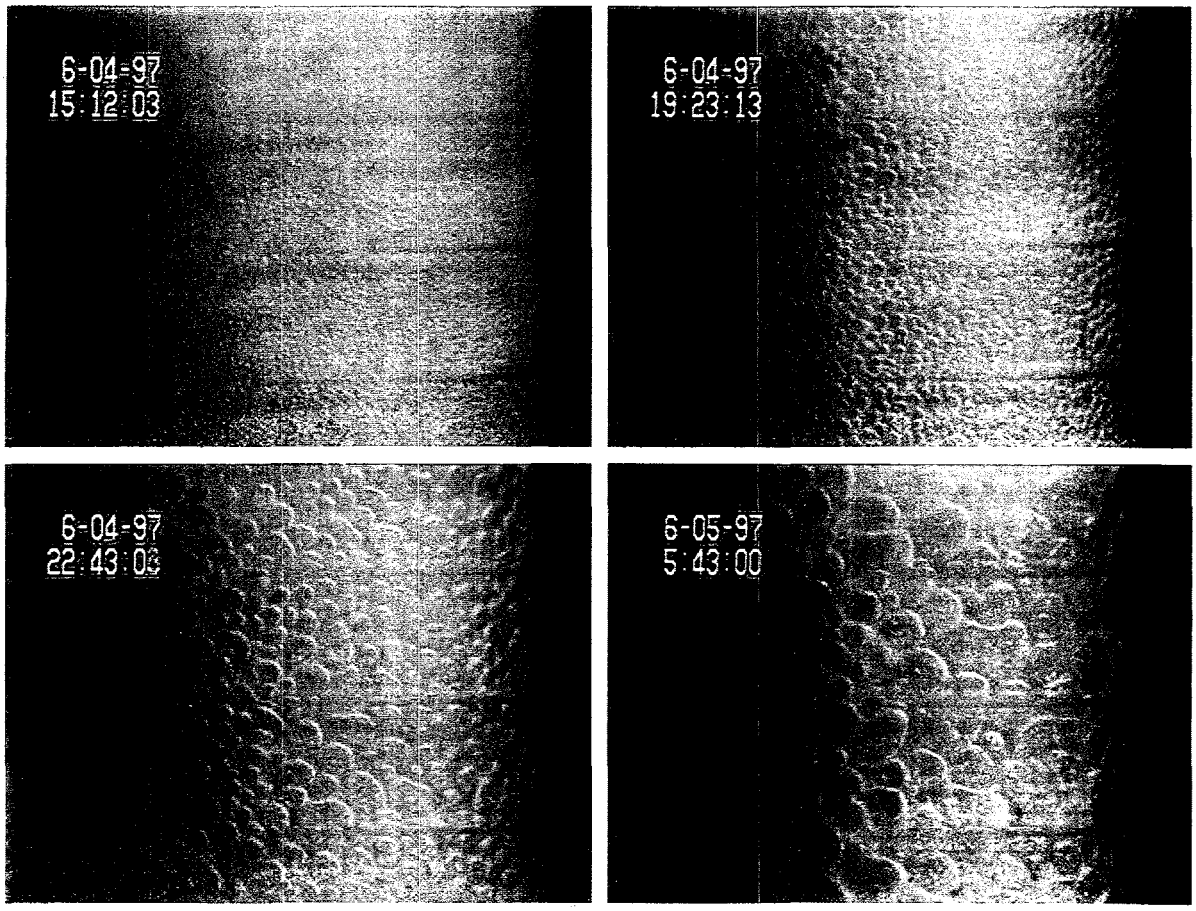

Figure 5.7. Gas Bubbles in the One-Day AN-103 Composite Experiment: (UL) Pre-Evacuation, 0% Growth; (UR) 8% Gas Growth; (LL) 14% Gas Growth; (LR) 27% Gas Growth

In the four-day AN-103 experiment, both the quantitative and visual gas retention data deviate from the shorter experiments. Through 15% gas growth, the images from the three experiments (Figures 5.6–5.8) are outwardly similar. On closer examination, however, the average bubble diameter in the four-day test shown in Figure 5.8 appears to be greater at both 8% gas growth (0.7 versus 0.6 mm) and 15% gas growth (1.9 versus 1.5 mm). The relative coarsening of the bubbles in the longer experiment may reflect slow dynamics for bubble coalescence in the waste type. At 26% gas growth, distinctions in the four-day experiment are clearly obvious. The bubble size distribution shown in Figure 5.8 is very nonhomogeneous, with bubbles as large as 3.8 mm and smaller than 0.3 mm readily visible. The smaller bubbles appear to be second-generation, likely resulting from dissolution of liquid dissolved species into gaseous nucleation sites during evacuation. The wall surface density of gas is much more appropriate for the gas

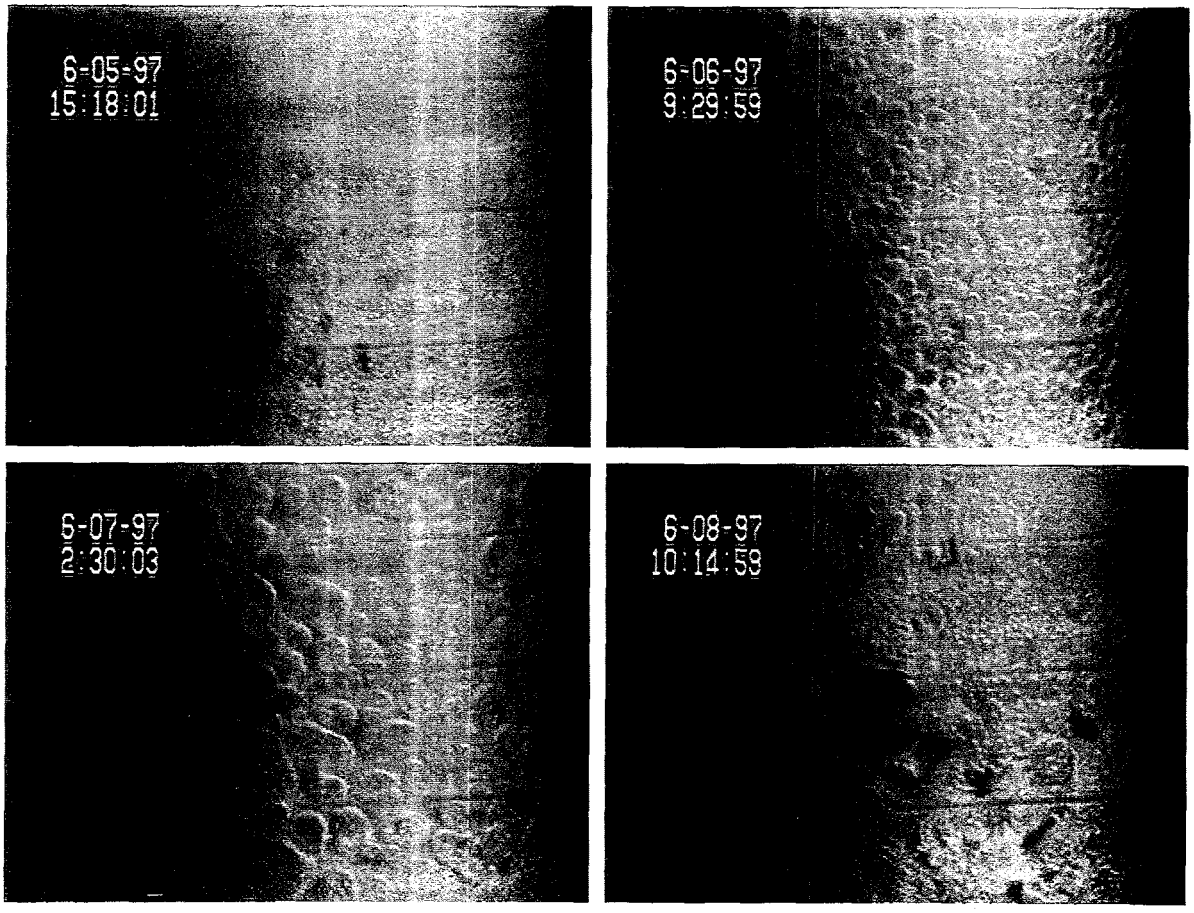

Figure 5.8. Gas Bubbles in the Four-Day AN-103 Composite Experiment: (UL) Pre-Evacuation, 0% Growth; (UR) 8% Gas Growth; (LL) 15% Gas Growth; (LR) 26% Gas Growth

content within the sample, and it suggests that considerable retained gas either migrated (out of camera view) up the vessel wall or moved into the core of the sample. The reduced density of gas at the wall may also contribute to the reduced wall effects noted in the long test (Section 4.4). As discussed in more detail in Sections 4.3 and 4.4, differences in the AN-103 four-day test from the two-hour and one-day tests cannot be conclusively attributed to differences in experimental duration due to AN-103 composite inhomogeneities.

In Figure 5.8, the remaining visible large bubbles show a slightly distorted-round shape, similar to that observed in moderate strength (~67 Pa) bentonite clay simulants at high gas fraction (Gauglitz et al. 1996). The data suggest strengths in the bubble-laden AN-103 composite on the order of 100 Pa, more than an order of magnitude weaker than the measured shear strengths of the component materials prior to compositing.

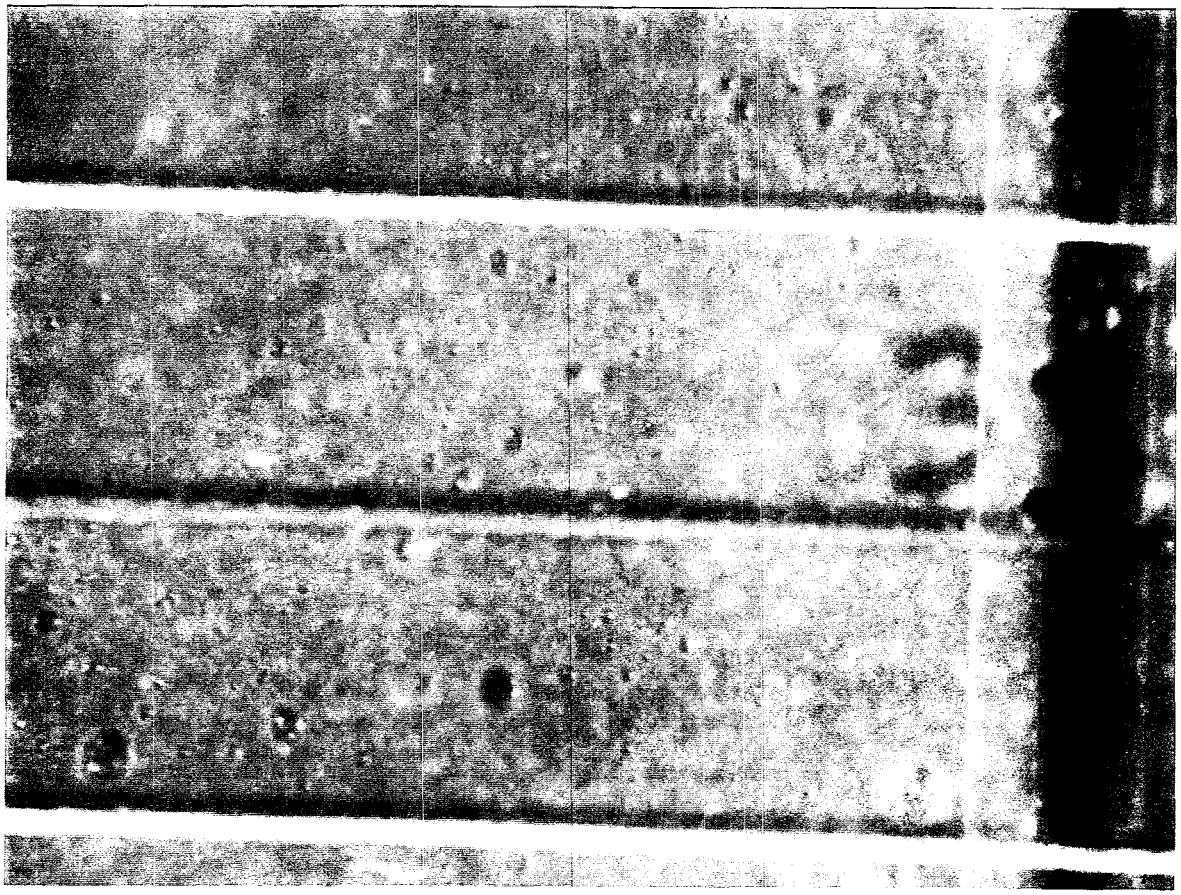

Figure 5.9. Gas Bubbles in Tank SY-103 Nonconvective Composite at ~21% Gas Growth

5.2.2 Retention Mechanisms in an Ultimate Retention Experiment

As shown in Figure 5.10, the gas retention characteristics in the AN-103 composite ultimate retention experiment were different than those observed in the retention-to-buoyancy experiments. Because the ultimate retention vessel (#9) was the last one filled in the vessel loading process, it is likely the least homogeneous of the AN-103 samples. In addition to a relatively high nonconvective layer density (1.86 g/mL), a slug of relatively strong cohesive material (i.e., stiffer than soft-serve ice cream) was observed while filling the vessel. This likely contributes to the unique and varied bubble shapes in that sample. Figure 5.10 includes two images centered at ~4.3 cm above the bottom of the vessel, one captured at a gas growth of 9% and the other at 27%. Although not shown in the figure, the bubble sizes and distribution after irradiation and before evacuation were similar to those observed in the other AN-103 tests. However, as the gas content increased, the distinctive character of the experiment became apparent. At a gas fraction of only 9%, a much greater variation in bubble sizes is noted with a few bubbles >2 mm in diameter and the majority closer to 0.6 mm. In some regions of the photograph, bubbles on the order of

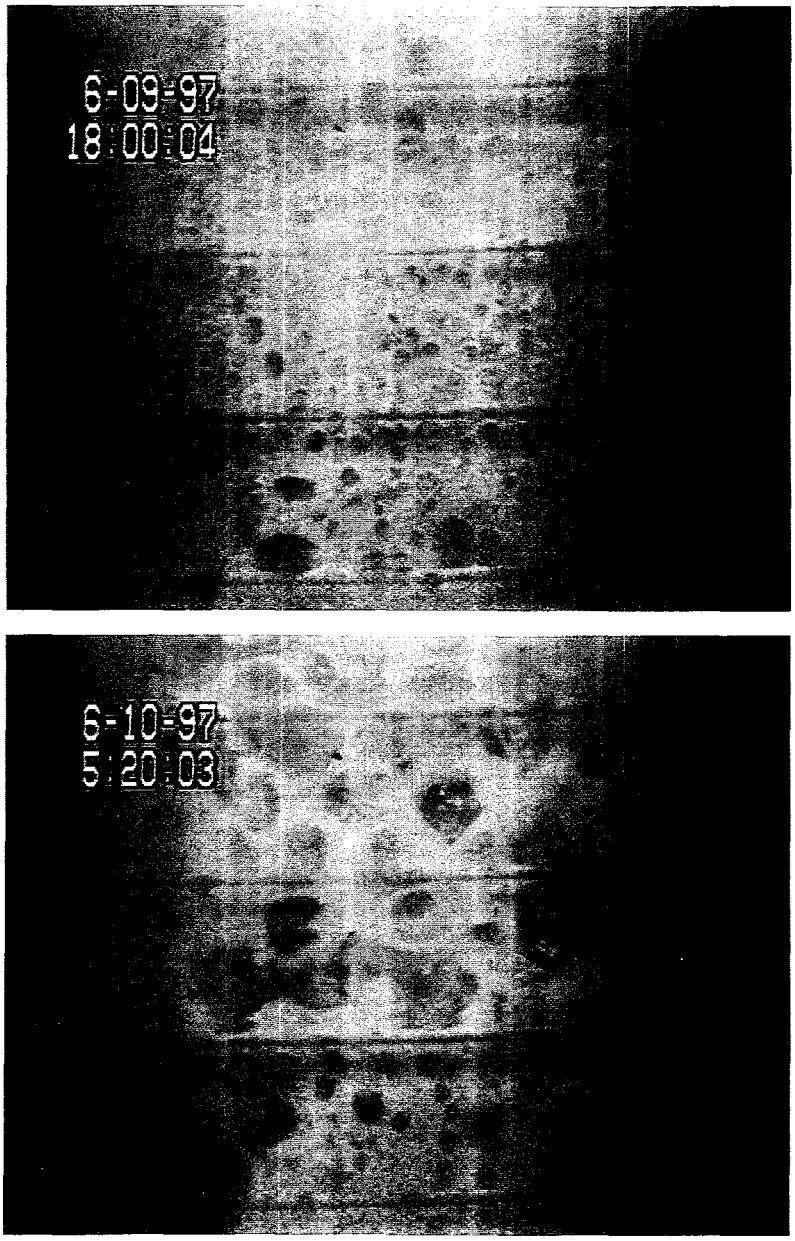

Figure 5.10. Gas Bubbles in AN-103 Composite During an Ultimate Retention Experiment: (upper) 9% Gas Growth; and (lower) 27% Gas Growth

1 mm diameter are clearly distorted from round, and this deformation appears to be the result of material strength as opposed to the close packing of bubbles. The lack of uniformity of bubble sizes and shapes is even more pronounced at 27% gas growth. For example, near the center of the lower photograph in Figure 5.10, a rather long (~9 mm) and narrow (<2.5 mm) horizontal bubble (or pair of bubbles) with round and angular surfaces dominates, suggesting a relatively high

material strength, perhaps greater than 100 Pa, in the vicinity. Other distorted round bubbles approximately 2 mm in diameter occupy the upper field of view, and a region of smaller round bubbles (< 1 mm) is observed in the lower areas of the image.

5.3 Foam, Froth, and Armored Bubbles

In a previous investigation,[a] the ability of SY-103 waste particles to armor bubbles and create stable froths was studied. To probe bubble armoring, froths were created by sparging gas through SY-103 supernatant liquid containing various amounts of SY-103 waste particles, and their stability (lifetime) was monitored. The froths were consistently short-lived (less than one hour), and it appeared that relatively little bubble armoring occurred. The armored bubble retention mechanism and its relationship to gas retention in Hanford tank wastes have been studied at a more fundamental level by Rossen and coworkers (Rossen and Kam 1996; Rossen and Das 1995). Although, the ability of particles to armor bubbles has been demonstrated, it is generally believed that the armored bubble retention mechanism plays a relatively minor role in the overall retention of gas in Hanford tank wastes. In the AN-103 waste samples much more stable froths were observed, although controlled frothing experiments for quantifying armored bubble creation were not conducted.

As shown in Figure 5.11, stable foams were observed in AN-103 composite samples. Apparently gas bubbles were entrained in the composite during homogenization and were decanted into the sample vessels. The foam creamed on top of the supernatant liquid layer and remained stable throughout a more than three-week settling/irradiation period and the sample evacuation. The image in Figure 5.11 was captured before evacuation started. The stability of the 2–3 mm-thick layer of foam is clearly dependent on the waste chemistry. For example, compare Figure 5.11 with the liquid-gas interface of an AW-101 composite sample shown in Figures 5.3 and 5.4. Prior to the gas release in Figure 5.3, only a few gas bubbles pinned near the intersection of the vessel wall and the liquid-gas interface are present. After gas releases, in both figures, the number of bubbles at the interface increases, but the number of bubbles is clearly less than in the AN-103 foam, and the bubbles in the AW-101 composite were relatively short-lived. The stability of foam in the AN-103 samples may be related to the relatively thick crust observed in that tank (Meyer et al. 1997).

Figure 5.12 shows the expansion of the initial stable foam (Figure 5.11) resulting from sample evacuation. At the time the photograph was taken, the system pressure was nearly 84 mm Hg, and the nonconvective layer growth gas fraction was approximately 0.25. Of particular interest in the upper image are the domed shape of the foam and the attachment of bubbles on the walls in the upper liquid region. The shape of the foam layer suggests a strong interaction of the foam with the vessel walls, which limits the upward rise (expansion) of the foam near the wall. The adhesion of individual gas bubbles of ~1 mm diameter in the middle to upper liquid layer also indicates strong interaction of gas with the vessel surface. The sudden transition in the liquid layer from essentially no bubble attachment (lower liquid) to a relatively dense region of attachment coincides with the initial, pre-evacuation interface of the supernatant liquid and dome space gas. The walls were apparently populated with the gas bubbles during earlier, small gas releases at lower overall sample height, when the bubbles were trapped below the foam layer. The data indicate poor wetting of the vessel walls by the AN-103 convective liquid.

(a) A draft PNNL report entitled "Bubble Retention by Armored Bubbles: Results for Hanford Waste Tank 241-SY-103" by Gauglitz and coworkers summarizes an experimental study conducted in 1996.

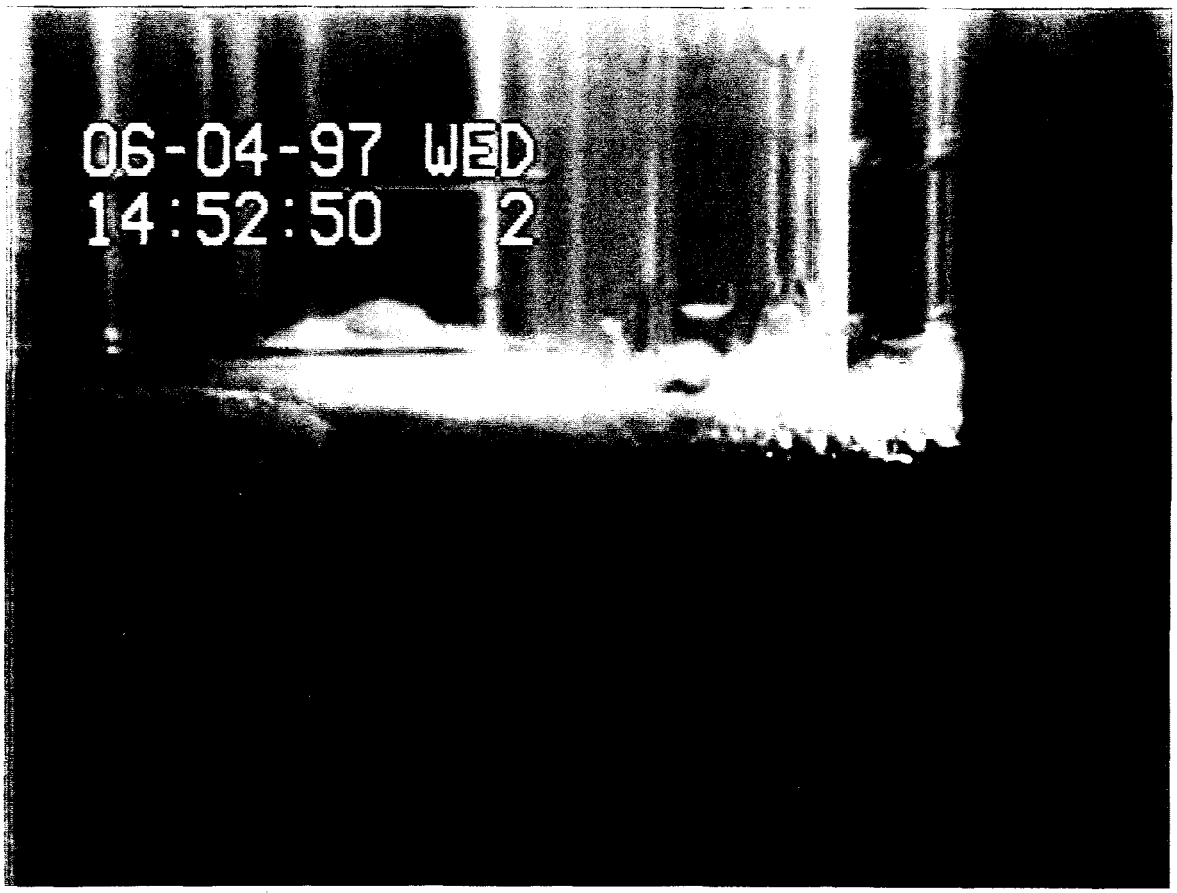

Figure 5.11. Stable Foam Atop Supernatant Liquid of AN-103 Composite Before Evacuation

The lower image in Figure 5.12 was taken at a system pressure of 59 mm Hg, long after the solids layer became neutrally buoyant (64 Pa) and attained maximum retention. In fact, the sample continued to expand beyond the point of neutral buoyancy as the pressure was further reduced, and this is depicted in the photograph. The waste structure is layered, consisting of a gas/solid/liquid froth, dynamically stabilized by the reduced pressure of the evacuated system, underneath the foam cap; below the froth (not shown in the photograph), the now more dense liquid was pooled. There appears to be a gradation in bubble sizes within the froth layer with the smallest diameters just below (and in) the foam, progressing to bubbles ~2 mm and larger deeper in the waste. This indicates increased bubble stabilization in the upper froth and increased bubble coalescence in the less-stable lower regions, where the liquid fraction is expected to be higher due to drainage.

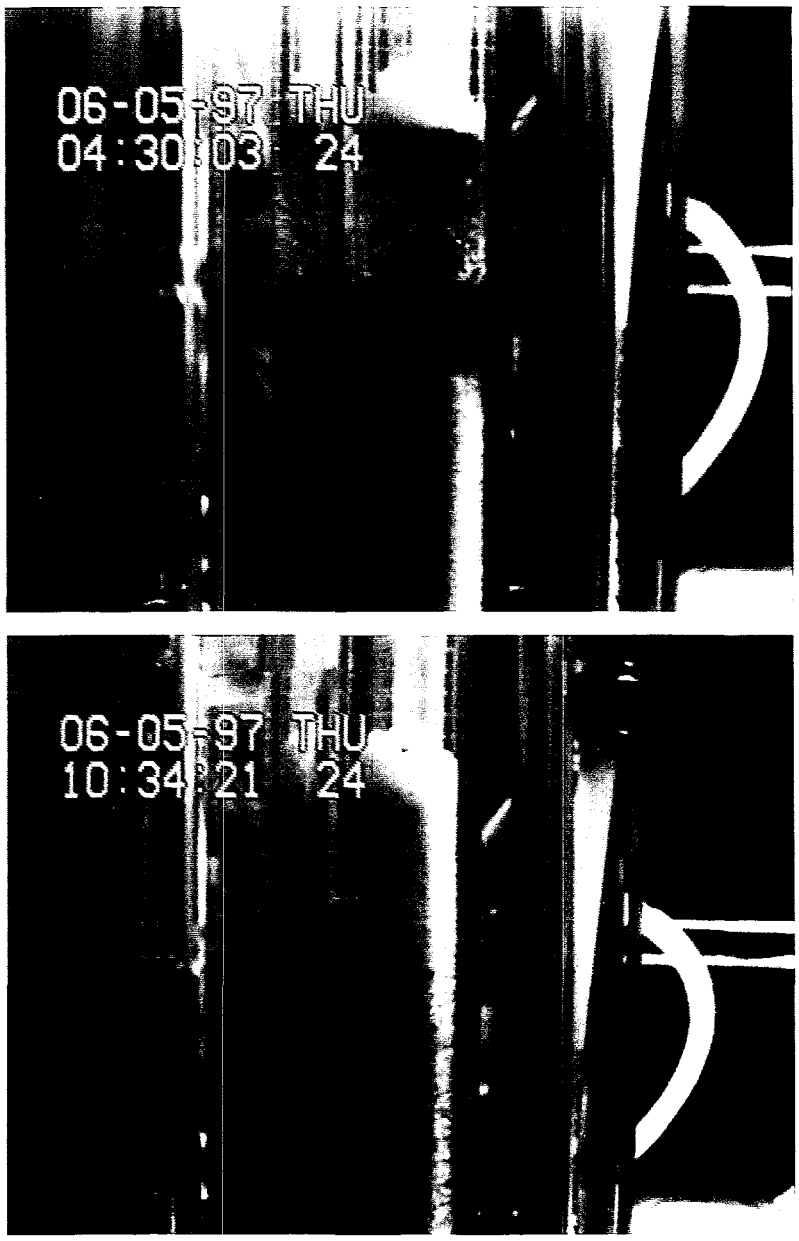

Figure 5.12. Foam and Froth in the AN-103 Composite During Evacuation: (upper) Expanding Foam Atop the Supernatant Liquid; and (lower) Buoyant Waste Froths Below a Foam Dome

6.0 Summary: Present, Past, and Future

In the current study, the mechanisms of gas bubble retention and release were investigated experimentally using two additional waste types from Hanford Tanks AW-101 and AN-103. These studies follow on our previous investigations of Hanford wastes, including S-102 and SY-103 (Gauglitz et al. 1996; Bredt and Tingey 1996) and SY-101 (Bredt et al. 1995). In Section 6.1 the current experimental results are summarized. These results are placed in the context of the previous laboratory gas retention studies, including simulated waste experiments, in Section 6.2. Section 6.3 then addresses some experiments needed in the future to refine and solidify our understanding of gas retention and release mechanisms in Hanford tank wastes.

6.1 Summary of AW-101 and AN-103 Experimental Results

The mechanisms of gas bubble retention and release in AW-101 and AN-103 samples were quantified through waste level and other measurements. Photographic evidence of retained gas bubbles supports those findings qualitatively. The following are our conclusions:

- AN-103 and AW-101 waste types retained gas in particle-displacing bubbles. These bubbles were typically round when small but tended to be slightly distorted from round at 1 mm in diameter or larger. The data indicate a moderate material strength in each waste type, probably on the order of 75 Pa. Somewhat more deformed and elongated bubbles were observed in a portion of the AN-103 ultimate retention sample, indicative of a region containing higher-strength material.

- Stable foams, potentially resulting from an armored bubble retention mechanism and a viable pathway to crust formation, were observed atop the supernatant liquid in the AN-103 composite retention-to-buoyancy experiments. In addition, once the samples attained neutral buoyancy, the buoyant mass formed a froth that continued to retain more gas and expand with pressure reductions.

- Unusually high gas fractions (0.8–0.9) near the vessel wall were observed in the AN-103 retention-to-buoyancy experiments. This phenomenon appears to be intimately linked to the attachment of bubbles to the vessel walls and the excess gas content when the samples attained buoyancy.

A limitation of some earlier gas retention results is that the tests were run too quickly. It is speculated that longer experiments would result in a wider distribution of bubble sizes more realistic of actual tank conditions. A primary focus of the current experiments was to evaluate the effects of experiment duration and waste growth rate on gas retention behavior. To effect a specified growth rate, a new electronic vacuum pressure control system was developed and pressure programs were applied such that linear sample growth rates were attained (in the absence of gas release). The following results were obtained:

- In two-hour, half-day, and one-day AW-101 retention-to-buoyancy tests, the maximum gas fractions were essentially equal. However, gas release behavior was varied: the nonconvective layer became buoyant in the supernatant liquid only in the most quickly evacuated sample; but the gas release rate (as a function of pressure) following maximum retention was greatest in the slowest (one-day) experiment. One day was established as the new standard for these evacuation gas retention experiments, superseding the previous two-hour standard.

- In the AN-103 retention-to-buoyancy tests, higher maximum gas growth was observed in the two-hour and one-day experiments than in the four-day test. In addition, more gas release activity prior to maximum retention was evident in the longer AN-103 test. However, because of inhomogeneities in the AN-103 composite sample, differences in the AN-103 four-day test from the shorter tests cannot be attributed conclusively to variations in the experiment duration.

Wall effects influenced the extent of gas retention in both AW-101 and AN-103 retention-to-buoyancy experiments, and the interaction strength between the waste samples and the vessel walls was quantified:

- In AW-101 Composites 1 and 2 tests, maximum gas volume growth of 19% was observed, and only 9% growth was expected to reach neutral buoyancy. A wall/sample interaction strength of 9–10 Pa was calculated to account for the excess retained gas.

- In the two-hour and one-day AN-103 experiments, a maximum 30–32% gas volume increase to neutral buoyancy was measured, and only 15–16% growth was predicted from density data. The excess gas retention was attributed to a 16–19 Pa wall effect. In the four-day AN-103 experiment, the deviation of the expected (20%) and measured (28%) maximum gas growths was considerably less. This corresponds to a lesser apparent wall interaction strength of 8 Pa. Additionally, in the long AN-103 test, the initiation of a slow buoyant rise of the nonconvective layer was detected at a gas volume increase of 22% or less, in very good agreement with the predicted neutral buoyancy gas content.

The ultimate retention of each of the waste types was determined by removing the supernatant liquid layer and thereby eliminating the buoyant rollover as a mechanism for gas release.

- A maximum gas growth of 37% was measured in the AN-103 ultimate retention experiment, and only 28–32% gas growth was observed in the retention-to-buoyancy tests. The AW-101 ultimate retention maximum gas growth (22–27%) was also greater than in the corresponding retention-to-buoyancy experiment (19%). Interestingly, a pressure upset during the AW-101 ultimate retention experiment caused a very rapid gas release, resulting in a relatively large retained gas decrease from 17 to 5% of the nonconvective layer volume.

- The maximum absolute gas content in all the AW-101 and AN-101 waste samples tested is 2–4% higher in gas than the reported maximum growth gas content owing to gas present in the samples before sample evacuation. The minimum initial nonconvective layer gas content due to sample irradiation was 2–3%, and the maximum initial gas content determined from initial growth rates ranged from 3 to 5%.

6.2 Gas Retention Mechanisms: Summary of Current and Previous Investigations

Figure 6.1 summarizes the current and previous experimental investigations of gas retention mechanisms in numerous Hanford tank wastes and several simulated waste types. The montage includes photographs of gas bubbles in various samples and locates the wastes on a Bond number plot. The plot classifies the bubble retention mechanisms based on the three dimensionless groups discussed in Section 1.3. Many of the parameter values used to place the wastes on the Bond number plot are estimated. Some uncertainty in the parameter values was also allowed, and this is reflected in the oval window of data values, instead of a single datum, for each waste type. The selected parameter values for each of the actual waste types represented in the Bond number

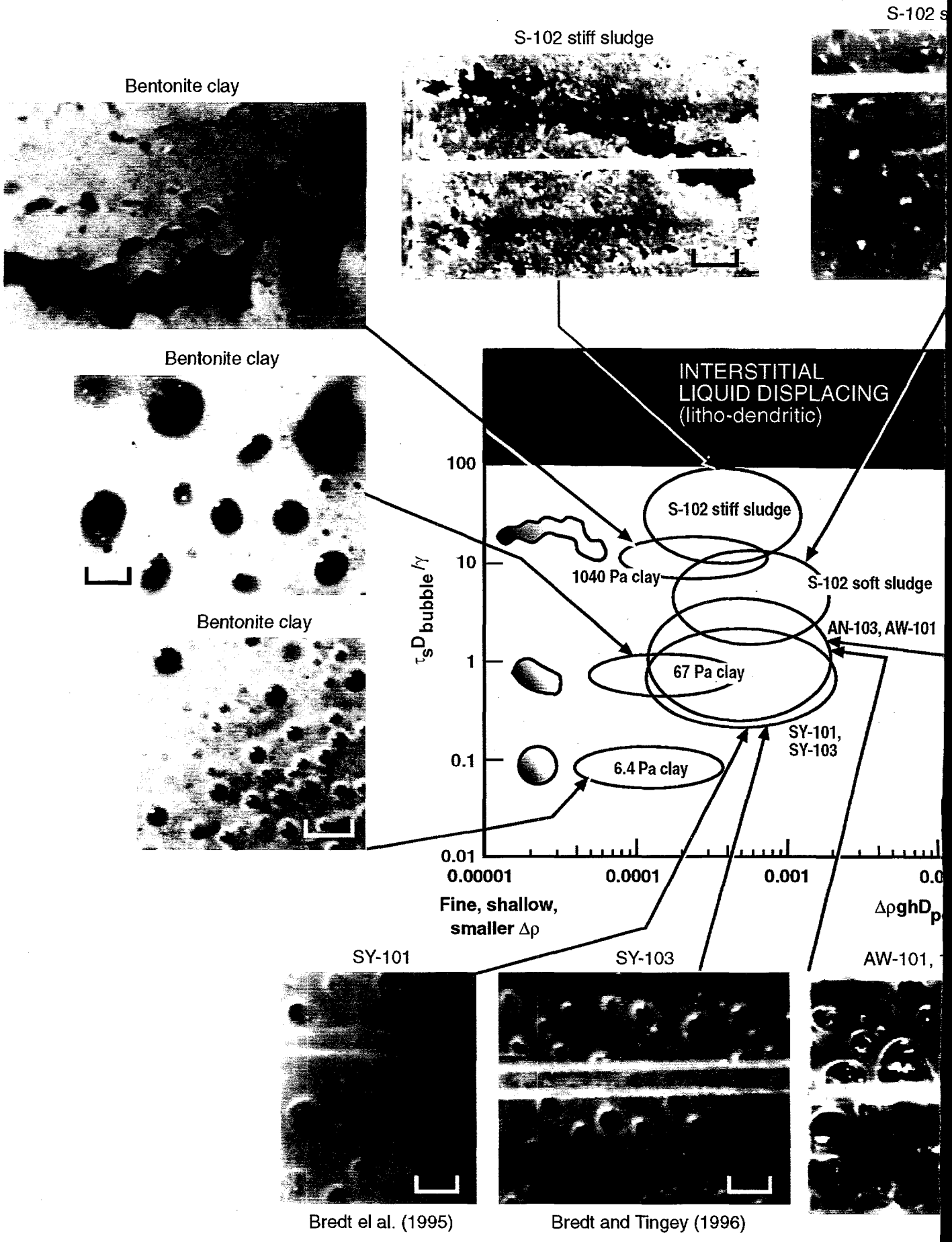

Bredt el al. (1995)

Bredt and Tingey (1996)

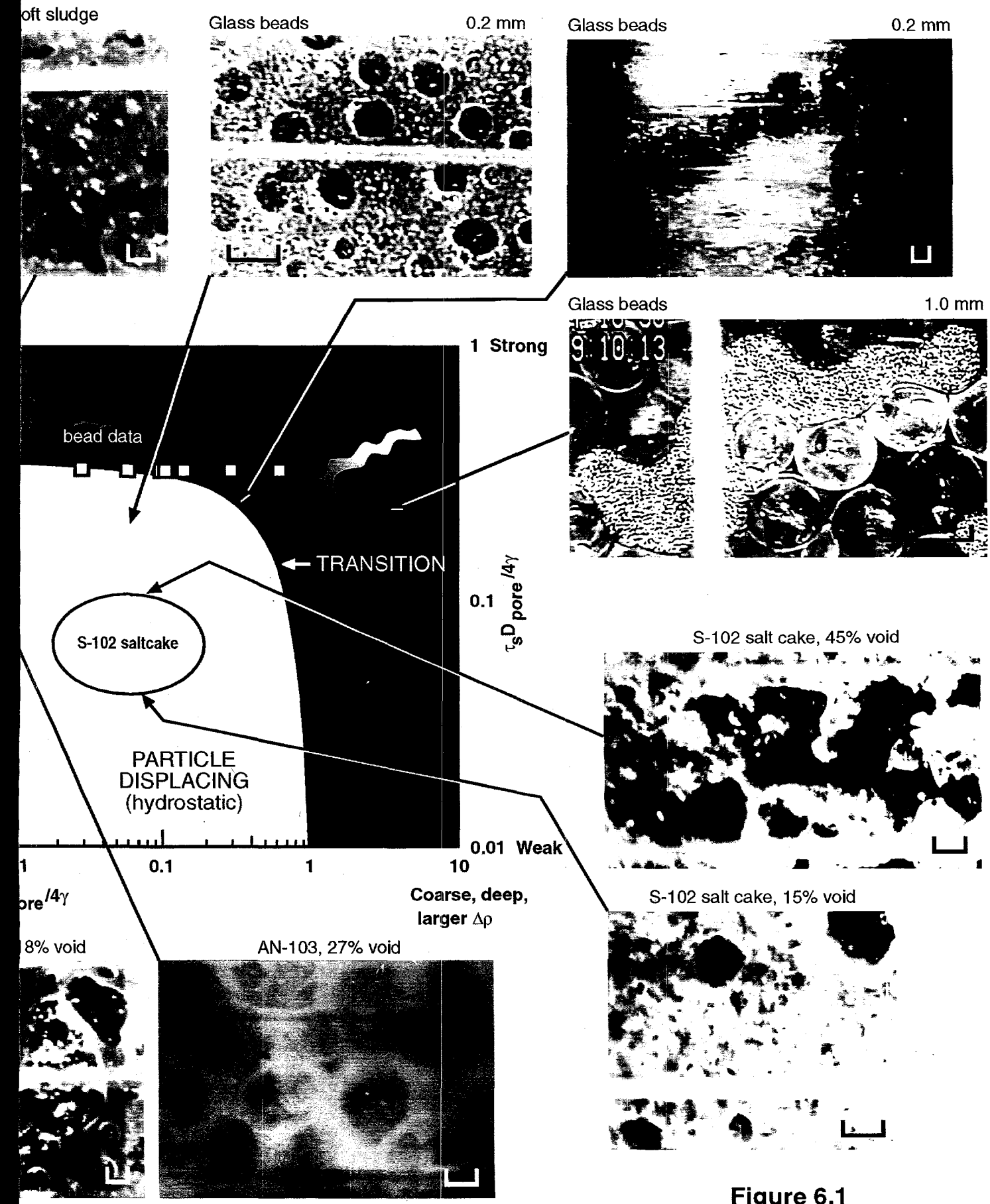

Figure 6.1
Gas Bubble Retention Mechanisms

depicts 1 mm

SG97070054.1

plot are tabulated in Appendix C. Considering the degree of uncertainty in estimating the parameter values for actual wastes, which may exceed the bounds depicted, the analysis should be deemed semi-quantitative at best. The relative positions of data are, in general, soundly based. The main function and benefit of the figure is to succinctly summarize a breadth of qualitative visual and quantitative parameter data.

The dominant mechanisms of gas bubble retention are yield strength retention for particle-displacing bubbles and capillary retention for interstitial liquid-displacing bubbles. The particle-displacing bubbles are located in the yellow region of Figure 6.1 and the interstitial liquid-displacing bubbles are located in the blue region. All of our actual waste results, including the results for AN-103 and AW-104, show particle-displacing bubbles. The AN-103 and AW-101 waste samples demonstrated gas retention behavior similar to those in earlier SY-101 and SY-103 tests. Bubbles of the order 1 mm and larger were a somewhat distorted round shape. The bubbles in AN-103 demonstrated somewhat greater shape deformity, so this waste type (along with AW-101) is placed at a higher vertical position on the map to denote the apparently higher material strength. The previously examined S-102 sludge samples clearly were stronger materials, because the retained gas bubbles were highly compressed dendritic entities, much like those observed in strong bentonite clay simulants.

To date, in our laboratory, interstitial liquid-displacing bubbles have been observed only for simulated wastes made up of sands (Gauglitz et al. 1994b) and glass or polymethylmethacrylate (PMMA) beads of varying diameter (Gauglitz et al. 1995) in water. In these relatively large-particle and high-density difference systems, transitions were observed from interstitial liquid-displacing bubbles deeper in the waste to round, particle-displacing bubbles nearer the liquid surface. The transition data for the glass and PMMA bead experiments are shown in Figure 6.1. In actual waste experiments, only particle-displacing bubbles have been observed, and the visual evidence is summarized in the figure. Neither the actual waste properties (i.e., difference in non-convective layer and interstitial liquid densities; particle size) or the experimental conditions (shallow waste depth) used in laboratory tests thus far have been conducive for observing interstitial liquid-displacing bubbles.

It should be emphasized that the locations of the simulated and actual waste types on the Bond number map are based on the laboratory experimental conditions under which the retention mechanisms were actually observed. Under actual tank conditions, it is likely that certain waste types retain gas by the interstitial liquid-displacing bubble mechanism at sufficient depth. A plausible example is S-102 saltcake waste. In the laboratory, the sample (observation) depth, h, is small (typically ~0.1 m), whereas actual tank waste depths can be one to two orders of magnitude larger. By increasing the depth a hundred-fold, the experiment-based abscissa values shown for S-102 saltcake would be shifted to greater than one, above the transition line. The other waste types shown in Figure 6.1 would be similarly affected by increasing waste depth, but it is less likely that these other materials give interstitial liquid-displacing bubbles. For other than S-102 saltcake, it is estimated that three to four orders of magnitude greater waste depth (100-1000 m) would be required.

The majority of the actual waste data presented in Figure 6.1 are isolated to a narrow band of abscissa values (~0.0005), primarily because an identical pore diameter (~particle diameter) of 1 μm was assigned for all the actual wastes except for the S-102 saltcake (100 μm). A much greater divergence in the ordinate values is depicted, corresponding to large variations in both material strengths and bubble shape distortion.

6.3 Future Direction

The summary map (Figure 6.1) helps to identify gas retention regimes and waste types where additional studies are required to solidify our understanding of the primary gas retention mechanisms in Hanford tank wastes. In our review of existing actual waste experimental gas retention data, a particularly notable deficiency was the lack of evidence of retained interstitial liquid-displacing bubbles. To this end, experiments are needed to provide an actual waste example of retained gas bubbles in the capillary retention regime. To date, experimental waste samples have been too small (short) to observe anything but the particle-displacing bubbles. Due to limitations on the amounts of available actual waste and practical restrictions on the height of an actual waste experiment, it is proposed to mimic a tall waste sample by placing a static load on top of a non-convective layer during a gas retention experiment. To probe the effect of waste depth on the transition from interstitial liquid-displacing to particle-displacing bubbles, the load would be varied. In support of this endeavor, particle size data and other physical property information on the waste are needed to be able to model the behavior better.

Although waste characteristics may be such that they appear to represent nearly identical gas retention behaviors when shown in Figure 6.1, each waste is unique and presents fresh information. For example, SY-103 and AN-103 wastes overlap in the Figure 6.1 plot, but this does not depict the unique foaming characteristics of the AN-103 material and the relatively weak foam stability in SY-103. In addition, the summary plot does not convey information about the maximum gas retention of the various waste types. To provide a broad basis for understanding bubble retention mechanisms and maximum gas retention, experiments are necessary on many additional significant waste tank samples. Preferably these will be selected from different waste tanks of highest priority to the Flammable Gas Project. The improved understanding gained from these tests would be valuable to SCOPE because it it would provide a basis for estimating the uncertainty and variability in retained gas among tanks and the range of likely releases and release mechanisms. Since the gas retention experimental approach described here provides quite reproducible results, we suggest increasing the number of unique sample types and reducing the number of replicate analyses. However, it must be emphasized that a unique sample does not need to come from a distinct waste tank. A wide variety of waste physical properties and gas retention behavior may exist within a single heterogeneous tank (e.g., S-102).

The overall objective of these studies is to quantify the pertinent mechanisms of gas bubble retention and release under conditions that, as accurately as reasonably possible, reflect the actual tank conditions. The current standard method, in which retained gas volume is created and expanded by applying a vacuum to the sample, occurs on time scales that are quite rapid compared with the actual tank processes. An alternative would be to accelerate the radiolytic gas generation mechanism naturally occurring in the tanks. In this approach, gas retention and release would occur over months rather than hours or days. By increasing the experiment duration it is anticipated that novel gas retention and release characteristics will be observed. Gas diffusion and bubble migration will play a more significant role, and it is expected that a wider distribution of bubble sizes will result. To understand the role of bubble migration in the actual waste results, it is necessary to study the creep of individual bubbles in simulants and develop techniques to follow the slow creep of bubbles relative to the surrounding waste.

In addition to the experimental needs addressed above, it is also important to understand the importance and role of bubble-particle interactions better and to more clearly tie gas retention observations to tank chemistry, specifically, the presence or absence of surfactant-type chemical species. For example, in the current results on AN-103 waste, stable foams and tremendous frothing were observed, and the particular waste chemistry responsible for this phenomenon is as yet unclear. Simulant studies of known chemical composition could be used to screen for key chemical species or key interactions, and thereby supplement actual waste studies.

7.0 References

Benar CJ. 1997. *Final Report for Tank 241-AW-101, Push Mode Cores 132 and 139.* WHC-SD-WM-DP-192, Westinghouse Hanford Company, Richland, Washington.

Brager HR. 1994. *Summary of Information of Flammable Gas Watch List Tanks.* WHC-EP-0711, Westinghouse Hanford Company, Richland, Washington.

Bredt PR and SM Tingey. 1996. *The Effect of Dilution on the Gas Retention Behavior of Tank 241-SY-103 Waste.* PNL-10893, Pacific Northwest National Laboratory, Richland, Washington.

Bredt PR, SM Tingey, and EH Shade. 1995. *The Effect of Dilution on the Gas-Retention Behavior of Tank 241-SY-101 Waste.* PNL-10781, Pacific Northwest Laboratory, Richland, Washington.

Chhabra RP. 1993. *Bubbles, Drops, and Particles in Non-Newtonian Fluids*, Ch. 3, Sec. IV-B. CRC Press, Boca Raton, Florida.

Chhabra RP and PHT Uhlherr. 1986. "Static Equilibrium and Motion of Spheres in Viscoplastic Liquids." *Encyclopedia of Fluid Mechanics,* Vol. 21, NP Cheremisinoff, ed. Gulf Publishing Company, Houston, pp. 611-633.

Dullien FAL. 1992. *Porous Media: Fluid Transport and Pore Structure.* Academic Press, San Diego.

Gauglitz PA, SD Rassat, PR Bredt, JH Konynenbelt, SM Tingey, and DP Mendoza. 1996. *Mechanisms of Gas Bubble Retention and Release: Results for Hanford Waste Tanks 241-S-102 and 241-SY-103 and Single-Shell Tank Simulants.* PNNL-11298, Pacific Northwest National Laboratory, Richland, Washington.

Gauglitz PA, SD Rassat, MR Powell, RR Shah, and LA Mahoney. 1995. *Gas Bubble Retention and its Effect on Waste Properties: Retention Mechanisms, Viscosity, and Tensile and Shear Strengths.* PNL-10740, Pacific Northwest Laboratory, Richland, Washington.

Gauglitz PA, LA Mahoney, DP Mendoza, and MC Miller. 1994a. *Mechanisms of Gas Bubble Retention.* PNL-10120, Pacific Northwest Laboratory, Richland, Washington.

Gauglitz PA, RR Shah, and RL Davis. 1994b. *Gas Distribution Effects on Waste Properties: Viscosity of Bubbly Slurries.* PNL-10112, Pacific Northwest Laboratory, Richland, Washington.

Grigsby JM and CE Leach. 1996. *Flammable Gas/Slurry Growth Unreviewed Safety Question: Justification for Continued Operation for the Tank Farms.* WHC-SD-WM-JCO-007 Rev. 0A, Westinghouse Hanford Company, Richland, Washington.

Hanlon BM. 1995. *Waste Tank Summary Report for Month Ending August 31, 1995.* WHC-EP-0182-89, Westinghouse Hanford Company, Richland, Washington.

Hanlon BM. 1997. *Waste Tank Summary Report for Month Ending April 30, 1997.* HNF-EP-0182-109, Lockheed Martin Services Inc., Richland, Washington.

Heath WO. 1987. *Development of an In Situ Method to Define the Rheological Properties of Slurries and Sludges Stored in Underground Tanks.* PNL-6083, Pacific Northwest Laboratory, Richland, Washington.

Johnson GD, WB Barton, JW Brothers, SA Bryan, PA Gauglitz, RC Hill, LR Pederson, CW Stewart, and LM Stock. 1997a. "Evaluation of High-level Nuclear Waste Tanks Having a Potential Flammable Gas Hazard." In *Proceedings of Waste Management 97*, Tucson, Arizona.

Johnson GD, WB Barton, JW Brothers, SA Bryan, PA Gauglitz, RC Hill, LR Pederson, CW Stewart, and LM Stock. 1997b. *Flammable Gas Project Topical Report.* HNF-SP-1193 Rev. 2 (PNNL-11500), Lockheed Martin Services Inc., Richland, Washington

Johnson GD. 1997. *Strategy for Resolution of the Flammable Gas Safety Issue.* HNF-SD-WM-ER-680, Lockheed Martin Services Inc., Richland, Washington.

King CM, LR Pederson, and SA Bryan. 1997. *Thermal and Radiolytic Gas Generation form Tank 241-S-102 Waste.* PNNL-11600, Pacific Northwest National Laboratory, Richland, Washington.

Meyer PA, ME Brewster, SA Bryan, G Chen, LR Pederson, CW Stewart, and G Terrones. 1997. *Gas Retention and Release Behavior in Hanford Double-Shell Waste Tanks.* PNNL-11536 Rev. 1, Pacific Northwest National Laboratory, Richland, Washington.

Nguyen QD and DV Boger. 1992. "Measuring the Flow Properties of Yield Stress Fluids." *Annu. Rev. Fluid Mech.*, 24:47-88.

Rassat SD and PA Gauglitz. 1995. *Bubble Retention in Synthetic Sludge: Testing of Alternative Gas Retention Apparatus.* PNL-10661, Pacific Northwest Laboratory, Richland, Washington.

Rossen WR and SI Kam. 1996. *Mechanisms of Stability of Armored Bubbles: FY1996 Final Report.* PNNL-11416, Pacific Northwest National Laboratory, Richland, Washington.

Rossen WR and SK Das. 1995. *Mechanisms of Stability of Armored Bubbles: FY 1995 Progress Report.* PNNL-11133, Pacific Northwest National Laboratory, Richland, Washington.

Sathyanarayana P. 1994. *Tank 241-AW-101 Tank Characterization Plan.* WHC-SD-WM-TP-229, Westinghouse Hanford Company, Richland, Washington.

Shekarriz A, DR Rector, LA Mahoney, MA Chieda, JM Bates, RE Bauer, NS Cannon, BE Hey, CG Linschooten, FJ Reitz, and ER Siciliano. 1997. *Composition and Quantities of Retained Gas Measured in Hanford Waste Tanks 241-AW-101, A-101, AN-105, AN-104, and AN-103.* PNNL-11450 Rev. 1, Pacific Northwest National Laboratory, Richland, Washington.

Slezak SC and DR Bratzel. 1997. Safety Controls Optimization by Performance Evaluation (SCOPE) Analysis Framework. HNF-SD-WM-ES--410 Rev. 0, Lockheed Martin Services Inc., Richland, Washington.

Stewart CW, ME Brewster, PA Gauglitz, LA Mahoney, PA Meyer, KP Recknagle, and HC Reid. 1996. *Gas Retention and Release Behavior in Hanford Single-Shell Waste Tanks.* PNNL-11391, Pacific Northwest National Laboratory, Richland, Washington.

Walker DD, CL Crawford, and NE Bibler. 1994. "Radiolytic Bubble Formation and Level Changes in Simulated High-Level Waste Salts and Sludges - Application to HLW Storage Tanks." Proceedings of Waste Management 1994, Tucson, Arizona, pp. 393-396.

WHC. 1996a. *A Safety Assessment of Push-Mode and Rotary-Mode Core Sampling in Flammable Gas Single-Shell Tanks: Hanford Site, Richland, Washington.* WHC-SD-WM-SAD-035 Rev. 1, Westinghouse Hanford Company, Richland, Washington.

WHC. 1996b. *A Safety for Salt Well Jet Pumping Operations in Tank 241-A-101: Hanford Site, Richland, Washington,* WHC-SD-WM-SAD-036 Rev. 0, Westinghouse Hanford Company, Richland, Washington.

Appendix A

Tank 241-AW-101 Retention Data

Table A.1. Gas Retention Data for AW-101 Composite 1 in Vessel 1

Date	Time	Solids Layer Height, cm	Total (Liquid) Height, cm	Growth Volume, mL	Growth Gas Fraction	Pressure, mm Hg
5/14/97	10:14:53	10.95	13.20	0.0	0.000	753.7
	10:18:01	11.05	13.35	0.7	0.014	545.1
	10:21:01	11.20	13.45	1.2	0.022	429.3
	10:24:01	11.25	13.50	1.5	0.027	392.4
	10:28:01	11.45	13.75	2.7	0.048	320.0
	10:37:01	11.50	13.80	3.0	0.052	304.5
	10:41:01	11.60	13.90	3.4	0.060	277.3
	10:45:01	11.70	14.00	3.9	0.068	254.9
	10:49:01	11.85	14.15	4.7	0.080	235.5
	10:53:01	12.00	14.30	5.4	0.091	219.2
	10:57:01	12.10	14.40	5.9	0.099	205.1
	11:01:01	12.15	14.45	6.2	0.103	192.8
	11:05:01	12.30	14.60	6.9	0.114	181.1
	11:09:01	12.40	14.70	7.4	0.121	171.1
	11:13:01	12.55	14.85	8.1	0.131	162.6
	11:17:01	12.60	14.90	8.4	0.135	154.6
	11:21:01	12.75	15.05	9.1	0.145	146.9
	11:25:01	12.90	15.20	9.9	0.155	140.5
	11:29:01	13.00	15.30	10.3	0.161	134.2
	11:33:01	13.15	15.40	10.8	0.167	129.1
	11:37:01	13.35	15.55	11.6	0.177	123.3
	11:41:01	13.50	15.65	12.1	0.183	118.7
	11:43:01		15.55	11.6	0.177	116.5
	11:45:01		15.60	11.8	0.180	115.0
	11:49:01		15.70	12.3	0.186	111.6
	11:50:31		15.75	12.6	0.189	108.7
	11:51:26		15.55	11.6	0.177	107.5
	11:54:31		15.40	10.8	0.167	104.6
	12:00:11		15.50	11.3	0.174	99.7
	12:00:31		15.40	10.8	0.167	100.2
	12:05:31		15.40	10.8	0.167	96.3
	12:10:31		15.40	10.8	0.167	92.2
	12:15:30		15.45	11.1	0.171	90.0
	12:25:30		15.60	11.8	0.180	84.0
	12:30:30		15.55	11.6	0.177	81.3
	12:35:30		15.60	11.8	0.180	77.7
	12:40:30		15.70	12.3	0.186	76.2
	12:43:30		15.55	11.6	0.177	75.2
	12:48:30		15.55	11.6	0.177	71.6
	12:53:30		15.35	10.6	0.164	70.4
	12:58:30		15.15	9.6	0.151	68.4
	13:01:30		15.20	9.9	0.155	67.7
	13:06:30		15.10	9.4	0.148	65.5
	13:11:30		14.95	8.6	0.138	63.8
	13:16:30		14.50	6.4	0.106	62.6

Table A.2. Gas Retention Data for AW-101 Composite 1 in Vessel 2

Date	Time	Solids Layer Height, cm	Total (Liquid) Height, cm	Growth Volume, mL	Growth Gas Fraction	Pressure, mm Hg
5/14/97	16:47:11	10.75	12.85	0.0	0.000	752.2
	17:00:01	10.75	12.85	0.0	0.000	710.0
	17:30:01	10.80	12.90	0.2	0.005	618.7
	18:00:00	10.85	12.95	0.5	0.009	548.3
	18:30:00	10.90	13.00	0.7	0.014	491.9
	19:00:00	10.95	13.05	1.0	0.018	446.3
	19:30:00	11.00	13.15	1.5	0.027	408.1
	20:00:00	11.05	13.20	1.7	0.031	376.1
	20:30:00	11.10	13.30	2.2	0.040	348.9
	21:00:00	11.20	13.35	2.5	0.044	324.4
	21:30:00	11.25	13.40	2.7	0.049	303.5
	22:00:00	11.35	13.50	3.2	0.057	286.2
	22:30:09	11.45	13.60	3.7	0.065	270.2
	23:00:09	11.50	13.65	3.9	0.069	255.4
	23:30:09	11.60	13.75	4.4	0.077	242.3
	23:44:09	11.65	13.80	4.7	0.081	236.9
5/15/97	0:30:09	11.80	13.95	5.4	0.093	220.0
	1:00:09	11.95	14.05	5.9	0.100	210.2
	1:30:09	12.00	14.10	6.2	0.103	201.7
	2:00:08	12.05	14.20	6.6	0.111	193.5
	2:30:08	12.15	14.30	7.1	0.118	186.0
	3:00:08	12.30	14.40	7.6	0.125	179.2
	3:30:08	12.40	14.45	7.9	0.128	172.4
	4:00:08	12.50	14.50	8.1	0.131	166.5
	4:30:09	12.60	14.60	8.6	0.138	160.9
	5:00:06	12.75	14.70	9.1	0.146	155.6
	5:30:06	12.85	14.80	9.6	0.153	151.0
	6:00:05	12.95	14.90	10.1	0.159	146.1
	6:30:05	13.05	14.95	10.3	0.163	141.0
	7:00:04	13.20	15.05	10.8	0.169	137.1
	7:30:04	13.35	15.05	10.8	0.169	133.3
	8:00:04	13.50	15.10	11.1	0.172	130.3
	8:30:04	13.80	15.20	11.6	0.178	126.7
	9:00:04	13.85	15.30	12.1	0.185	123.5
	9:30:04	13.90	15.40	12.6	0.191	119.7
	10:00:04	13.90	15.45	12.8	0.194	117.2
	10:15:04		15.30	11.3	0.175	116.3
	10:30:04		14.70	9.1	0.146	115.3
	10:45:04		14.45	7.9	0.129	113.3
	11:00:04		14.35	7.4	0.122	112.6
	11:30:04		14.35	7.4	0.122	109.5
	12:00:04		14.40	7.6	0.125	108.0
	12:30:04		14.25	6.9	0.115	105.1
	13:00:03		14.15	6.4	0.107	105.1
	13:30:03		14.05	5.9	0.100	105.1
	14:00:03		14.00	5.7	0.096	105.1
	14:30:03		14.00	5.7	0.096	105.1

Table A.2. Gas Retention Data for AW-101 Composite 1 in Vessel 2

Date	Time	Solids Layer Height, cm	Total (Liquid) Height, cm	Growth Volume, mL	Growth Gas Fraction	Pressure, mm Hg
	15:00:03		14.05	5.9	0.100	105.1
	15:13:03		14.10	6.2	0.104	93.9
	15:20:03		14.15	6.4	0.107	92.9
	15:25:03		14.05	5.9	0.100	92.9
	16:58:05		13.65	3.9	0.069	77.2
	18:30:05		13.35	2.5	0.044	64.5
	20:20:03		13.15	1.5	0.027	54.8
	22:30:02		13.35	2.5	0.044	45.6
5/16/97	2:00:02		13.30	2.2	0.040	36.9
	4:00:02		13.20	1.7	0.031	33.0
	7:08:02		13.05	1.0	0.018	28.4
	8:00:01		13.05	1.0	0.018	27.4

Table A.3. Gas Retention Data for AW-101 Composite 2 in Vessel 3

Date	Time	Solids Layer Height, cm	Total (Liquid) Height, cm	Growth Volume, mL	Growth Gas Fraction	Pressure, mm Hg
5/19/97	16:02:16	10.85	13.00	0.0	0.000	746.9
	16:30:06	10.95	13.10	0.5	0.009	616.0
	17:00:06	11.00	13.20	1.0	0.018	511.8
	17:30:06	11.10	13.35	1.7	0.032	437.5
	18:00:06	11.25	13.45	2.2	0.040	382.2
	18:30:06	11.40	13.60	3.0	0.053	338.9
	19:00:06	11.50	13.70	3.4	0.061	305.2
	19:30:06	11.65	13.85	4.2	0.073	276.8
	20:00:06	11.85	14.00	4.9	0.084	254.4
	20:30:06	11.95	14.10	5.4	0.092	233.6
	21:00:06	12.10	14.25	6.2	0.103	217.5
	21:30:06	12.30	14.40	6.9	0.114	202.7
	22:00:06	12.45	14.50	7.4	0.120	190.1
	22:30:06	12.55	14.65	8.1	0.131	177.9
	23:00:06	12.80	14.80	8.9	0.141	168.5
	23:30:06	12.95	14.95	9.6	0.151	159.7
5/20/97	0:00:06	13.20	15.05	10.1	0.159	152.0
	0:30:05	13.30	15.15	10.6	0.165	144.2
	1:00:05	13.40	15.30	11.3	0.175	137.4
	1:30:05	13.55	15.40	11.8	0.181	131.3
	2:00:00	13.65	15.50	12.3	0.187	126.5
	2:18:04	13.75	15.60	12.8	0.193	122.3
	2:30:04		15.35	11.6	0.178	120.9
	3:00:04		15.10	10.3	0.162	116.7
	3:30:04		15.10	10.3	0.162	111.9
	4:00:04		15.05	10.1	0.159	108.0
	4:30:04		15.10	10.3	0.162	104.1
	5:00:04		15.15	10.6	0.165	101.0
	5:30:03		15.25	11.1	0.172	97.1
	5:31:03		15.10	10.3	0.162	97.3
	6:00:03		15.15	10.6	0.165	94.4
	6:30:02		15.25	11.1	0.172	91.5
	6:47:02		15.30	11.3	0.175	89.5
	6:50:02		15.15	10.6	0.165	89.5
	7:00:02		15.20	10.8	0.168	88.8
	7:05:02		15.00	9.8	0.155	88.6
	7:30:01		15.05	10.1	0.159	86.4
	8:00:01		15.05	10.1	0.159	83.5
	8:30:01		15.10	10.3	0.162	81.5
	8:57:01		15.20	10.8	0.168	79.8
	9:15:01		15.25	11.1	0.172	78.9
	9:30:01		15.15	10.6	0.165	76.2
	9:45:01		15.20	10.8	0.168	75.7
	10:00:01		15.05	10.1	0.159	74.3
	10:11:01		15.10	10.3	0.162	75.0
	10:13:01		14.90	9.4	0.149	75.0

Table A.3. Gas Retention Data for AW-101 Composite 2 in Vessel 3

Date	Time	Solids Layer Height, cm	Total (Liquid) Height, cm	Growth Volume, mL	Growth Gas Fraction	Pressure, mm Hg
	10:30:01		14.95	9.6	0.152	73.8
	10:32:01		14.65	8.1	0.132	73.3
	10:53:01		14.70	8.4	0.135	72.1
	11:00:01		14.45	7.1	0.118	72.1
	11:06:01		14.30	6.4	0.107	71.3
	11:30:01		14.35	6.6	0.111	69.9
	12:00:02		14.35	6.6	0.111	68.2
	12:15:02		14.40	6.9	0.114	68.2
	12:20:02		14.30	6.4	0.107	67.0
	12:30:02		14.30	6.4	0.107	67.5
	12:40:02		14.35	6.6	0.111	66.0
	12:45:02		14.15	5.7	0.096	66.2
	13:00:02		14.20	5.9	0.099	65.0
	13:17:02		14.10	5.4	0.092	64.5
	13:30:02		14.10	5.4	0.092	64.3
	13:40:02		14.05	5.2	0.088	63.1

Table A.4. Gas Retention Data for AW-101 Composite 2 in Vessel 4

Date	Time	Solids Layer Height, cm	Total (Liquid) Height, cm	Growth Volume, mL	Growth Gas Fraction	Pressure, mm Hg
5/21/97	15:59:33	7.25	7.35	0.0	0.000	753.0
	16:30:03	7.30	7.35	0.0	0.000	604.4
	17:00:03	7.35	7.40	0.2	0.007	504.1
	17:30:03	7.40	7.45	0.5	0.013	431.7
	18:00:03		7.50	0.7	0.020	377.8
	18:30:03		7.60	1.2	0.033	335.8
	19:00:03		7.65	1.5	0.039	302.0
	19:30:03		7.75	2.0	0.052	274.1
	20:00:03		7.80	2.2	0.058	252.7
	20:30:03		7.85	2.5	0.064	233.3
	21:00:03		7.95	3.0	0.076	216.1
	21:30:03		8.00	3.2	0.081	202.0
	22:00:03		8.05	3.5	0.087	188.9
	22:30:03		8.15	4.0	0.098	176.7
	23:00:03		8.25	4.5	0.109	167.3
	23:30:03		8.35	4.9	0.120	158.8
5/22/97	0:00:03		8.40	5.2	0.125	150.7
	0:30:03		8.45	5.4	0.131	143.9
	1:00:03		8.50	5.7	0.136	137.4
	1:30:03		8.55	5.9	0.141	131.3
	2:00:03		8.65	6.4	0.151	125.2
	2:30:03		8.75	6.9	0.160	120.4
	3:00:03		8.85	7.4	0.170	115.5
	3:30:03		8.90	7.7	0.175	111.6
	4:00:03		8.95	7.9	0.179	107.8
	4:01:33		8.85	7.4	0.170	106.3
	4:30:03		8.90	7.7	0.175	104.1
	4:50:03		8.85	7.4	0.170	101.2
	5:00:03		8.85	7.4	0.170	100.2
	5:30:03		8.90	7.7	0.175	97.3
	6:00:03		8.95	7.9	0.179	93.9
	6:23:03		9.00	8.2	0.184	90.5
	6:30:03		8.90	7.7	0.175	91.2
	7:00:03		8.95	7.9	0.179	88.3
	7:30:03		9.00	8.2	0.184	85.9
	8:00:03		9.05	8.4	0.188	83.5
	8:30:03		9.05	8.4	0.188	81.5
	9:00:03		9.10	8.7	0.193	78.9
	9:30:03		9.20	9.1	0.202	76.7
	9:35:03		9.15	8.9	0.197	76.7
	10:00:04		9.20	9.1	0.202	74.7
	10:30:04		9.25	9.4	0.206	73.0
	11:00:04		9.30	9.6	0.210	71.6
	11:30:04		9.40	10.1	0.219	69.9
	11:40:04		9.30	9.6	0.210	68.9
	12:00:04		9.40	10.1	0.219	67.7

Table A.4. Gas Retention Data for AW-101 Composite 2 in Vessel 4

Date	Time	Solids Layer Height, cm	Total (Liquid) Height, cm	Growth Volume, mL	Growth Gas Fraction	Pressure, mm Hg
	12:30:04		9.40	10.1	0.219	66.7
	12:35:04		9.30	9.6	0.210	65.5
	13:00:04		9.30	9.6	0.210	65.0
	13:30:04		9.30	9.6	0.210	64.1
	14:00:04		9.35	9.9	0.214	62.1
	14:30:04		9.35	9.9	0.214	61.1
	14:56:04		9.40	10.1	0.219	60.2
	15:30:04		9.45	10.4	0.223	59.2
	16:00:04		9.45	10.4	0.223	57.0
	16:30:04		9.45	10.4	0.223	56.0
	17:00:04		9.45	10.4	0.223	55.3
	17:08:34		9.45	10.4	0.223	55.6
	17:08:44		9.80	12.1	0.251	49.7
	17:08:54		10.00	13.1	0.266	38.3
	17:12:14		9.75	11.9	0.247	42.4
	17:14:44		9.35	9.9	0.214	43.2
	17:16:54		9.00	8.2	0.184	50.7
	17:19:24		8.85	7.4	0.170	55.1
	17:20:44		8.85	7.4	0.170	51.2
	17:21:04		7.80	2.2	0.058	51.7
	17:30:04		7.60	1.2	0.033	51.9
	18:00:04		7.60	1.2	0.033	49.7
	18:30:04		7.60	1.2	0.033	47.5
	19:00:04		7.70	1.7	0.046	45.4
	19:30:04		7.80	2.2	0.058	43.2
	20:00:04		7.95	3.0	0.076	41.5
	20:30:04		8.05	3.5	0.087	40.7
	21:00:04		8.15	4.0	0.098	38.6
	21:30:04		8.15	4.0	0.098	37.8
	22:00:04		8.25	4.5	0.109	36.1
	22:05:04		8.00	3.2	0.081	35.4
	22:30:05		8.05	3.5	0.087	34.9
	23:00:05		8.05	3.5	0.087	33.7
	23:15:05		8.10	3.7	0.093	32.0
	23:30:05		8.05	3.5	0.087	32.7
5/23/97	0:00:05		8.05	3.5	0.087	31.8
	0:30:05		8.10	3.7	0.093	30.8
	1:00:05		8.15	4.0	0.098	29.8
	1:30:05		8.20	4.2	0.104	28.8
	2:00:05		8.05	3.5	0.087	28.4
	2:15:05		8.00	3.2	0.081	27.9
	2:30:05		8.00	3.2	0.081	27.9
	3:00:05		7.90	2.7	0.070	26.9
	3:30:05		8.00	3.2	0.081	25.9
	4:00:05		8.00	3.2	0.081	25.9
	4:30:05		8.00	3.2	0.081	25.0
	5:00:05		8.15	4.0	0.098	23.7

Table A.4. Gas Retention Data for AW-101 Composite 2 in Vessel 4

Date	Time	Solids Layer Height, cm	Total (Liquid) Height, cm	Growth Volume, mL	Growth Gas Fraction	Pressure, mm Hg
	5:30:05		8.15	4.0	0.098	24.0
	6:00:05		8.00	3.2	0.081	23.0
	6:30:05		8.00	3.2	0.081	23.3
	7:00:05		8.00	3.2	0.081	22.0
	7:30:05		8.00	3.2	0.081	22.0
	8:30:05		7.90	2.7	0.070	21.1
	8:48:05		7.80	2.2	0.058	21.1
	9:00:05		7.75	2.0	0.052	19.6
	9:30:05		7.65	1.5	0.039	20.1

Appendix B

Tank 241-AN-103 Retention Data

Table B.1. Gas Retention Data for AN-103 Composite in Vessel 6

Date	Time	Solids Layer Height, cm	Total (Liquid) Height, cm	Growth Volume, mL	Growth Gas Fraction	Pressure, mm Hg
6/2/97	14:18:04	9.35	14.65	0.0	0.000	755.2
	14:20:59	9.40	14.65	0.0	0.000	609.7
	14:23:59	9.45	14.75	0.5	0.011	507.5
	14:26:59	9.55	14.80	0.7	0.016	434.1
	14:29:59	9.65	14.85	1.0	0.021	380.0
	14:32:59	9.75	14.95	1.5	0.031	337.5
	14:34:04	9.80	15.00	1.7	0.036	324.4
	14:35:59	9.85	15.05	2.0	0.040	303.7
	14:38:59	9.90	15.10	2.2	0.045	275.8
	14:41:59	9.90	15.20	2.7	0.055	253.2
	14:44:19	9.80	15.25	3.0	0.061	237.2
	14:48:04	10.15	15.45	3.9	0.079	215.8
	14:52:04	10.30	15.50	4.2	0.082	197.4
	14:56:04	10.35	15.65	4.9	0.096	181.3
	15:00:04	10.45	15.80	5.7	0.110	167.7
	15:04:04	10.65	15.90	6.1	0.117	156.1
	15:08:04	10.70	16.00	6.6	0.126	146.1
	15:12:04	10.75	16.15	7.4	0.139	137.1
	15:16:04	10.95	16.35	8.4	0.155	129.4
	15:20:04	11.05	16.45	8.9	0.162	122.3
	15:24:04	11.20	16.55	9.3	0.169	116.0
	15:28:04	11.35	16.75	10.3	0.185	110.4
	15:32:04	11.45	16.80	10.6	0.187	105.3
	15:36:04	11.65	17.00	11.6	0.201	100.2
	15:40:04	11.80	17.15	12.3	0.211	95.6
	15:44:04	11.95	17.25	12.8	0.217	91.7
	15:48:04	12.10	17.50	14.0	0.235	88.1
	15:52:04	12.25	17.55	14.3	0.236	85.7
	15:56:04	12.45	17.70	15.0	0.244	82.0
	16:00:04	12.55	17.85	15.7	0.254	79.8
	16:04:04	12.85	18.00	16.5	0.260	76.2
	16:08:04	13.00	18.20	17.5	0.272	73.8
	16:12:04	13.20	18.35	18.2	0.283	72.1
	16:16:04	13.45	18.50	18.9	0.291	70.1
	16:20:04	14.00	18.70	19.9	0.302	67.2
	16:21:14	14.30	18.75	20.2	0.304	66.2
	16:22:29	14.60	18.50	18.9	0.291	66.2
	16:23:29	16.00	18.45	18.7	0.288	66.5
	16:24:04	18.45	18.45	18.7	0.288	64.1

Table B.2. Gas Retention Data for AN-103 Composite in Vessel 7

Date	Time	Solids Layer Height, cm	Total (Liquid) Height, cm	Growth Volume, mL	Growth Gas Fraction	Pressure, mm Hg
6/4/97	15:13:01	9.75	14.65	0.0	0.000	753.7
	15:43:01	9.80	14.70	0.2	0.005	583.0
	16:13:01	9.85	14.75	0.5	0.010	473.5
	16:43:01	9.95	14.85	1.0	0.020	398.2
	17:13:01	10.05	14.95	1.5	0.030	343.6
	17:43:02	10.20	15.15	2.5	0.049	302.8
	18:13:02	10.30	15.20	2.7	0.054	269.5
	18:43:02	10.45	15.35	3.5	0.067	244.5
	19:13:02	10.50	15.50	4.2	0.081	221.7
	19:43:02	10.65	15.60	4.7	0.090	204.4
	20:13:02	10.80	15.65	5.0	0.093	188.9
	20:43:02	10.90	15.80	5.7	0.106	175.5
	21:13:02	11.00	15.95	6.4	0.119	164.6
	21:43:02	11.15	16.05	6.9	0.126	153.9
	22:13:02	11.30	16.20	7.7	0.138	144.9
	22:43:02	11.45	16.30	8.4	0.145	137.1
	23:13:02	11.60	16.45	9.2	0.156	130.3
	23:43:02	11.75	16.55	10.2	0.162	123.3
6/5/97	0:13:02	11.90	16.70	10.4	0.173	117.5
	0:43:02	12.00	16.85	10.9	0.184	112.6
	1:13:02	12.05	16.90	11.2	0.188	107.8
	1:43:02	12.15	17.00	11.7	0.194	102.9
	2:13:02	12.25	17.10	12.2	0.201	99.0
	2:43:02	12.50	17.30	13.1	0.213	95.1
	3:13:02	12.55	17.50	14.1	0.228	91.2
	3:43:02	12.75	17.65	14.9	0.236	88.6
	4:43:02	13.10	17.90	16.1	0.249	82.5
	5:13:02	13.25	18.00	16.6	0.254	79.6
	5:43:02	13.40	18.20	17.6	0.266	77.7
	6:13:01	13.55	18.40	18.6	0.278	74.7
	6:43:01	13.80	18.50	19.1	0.284	72.8
	7:13:01	14.00	18.65	19.8	0.292	70.6
	7:43:01	14.30	18.85	20.8	0.302	68.9
	8:13:01	14.65	19.00	21.6	0.310	67.0
	8:43:01	14.95	19.20	22.6	0.319	65.0
	8:45:41	15.00	19.20	22.6	0.319	65.0
	8:53:31	15.60	19.20	22.6	0.319	65.0
	8:56:51	16.00	19.25	22.8	0.322	64.1
	9:01:41	16.25	19.20	22.6	0.319	64.1
	9:04:31	18.00	19.15	22.3	0.317	64.1
	9:05:31	19.15	19.15	22.3	0.317	64.1

Table B.3. Gas Retention Data for AN-103 Composite in Vessel 8

Date	Time	Solids Layer Height, cm	Total (Liquid) Height, cm	Growth Volume, mL	Growth Gas Fraction	Pressure, mm Hg
6/5/97	15:18:09	10.35	13.20	0.0	0.000	757.1
	17:30:09	10.35	13.25	0.2	0.005	570.1
	20:00:09	10.40	13.30	0.5	0.010	444.1
	22:30:09	10.50	13.45	1.2	0.024	364.0
6/6/97	1:00:09	10.55	13.55	1.7	0.033	307.1
	3:30:09	10.65	13.70	2.5	0.047	266.3
	6:00:09	10.80	13.90	3.4	0.065	235.5
	9:00:09	10.95	14.05	4.2	0.078	206.4
	12:00:09	11.10	14.20	4.9	0.090	183.5
	14:30:13	11.25	14.35	5.6	0.102	168.0
	17:00:13	11.35	14.45	6.1	0.110	155.4
	19:30:13	11.45	14.50	6.4	0.114	143.7
	22:00:13	11.50	14.60	6.9	0.122	133.7
6/7/97	0:30:13	11.55	14.75	7.6	0.134	126.2
	3:00:13	11.70	14.95	8.6	0.150	118.4
	5:30:13	11.85	15.10	9.3	0.161	111.4
	8:00:13	12.05	15.20	9.8	0.166	105.6
	10:30:13	12.20	15.35	10.5	0.176	101.0
	11:20:13	12.30	15.45	11.0	0.183	98.8
	11:34:13	12.25	15.35	10.5	0.176	97.8
	13:00:13	12.30	15.40	10.8	0.179	95.9
	15:30:13	12.40	15.50	11.3	0.186	91.0
	18:00:13	12.60	15.60	11.8	0.191	87.1
	20:30:13	12.80	15.75	12.5	0.199	83.2
	23:00:13	13.05	15.95	13.5	0.211	80.6
6/8/97	1:30:13	13.45	16.10	14.2	0.223	76.7
	4:00:13	14.00	16.30	15.2	0.234	74.7
	6:30:13	14.70	16.50	16.2	0.246	71.6
	9:00:13	15.45	16.60	16.7	0.251	68.7
	11:30:13	16.10	16.90	18.1	0.268	66.7
	14:00:13	17.00	17.00	18.6	0.273	64.8
	14:05:13	17.10	17.10	19.1	0.278	64.3

Table B.4. Gas Retention Data for AN-103 Composite in Vessel 9

Date	Time	Solids Layer Height, cm	Total (Liquid) Height, cm	Growth Volume, mL	Growth Gas Fraction	Pressure, mm Hg
6/9/97	14:04:09	7.45	7.55	0.0	0.000	753.9
	14:40:07	7.55	7.65	0.5	0.013	557.0
	15:20:07	7.65	7.75	1.0	0.026	429.8
	16:00:06	7.75	7.85	1.5	0.039	350.1
	16:40:06	7.90	8.00	2.2	0.057	295.5
	17:20:06	8.00	8.10	2.7	0.069	255.2
	18:00:06	8.15	8.25	3.5	0.086	224.6
	18:40:06	8.30	8.35	3.9	0.097	201.3
	19:20:06	8.40	8.45	4.4	0.108	181.6
	20:00:05		8.55	4.9	0.119	164.8
	20:40:05		8.75	5.9	0.139	151.0
	21:20:04		8.85	6.4	0.149	140.3
	22:00:04		8.95	6.9	0.159	130.8
	22:40:04		9.10	7.6	0.173	122.1
	23:20:03		9.25	8.4	0.186	114.1
6/10/97	0:00:03		9.45	9.4	0.204	107.3
	0:40:03		9.60	10.1	0.216	101.7
	1:20:03		9.80	11.1	0.233	96.8
	2:00:02		9.95	11.8	0.244	91.7
	2:40:02		10.05	12.3	0.252	87.1
	3:20:02		9.90	11.6	0.240	83.0
	4:00:03		10.00	12.1	0.248	80.1
	4:40:03		10.25	13.3	0.267	76.2
	5:20:03		10.30	13.6	0.270	73.3
	6:00:03		10.50	14.5	0.284	70.4
	6:40:03		10.55	14.8	0.288	68.4
	7:20:03		10.70	15.5	0.298	65.5
	7:47:00		11.00	17.0	0.317	63.6
	8:00:03		10.85	16.3	0.308	63.6
	9:00:03		11.05	17.3	0.320	59.4
	10:00:03		11.25	18.2	0.333	57.7
	11:00:03		11.40	19.0	0.342	54.8
	12:00:01		11.20	18.0	0.330	52.2
	13:00:01		11.15	17.7	0.327	50.2
	14:00:01		11.30	18.5	0.336	48.0
	15:30:01		11.45	19.2	0.344	45.1
	17:00:00		11.60	20.0	0.353	42.9
	17:10:00		11.90	21.4	0.369	43.2
	18:30:00		11.50	19.5	0.347	41.0
	20:00:00		11.75	20.7	0.361	39.3
	21:30:00		11.45	19.2	0.344	37.3
	23:00:00		11.50	19.5	0.347	35.4
	23:28:00		11.65	20.2	0.356	33.7
6/11/97	0:30:00		11.45	19.2	0.344	33.5
	2:00:00		11.20	18.0	0.330	32.5
	3:30:09		11.20	18.0	0.330	31.3
	5:00:09		11.20	18.0	0.330	29.3

Appendix C

Gas Retention Mechanism Parameter Summary

Appendix C

Gas Retention Mechanism Parameter Summary

The gas retention mechanism summary plot shown in Figure 6.1 of the main report requires the calculation of three dimensionless quantities for each waste type represented. The parameter values used to compute these quantities for each distinct actual waste sample represented on the figure are summarized below.

As noted in Section 1.3 of the report, the distinction between the two dominant mechanisms of retention, interstitial liquid-displacing bubbles or particle-displacing bubbles, depends on two dimensionless groups that relate surface tension, gravitational, and waste strength forces (Gauglitz et al. 1994a, 1995, 1996). These relationships are reproduced here for convenience:

$$\frac{\text{Gravitational Force}}{\text{Surface Tension Force}} = \frac{\Delta\rho g h D_{particle}}{4\gamma} \qquad \text{(C.1)}$$

$$\frac{\text{Strength Force}}{\text{Surface Tension Force}} = \frac{\tau_s D_{particle}}{4\gamma}\left(\frac{A_2}{A_1}\right) \qquad \text{(C.2)}$$

The parameters in these equations are defined in Table C.1. Equation (C.1) is used to locate waste types on the abscissa of Figure 6.1, and the right-hand ordinate of the figure is calculated using Equation (C.2). The constant A_2/A_1, a ratio of areas that resulted from the original analysis (Gauglitz et al. 1995), was assigned a value of 1 in this study.

A third dimensionless group further refines the range of bubble behavior for particle-displacing bubbles. When these bubbles grow in a deformable material, the dominant factors controlling their growth are surface tension forces, which seek to keep the bubbles round, and the strength of the material that the bubble must overcome to displace the particles; this is represented by the following quantity:

$$\frac{\text{Strength Force}}{\text{Surface Tension Force}} = \frac{\tau_s D_{bubble}}{\gamma} \qquad \text{(C.3)}$$

Again, the parameters of Equation (C.3) are defined in Table C.1.

Table C.1. Definitions of Parameters Used in Gas Retention Mechanism Analyses

Parameter	Definition
$\Delta\rho$	Density difference between the nonconvective layer, including gas content, and the liquid
g	Gravitational acceleration, 9.8 m/s^2
h	Depth below the top of the settled solids
$D_{particle}$	Pore-throat diameter is approximated as the particle diameter
γ	Surface tension
τ_s	Shear strength, or more generally the strength of the material
D_{bubble}	Bubble diameter; 10^{-3} m (1 mm) specified throughout

The parameter values assigned for each actual tank waste type represented in Figure 6.1 are tabulated in Table C.2. To reflect uncertainty in the parameter values, a range of values is used in computing bounding values of the dimensionless quantities in Equations (C.1), (C.2), and (C.3). A central parameter value is assigned, and the range of values calculated relative to this follows:

$$P_- = P - k_P P \quad \text{(C.4)}$$

$$P_+ = P + k_P P \quad \text{(C.5)}$$

Equation (C.4) represents the lower bound, P_-, of the central parameter value P. Similarly, P_+ in Equation (C.5) is the upper bound of the parameter range. The multiplicative factor k_P defines uncertainty in the parameter value. These are also shown in Table C.2 for each parameter entry.

Table C.2. Actual Waste Gas Retention Parameter Values

Waste Type	$\Delta\rho$, g/mL	$k_{\Delta\rho}$	h, m	k_h	$D_{particle}$, m	$k_{Dparticle}$	γ, dyne/cm	k_γ	τ_s, Pa	k_τ
SY-103	0.22	1.2	0.05	1.26	10^{-6}	3	80	1.04	50	3.2
SY-101	0.22	1.2	0.1	1.26	10^{-6}	3	80	1.04	50	3.2
S-102 saltcake	0.4	1.2	0.05	1.26	10^{-4}	3	80	1.04	85	3.2
S-102 soft sludge	0.38	1.2	0.05	1.26	10^{-6}	3	80	1.04	320	3.2
S-102 stiff sludge	0.23	1.2	0.05	1.26	10^{-6}	3	80	1.04	3200	3.2
AN-103	0.33	1.15	0.065	1.26	10^{-6}	3	80	1.04	80	3.9
AW-101	0.18	1.25	0.065	1.26	10^{-6}	3	80	1.04	80	3.9

Distribution

No. of Copies

Offsite

2 Office of Scientific and Technical Information

H. Babad
2540 Cordoba Ct
Richland, WA 99352

C. W. Forsberg
Oak Ridge National Laboratory
P.O. Box 2008 MS 6495
Oak Ridge, TN 37831

B. C. Hudson
P.O. Box 271
Lindsborg, KA 67456

T. E. Larson
2711 Walnut St.
Los Alamos, NM 87544

Los Alamos National Laboratory
P.O. Box 1663
Los Alamos, NM 87545
Attn: D. R. Bennett K575

J. L. Kovach
Nuclear Consulting Services, Inc.
P.O. Box 29151
Columbus, OH 43229-0151

D. A. Powers
Sandia National Laboratories
MS-0744
Albuquerque, NM 87185-0744

No. of Copies

S. E. Slezak
Sandia National Laboratory
P.O. Box 5800 MS 1004
Albuquerque, NM 87110

A. B. Stone
Washington Department of Ecology
1315 W. 4th, B5-18
Kennewick, WA 00336

Onsite

5 DOE Richland Operations Office

K. Chen	S7-54
C. A. Groendyke	S7-54
G. W. Rosenwald	S7-54
J. M. Gray	S7-54
G. M. Neath	S7-51

14 Project Hanford Management Contract Team

W. B. Barton	R2-11
R. E. Bauer	S7-14
D. R. Bratzel	S7-14
R. J. Cash	S7-14
K. M. Hodgson	R2-11
G. D. Johnson (3)	S7-15
N. W. Kirch	R2-11
D. A. Reynolds	R2-11
E. R. Siciliano	H0-31
L. M. Stock	S7-14
R. J. Van Vleet	R3-27

No. of Copies		
29	Pacific Northwest National Laboratory	
	S. Q. Bennett	K7-90
	J. W. Brothers (5)	K9-20
	P. R. Bredt	P7-41
	S. V. Forbes	P7-25
	P. A. Gauglitz (5)	P7-41
	L. A. Mahoney	K7-15
	L. M. Peurrung	P7-41
	S. D. Rassat (5)	P7-41
	A. Shekarriz	K7-15
	C. W. Stewart	K7-15
	G. Terrones	K7-15
	S. M. Tingey	P7-25
	Information Release (5)	K1-06